CALIFORNIA INSTITUTE OF TECHNOLOGY

EARTHQUAKE ENGINEERING RESEARCH LABORATORY

REAL-TIME LOSS ESTIMATION FOR INSTRUMENTED BUILDINGS

BY

K.A. PORTER, J.L. BECK, J.Y. CHING, AND
J. MITRANI-REISER
CALIFORNIA INSTITUTE OF TECHNOLOGY

AND

M. MIYAMURA, A. KUSAKA, T. KUDO, K. IKKATAI, AND
Y. HYODO
KAJIMA CORPORATION

REPORT NO. EERL 2004-08

A REPORT ON RESEARCH SUPPORTED BY THE
CUREE-KAJIMA JOINT RESEARCH PROGRAM, PHASE V

PASADENA, CALIFORNIA

SEPTEMBER, 2004

A REPORT ON RESEARCH SUPPORTED BY THE CUREE-KAJIMA JOINT RESEARCH PROGRAM PHASE V UNDER THE SUPERVISION OF K.A. PORTER AND J.L. BECK

Real-Time Loss Estimation for Instrumented Buildings

Final Report
CUREE-Kajima Joint Research Program
Phase V

September, 2004

Final Report for
CUREE-Kajima Phase V Project

REAL-TIME LOSS ESTIMATION FOR INSTRUMENTED BUILDINGS

CUREE	KAJIMA
K.A. Porter	M. Miyamura
J.L. Beck	A. Kusaka
J.Y. Ching	T. Kudo
J. Mitrani-Reiser	K. Ikkatai
	Y. Hyodo

September, 2004

REAL-TIME LOSS ESTIMATION FOR INSTRUMENTED BUILDINGS

K.A. Porter, J.L. Beck, J.Y. Ching, and J. Mitrani-Reiser
California Institute of Technology, Pasadena, CA

M. Miyamura, A. Kusaka, T. Kudo, K. Ikkatai, and Y. Hyodo
Kajima Corporation, Tokyo, Japan

Abstract

Motivation. *A growing number of buildings have been instrumented to measure and record earthquake motions and to transmit these records to seismic-network data centers to be archived and disseminated for research purposes. At the same time, sensors are growing smaller, less expensive to install, and capable of sensing and transmitting other environmental parameters in addition to acceleration. Finally, recently developed performance-based earthquake engineering methodologies employ structural-response information to estimate probabilistic repair costs, repair durations, and other metrics of seismic performance. The opportunity presents itself therefore to combine these developments into the capability to estimate automatically in near-real-time the probabilistic seismic performance of an instrumented building, shortly after the cessation of strong motion. We refer to this opportunity as (near-) real-time loss estimation (RTLE).*

Methodology. *This report presents a methodology for RTLE for instrumented buildings. Seismic performance is to be measured in terms of probabilistic repair cost, precise location of likely physical damage, operability, and life-safety. The methodology uses the instrument recordings and a Bayesian state-estimation algorithm called a particle filter to estimate the probabilistic structural response of the system, in terms of member forces and deformations. The structural response estimate is then used as input to component fragility functions to estimate the probabilistic damage state of structural and nonstructural components. The probabilistic damage state can be used to direct structural engineers to likely locations of physical damage, even if they are concealed behind architectural finishes. The damage state is used with construction cost-estimation principles to estimate probabilistic repair cost. It is also used as input to a quantified, fuzzy-set version of the FEMA-356 performance-level descriptions to estimate probabilistic safety and operability levels.*

CUREE demonstration building. *The procedure for estimating damage locations, repair costs, and post-earthquake safety and operability is illustrated in parallel demonstrations by CUREE and Kajima research teams. The CUREE demonstration is performed using a real 1960s-era, 7-story, non-ductile reinforced-concrete moment-frame building located in Van Nuys, California. The building is instrumented with 16 channels at five levels: ground level, floors 2, 3, 6, and the roof. We used the records obtained after the 1994 Northridge earthquake to hindcast performance in that earthquake. The building is analyzed in its condition prior to the 1994 Northridge Earthquake. It is found that, while hindcasting of the overall system performance level was excellent, prediction of detailed damage locations was poor, implying that either actual conditions differed substantially from those shown on the structural drawings, or inappropriate fragility functions were employed, or both. We also found that Bayesian updating of the structural model using observed structural response above the base of the building adds little information to the performance prediction. The reason is probably that*

structural uncertainties have only secondary effect on performance uncertainty, compared with the uncertainty in assembly damageability as quantified by their fragility functions. The implication is that real-time loss estimation is not sensitive to structural uncertainties (saving costly multiple simulations of structural response), and that real-time loss estimation does not benefit significantly from installing measuring instruments other than those at the base of the building.

Kajima demonstration building. *The Kajima demonstration is performed using a real 1960s-era office building in Kobe, Japan. The building, a 7-story reinforced-concrete shearwall building, was not instrumented in the 1995 Kobe earthquake, so instrument recordings are simulated. The building is analyzed in its condition prior to the earthquake. It is found that, while hindcasting of the overall repair cost was excellent, prediction of detailed damage locations was poor, again implying either that as-built conditions differ substantially from those shown on structural drawings, or that inappropriate fragility functions were used, or both. We find that the parameters of the detailed particle filter needed significant tuning, which would be impractical in actual application. Work is needed to prescribe values of these parameters in general.*

Opportunities for implementation and further research. *Because much of the cost of applying this RTLE algorithm results from the cost of instrumentation and the effort of setting up a structural model, the readiest application would be to instrumented buildings whose structural models are already available, and to apply the methodology to important facilities. It would be useful to study under what conditions RTLE would be economically justified. Two other interesting possibilities for further study are (1) to update performance using readily observable damage; and (2) to quantify the value of information for expensive inspections, e.g., if one inspects a connection with a modeled 50% failure probability and finds that the connect is undamaged, is it necessary to examine one with 10% failure probability?*

CONTENTS

FIGURES

TABLES

1 INTRODUCTION

1.1 BACKGROUND

The implications of seismic networks, instrumented buildings, performance-based earthquake engineering (PBEE), and state estimation. Seismic networks such as TriNet (2002), the California Integrated Seismic Network (CISN 2001), and the currently-developing Advanced National Seismic System (ANSS, U.S. Geological Survey, 2000a), demonstrate that mature and reliable infrastructure exists to provide near-real-time and archived near-real-time information from sensors in the ground and in buildings.

At the same time, developments in performance-based earthquake engineering (PBEE) enable an engineering analysis to quantify building performance in terms of fatalities, repair costs, and repair duration ("dollars, deaths, and downtime"). Recent projects, supported by the CUREE-Kajima Joint Research Program, Phases III and IV, developed such a PBEE framework, illustrated in Figure 1-1. In the framework (Beck et al. 1999, 2002), the analyst considers one or more levels of seismic intensity, performs dynamic structural analysis to estimate structural response, uses structural response to calculate damage, and uses damage to calculate loss.

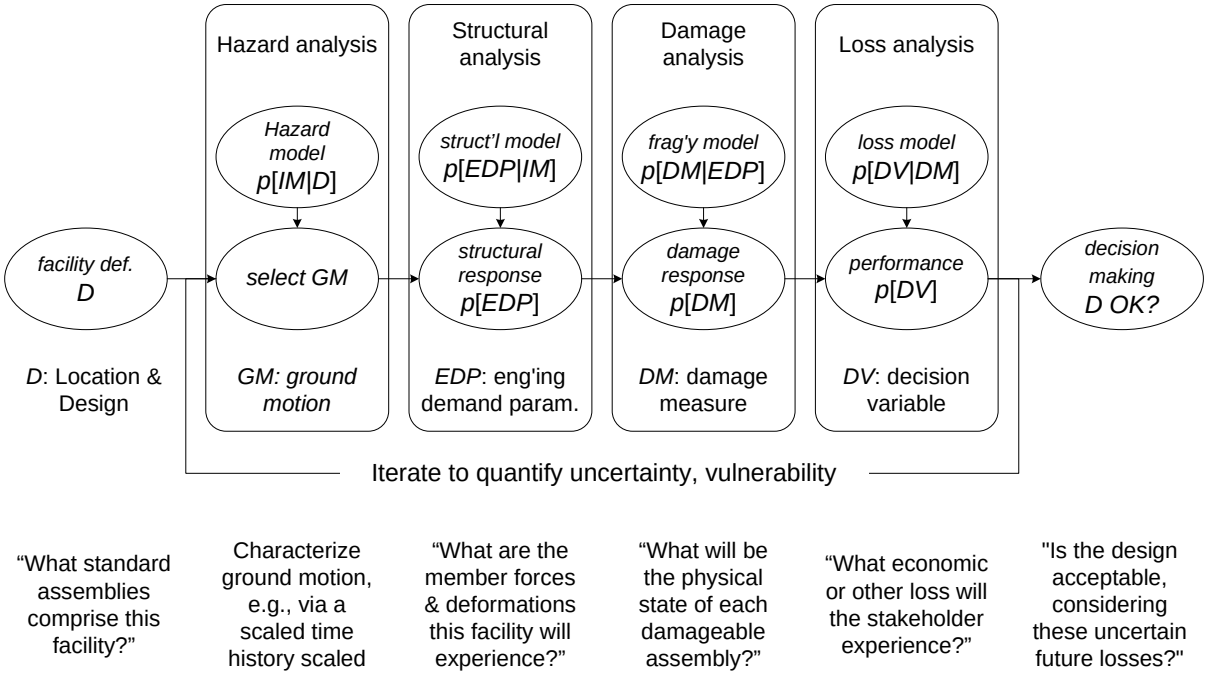

Figure 1-1. Framework of probabilistic PBEE methodologies

Considering these trends—advanced seismic networks, PBEE methods to estimate probabilistic damage and loss, along with advancements in state estimation, the opportunity arises to estimate automatically in near-real-time the probabilistic seismic performance of an instrumented building, shortly after the cessation of strong motion. We refer to this opportunity as (near-) real-time loss estimation (RTLE). The value of such a capability could be manifold:

- ***Safety and operability information.*** In a disaster, it can take days or more for engineers to perform a rapid visual safety assessment, and weeks before they complete a post-earthquake engineering analysis. During that time the owner and occupants may be in a state of uncomfortable uncertainty about their safety. A rapid damage analysis could provide a practical first-cut safety assessment or provide an indicator for prioritizing visual safety assessments, by estimating the probability that a building meets acceptable life-safety standards.
- ***Reduced inspection costs.*** Knowledge of the probable locations of concealed physical damage at a detailed level could greatly reduce post-earthquake inspection efforts by targeting those members or connections most likely to have suffered damage. In the case of welded-steel moment frames, the cost avoided can exceed $5,000 per connection. Knowledge of where to look for damage also reduces likely building-closure durations and consequent business-interruption costs.
- ***Accelerated recovery funding.*** Immediately after a disaster, building stakeholders usually want an estimate of restoration costs for recovery decisions. To contract for and carry out a structural analysis and cost estimate of an earthquake-damaged building can require the stakeholders to wait weeks or months before reliable information is available. An automated probabilistic loss estimate could provide valuable preliminary information to owners, insurers, banks and public-relief entities to begin funding restoration efforts.

1.2 PROJECT OBJECTIVES

Develop a near-real-time loss-estimation methodology. This project seeks to develop and illustrate the automated estimation of probabilistic damage at the component level, repair cost, safety, and operability immediately after strong motion for an instrumented building, using elements of a PBEE model of the building. Those elements include damage and loss analysis, plus the addition of a Bayesian state estimation procedure that uses a particle filter.

Applicable to instrumented buildings. The methodology is to be applicable to any building with strong-motion instruments recording base accelerations; additional sensors above the base are used to reduce uncertainty in the estimate of structural response, damage, and loss.

Informed by a stochastic structural model, and a damage and loss model. The methodology adapts the assembly-based vulnerability (ABV) methodology developed in previous CUREE-Kajima Joint Research projects (Beck et al. 1999, 2002) or Kajima Level-3 loss assessment (Beck et al. 2002). These models estimate physical damage at the component level, and overall performance at the system level, accounting for important sources of uncertainty. They are distinct from system-identification methods of damage assessment in that they apply fragility functions and construction-contracting principles to the performance evaluation.

Apply to US and Japanese demonstration facilities. The methodology is applied to demonstration facilities in the United States and Japan. The CUREE team will develop the method and apply it to the US demonstration facility; the Kajima team will apply it to the Japanese facility.

Design software (not implementation). Software to implement the methodology is not part of the project objectives. The algorithm to carry out the methodology can serve as pseudocode for such software. (In fact, some software to perform the particle-filter stage of the analysis is provided as part of the project, but this is in addition to the project objectives.)

1.3 ORGANIZATION OF REPORT

Chapter 2 presents a review of the relevant literature. The RTLE methodology is presented in Chapter 3. Chapter 4 illustrates the methodology by applying it to the CUREE demonstration building The Japanese demonstration building and application is presented in Chapter 5. Chapter 6 contains conclusions and offers suggestions for applications and further research. References are listed in Chapter 7. An appendix contains a supporting manuscript.

1.4 ACKNOWLEDGMENTS

This research was funded in part by the CUREE-Kajima Joint Research Program Phase V. In addition, some funding for Drs Porter and Ching was provided by the GW Housner Fund. We gratefully acknowledge the support of these entities.

2 LITERATURE REVIEW

2.1 NEAR-REAL-TIME GROUND MOTION INFORMATION

Near-real-time ground-motion information is available through a growing number of sources. TriNet (2002) is a collaborative project to determine seismic sources and collect seismograms and accelerograms for Southern California. It uses a network of 600 stations distributed throughout Southern California, of which approximately 450 have strong-motion instruments, and 150 that have both broadband seismometers and strong-motion accelerometers. The latter set provides continuous digital telemetry via TCP/IP to a central computing facility and to a redundant, active standby facility. The former send their recordings when triggered. When the instruments indicate that an earthquake has occurred, the central computing facility automatically determines the earthquake origin time, magnitude, location, and source information in near-real-time. Staff seismologists review computed earthquake information, and webservers display the information via a website. This infrastructure collects and archives the continuous telemetry at 20 samples per second. This means that anyone can recall a record from any of these 150 TriNet sites from any point in time since the instrument was installed, for any duration of interest. Furthermore, higher-sampling-rate records (up to 100 samples per second) are archived and available for any instrument in a region near an earthquake of magnitude $M \geq 1.8$, and from the entire network for events of magnitude $M \geq 4$.

TriNet began in 1997, a successor to earlier programs such as the 1990 Caltech US Geological Survey Broadcast of Earthquakes (CUBE) project to provide real-time earthquake information. The system is a collaborative effort of the California Institute of Technology, the U.S. Geological Survey, and the California Geological Survey (formerly the California Division of Mines and Geology). In 2002, TriNet finished, and merged with a similar, Northern-California effort to become the California Integrated Seismic Network (CISN 2001). CISN in turn will represent the California region of the currently-developing Advanced National Seismic System (ANSS, U.S. Geological Survey 2000), which if fully funded will be similar to TriNet and CISN, but with a national scope, a more extensive seismic network, and with the addition of instruments in buildings.

The methodologies for determining source information are fairly mature. TriNet, CISN, and eventually ANSS, represent examples of how these methodologies are implemented with sensors, communication, and computer facilities to provide publicly available, rapid, reliable estimates of source mechanism, origin time, location, and magnitude. The archive makes it easy to retrieve these earthquake data at a later time.

The California Strong-Motion Instrumentation Program (CSMIP, California Geological Survey 2002) since 1972 has maintained a network of accelerographs to measure strong shaking. In 2002, the network included more than 900 stations: 650 that record ground motion, 170 stations that are located in buildings, 20 that are on dams and 60 on bridges. The more modern of these instruments sends its telemetry automatically to CSMIP headquarters when it experiences strong motion. The strong-motion data are available for download from the California Geological Survey's Strong Motion Data Center (California Geological Survey 1999).

ShakeMap (TriNet 2001) is a product of TriNet and CISN that uses the strong-motion network to create maps of shaking severity. These images, called ShakeMaps, display

shaking severity for individual events in units of peak horizontal ground acceleration, peak ground velocity, and instrumental intensity (an estimate of MMI based on instrumental measurements). ShakeMaps are available in a format that can be input to the HAZUS software (Federal Emergency Management Agency 1999) for use in loss estimation. The ShakeMap working group notes that, with the current station distribution, data gaps are common, particularly for smaller events and earthquakes near or outside the edge of the network. They also note that, "Since ground motions and intensities typically can vary significantly over small distances, these maps are only approximate. At small scales, they should be considered unreliable."

2.2 STRUCTURAL HEALTH MONITORING

Structural health monitoring, or SHM for short, is a process of establishing some knowledge of the current condition of a structure based on data from sensors located on the structure. The ultimate goal is to determine the existence, location, and severity of damage in a structure if damage occurs. The need for this type of technology is demonstrated by the failure of structures due to gradual fatigue and corrosion type damage, such as the Mianus river bridge in Connecticut (Levy and Salvadori 1992) and Aloha Airlines flight 737 (Ott and O'lone 1988), as well as loss of structural integrity due to severe loading events, as seen in the connection failures of some steel frame structures during the Northridge earthquake in southern California in 1994 (EERI 1996).

A great deal of research in the past thirty years has been aimed at establishing effective local and global methods for health monitoring in civil, mechanical, and aerospace structures. An extensive survey of global methods which use vibration characteristics to perform SHM is presented in Doebling et al. (1996) and in a recent update by Sohn et al. (2004). One typical global approach involves comparing structural models identified using sets of modal data (i.e., frequencies and modeshapes) from a structure before and after damage has occurred. This model-based SHM approach relies on structural-model-updating methodologies to solve the inverse problem of determining the parameters of a structural model given some measured response time histories or some modal data. The basic idea is to use identified local stiffness loss as indicative of damage at that location. Farhat and Hemez (1993), Kim and Bartkowicz (1993) and Vanik et al. (2000) present examples of this type of SHM method. The critical assumption is made that changes in the stiffness parameters of the structural model imply damage in the parts of the real structure associated with the model parameters.

There are some inherent features of structural-model updating that lead to difficulties in the model-based SHM approach. The process of identifying the model parameters from the modal data is generally ill-conditioned. Thus, small changes in the modal data lead to proportionally larger changes in the model parameters. Model error and variations in the modal data due to noise and changing environmental conditions such as temperature and humidity, when combined with the ill-conditioning, can lead to large variations in the identified model parameters that are not due to true changes in the structure. Thus, there is uncertainty in whether changes in identified model parameters reflect actual damage in the structure.

Many of the available papers in the SHM literature do not consider this uncertainty. For example, they usually assume the structure under consideration is well-characterized by some analytical model, but analytical models rarely capture the full behavior of the structure. For

instance, the model may not account for effects such as thermally induced diurnal variations and excitation amplitude dependence of the modal parameters. Further, the available measured information is restricted by limits on the amount of instrumentation and the fact that only a few of the lower modes of a civil structure can generally be determined with confidence. Finally, measured modal data tend to show significant variation from one measurement to the next. Any SHM method applied in the case of civil structures should therefore account for the substantial uncertainty which arises in the identified structural model parameters.

In addition to neglecting the uncertainties, most methods tend to look for damage using only one set of data from the undamaged structure and another from the structure in a damaged state. In situations where the structure is only measured during infrequent inspections or following a severe loading event which had given cause to suspect the structure was damaged, such methods are potentially useful. However, there are a number of advantages to treating SHM as a continual monitoring process. First, the effects of noise in the data can potentially be mitigated by using multiple measurements. Also, by observing the structure continually, systematic changes may be separated from more random fluctuations whose source is unknown. Those systematic variations which are not due to damage, such as diurnal effects, can be included in the model to decrease model error.

Caltech researchers have introduced a continual on-line Bayesian probabilistic SHM technique which addresses the ill-conditioning inherent in the inverse problem (e.g., Vanik et al. 2000; Ching and Beck 2003). The approach requires a linear structural model whose stiffness matrix is parameterized to develop a class of possible models. The parameterization involves grouping the elements of the structural model into substructures. Modal data (i.e., frequencies and incomplete modeshapes) measured from a structure are used to identify the model substructure stiffness parameters. In a deterministic SHM scheme, differences in the best parameters identified from different modal data sets would be used as indicators of damage. However, rather than consider only single best models for each modal data set, the probabilistic method takes uncertainties in the identified model into account by treating the problem within a framework of plausible inference (Jaynes 2003). Bayes' theorem is invoked to develop a probability density function (PDF) for the model stiffness parameters conditional on measured modal data and the class of possible models. Using conditional PDFs derived from sets of modal data determined at different times, a probabilistic damage measure is developed. The probabilistic damage measure arises in answer to the question: Based on the available modal data and acknowledging the uncertainty, what is the probability that the current model stiffness parameters are less than a specified fraction of the corresponding undamaged stiffness parameters?

A testbed has been installed at Caltech for the development of on-line SHM. The technique implemented in the Caltech Online Monitoring and Evaluations Testbed (COMET; Lam and Beck 2004) is a computer-based system designed to receive, analyze, and disseminate near-real-time accelerometer data-streams from instruments in (currently) two facilities. The analytical tools calculate modal data of the monitored facilities from sensor information either received in near-real-time or retrieved from COMET's data warehouse of recorded motion. COMET can be accessed via a web browser on the Internet. In a similar spirit to COMET, the R-Shape system (Caltech 2002), provides real-time access to all 36 channels of data available in the Millikian Memorial Building, via a commercial software program. It offers alarms to indicate when predefined drift limits have been exceeded, and

calculates fast Fourier transforms of building vibration, which are indicative of modal periods and by extension stiffness degradation and damage.

Another interesting implementation of the same commercial system is presented by Celebi et al. (2004), which uses accelerometers in a 24-story steel-frame building to compute interstory drift ratios at a few story levels where sensors operate at two adjacent floors. These interstory drift ratios are then compared with (deterministic) drift limits associated with each of several FEMA 273-style performance levels: operational, immediately occupiable, life-safety, and collapse-prevention (FEMA 1997). When a drift limit is exceeded, the associated FEMA 273 performance level is assumed to be exceeded.

In the present report, a new approach is taken whereby fragility functions are employed to predict damage based on inferring engineering demand parameters from sensor data. This has an advantage that both structural and non-structural damage can be addressed and prior information about the fragility of these components is incorporated via the fragility functions. As in the previous Caltech approach to SHM (Vanik et al. 2000; Ching and Beck 2003), a full probabilistic description of the uncertainties at each stage is established and these uncertainties are propagated through to the final results.

2.3 STATE ESTIMATION

State estimation is the process of using dynamic data from a system to estimate quantities that give a complete description of the state of the system according to some representative model of it. For the Bayesian state-estimation algorithms, Kalman formulated the well-known Kalman filter (KF) (Kalman 1960; Kalman and Bucy 1961) for linear systems with Gaussian uncertainties. Later, KF was modified to give the extended Kalman filter (EKF) (Jazwinski 1970) to accommodate lightly nonlinear systems, and this is basically the dominant Bayesian state-estimation algorithm for nonlinear systems and non-Gaussian uncertainties for the last 30 years.

Although EKF has been widely used, it is only reliable for systems that are almost linear on the time scale of the updating intervals (Julier et al. 2000; Wan and van der Merwe 2000). However, civil engineering systems are often highly nonlinear when subject to severe loading events; in this case, the applicability of the Kalman filter and extended Kalman filter is often questionable. These older techniques have been used by civil engineering researchers for decades (Beck 1978; Yun and Shinozuka 1980; Hoshiya and Saito 1984; Koh and See 1994) although their applicability for nonlinear systems and non-Gaussian uncertainties is seldom verified either empirically or theoretically.

Several important breakthroughs (Alspach and Sorenson 1972; Gordon et al. 1993; Kitagawa 1996; Doucet et al. 2000; Julier et al. 2000) have produced Bayesian state-estimation algorithms that are applicable to highly nonlinear systems. State estimation for general nonlinear dynamical systems is still an active research area, and novel techniques (e.g., van der Merwe et al. 2000; van der Merwe and Wan 2003) can be found in the most recent signal-processing literature. Although these breakthroughs have had significant impact in the area of signal processing, they are rarely seen in the civil engineering literature and have not been implemented for civil engineering systems.

In Ching et al. (2004), some recent developments in real-time Bayesian state estimation that use Monte Carlo simulation (MCS), are introduced. The technique called particle filter (PF) is presented and discussed in this report. These Monte Carlo techniques have the

following advantages: 1) they are applicable to highly nonlinear systems with non-Gaussian uncertainties; 2) they are not limited to the first two moments as in KF and EKF; and 3) as the sample size approaches infinity, the resulting state estimates converge to their expected values. However, the simulation is usually computationally expensive, and sometimes the state estimates can be inaccurate due to insufficient samples. The authors introduce several recent developments that address the aforementioned difficulties and present new techniques that are useful to improve the convergence. The performance of different methods (i.e., EKF and PF) is compared through several numerical examples and a real-data case study.

2.4 ECONOMIC PERFORMANCE EVALUATION

A number of authors have performed empirical studies to attempt to relate recorded ground shaking with the observed damage and economic loss of buildings, considering key characteristics such as design date, structural system, size, and configuration. In general, the methodologies employ a common strategy: identify a study region and groups of buildings affected by one or more particular earthquakes, determine or estimate the shaking intensity experienced by each building in the study, tabulate the key characteristics of interest for each building, record the damage and economic loss measures of interest, and use regression analysis to attempt to discern correlation between loss and shaking intensity. Notable examples include the following.

Martel (1936) describes an effort designed, in part, to determine "if significant differences in damage [in an earthquake] resulted from differences in the building's subtype, occupancy, or adjacency to other buildings." The author examined 1,261 unreinforced-masonry buildings (UMBs) in Long Beach, CA, which were shaken by the March 10, 1933, Long Beach Earthquake, and in a supplementary study, a number of woodframe residences in Compton, CA. More recently, Rutherford & Chekene (1990) and Lizundia et al. (1993) set out with similar objectives and surveyed 2,007 unreinforced masonry buildings in San Francisco in the months after the 1989 Loma Prieta Earthquake.

FEMA 352 (SAC Joint Venture 2000), is an exemplar of a data-gathering procedure designed to inform a nuts-and-bolts-level structural-engineering decision process. It specifies data-gathering, analysis, and reporting procedures for evaluating the safety of welded-steel moment-frame (WSMF) buildings, and for determining required rehabilitation measures (relevant to repair cost).

McClure (1973) presents results of a detailed study of 169 single-family dwellings in the epicentral region of the 1971 San Fernando earthquake, all of which were subjected to peak ground acceleration of 0.25g to 1.0g. The author desired to observe the effects on seismic performance produced by differences in rise type (one story, one-and-two story, two-story, one-and-two-story split level, and other), seismic excitation (shaking only, and shaking and ground failure), soil condition (four types), and site grading (four types).

Schierle (2002a) examines woodframe dwelling losses of the 1994 Northridge earthquake. One important objective was to create seismic vulnerability functions—relationships between earthquake repair costs and shaking severity—for six categories of dwelling. Dwellings are categorized by plurality (i.e., single-family or multiple-family) and era of construction (pre-1941, 1941-1976, and 1977-1993). Repair costs are expressed in terms of the damage factor, i.e., as repair cost divided by an estimate of replacement cost, and in terms of cost per square foot of floorspace. Shaking severity is parameterized in terms of

peak ground acceleration, discretized in three levels: less than 0.30g, 0.30-0.60g, and greater than 0.60g.

The authors of ATC-13 (ATC 1985) set out to create a comprehensive model of the seismic vulnerability of a wide variety of buildings, bridges, and other facilities, relating physical damage and repair cost to shaking intensity. They found that for most categories of facilities, inadequate data exist to create such models from empirical data, and thus rely on expert opinion instead. The seismic vulnerability functions they produce account for structural system and height category, but do not address configuration or other detailed facility characteristics.

Several authors have attempted to formulate analytical methods to relate shaking and economic performance of individual buildings, accounting for their detailed structural and nonstructural design. Czarnecki (1973) was perhaps the first to suggest a method that relied on structural analysis to estimate structural response, and then to relate the resulting forces or deformations in structural and architectural elements to the cost to repair them. Kustu et al. (1982) advanced this approach by showing how laboratory and other empirical data could inform this second analytical stage, referred to here as the damage and loss analysis. Beck et al (1999, 2002), Porter (2000), Porter and Kiremidjian (2001), and Porter et al. (2002a) further added nonlinear time-history structural analysis at a number of intensity levels, offered a more-detailed taxonomy of components, suggested stochastic modeling at each analytical stage to propagate all important uncertainties, and demonstrated how one can estimate repair duration and post-earthquake usability. The Pacific Earthquake Engineering Research Center (PEER 2004) has employed similar techniques in its development of a second-generation performance-based earthquake engineering (PBEE) methodology, offering component-level fragility information, open-source structural analysis software, empirical fatality-rate information, and in general state-of-the-art principles of hazard and structural analysis.

2.5 SAFETY AND POST-EARTHQUAKE OPERABILITY

ATC-20 (ATC 1989, 1991, and 1996) has emerged as the dominant methodology to assess the post-earthquake safety of buildings based on observable damage. The procedures, developed for use by structural engineers and building department officials, provide for both rapid and detailed safety evaluations. For both levels of detail, the engineer completes a brief checklist, and based on the results, posts a placard on the building in one of three colors: red for unsafe, yellow for restricted use, or green for inspected. Under the rapid-evaluation procedure, any one of five readily-observable conditions makes a building unsafe to occupy, including various stages of collapse, significant residual drift, other structural, damage, falling hazards, and ground failure. ATC-20 offers simplicity, speed, and broad applicability; as a consequence it is used by most California cities and other jurisdictions.

FEMA 356 (ASCE 2000) represents the state of the practice in performance-based earthquake engineering for existing buildings. It offers analytical methods to estimate the future seismic performance of individual buildings subjected to various levels of shaking intensity. Several discrete levels of structural and nonstructural performance are defined, most notably four target levels: collapse prevention, life safety, immediate occupancy, and operational. Each target level is described in terms of detailed physical damage to a variety of structural and nonstructural systems and components. These descriptions are qualitative rather than quantitative, and are not suggested as tests for post-earthquake decision-making,

e.g., determining whether a building should be re-occupied after an earthquake. Nonetheless, they suggest a useful starting point for describing and estimating the post-earthquake usability of a building, given the detailed physical damage to structural and nonstructural systems.

3 METHODOLOGY

3.1 METHOLOGY OVERVIEW

The methodology employed in this project is illustrated in Figure 3-1. Closely related to Figure 1-1, it begins by defining the instrumented building in terms of structural and architectural design. One creates a stochastic structural model, i.e., a model in which one or more structural parameters (mass, damping, or force-deformation behavior) are uncertain and are reflected by a probability distribution whose parameters are known. One creates N realizations of the structural model by random sampling from these probability distributions. When an earthquake occurs, sensors record accelerations at the base and at one or more locations elsewhere in the building. For each realization of the structural model, a nonlinear time-history structural analysis is performed. The sample engineering demand parameter vector (*EDP*) from each structural analysis is recorded, along with the calculated motions at each accelerometer channel. Through a Bayesian-updating process described later, one compares the observed and calculated accelerations and calculates a weighting factor w to apply to each simulation; w depends on how closely the simulation matched the observed acceleration time histories. For each sample *EDP* vector, and each damageable assembly in the building, one uses assembly fragility functions to simulate physical damage to every assembly, producing N samples of the vector of damage measures, *DM*.

For each sample *DM* vector, one uses a loss model to simulate each decision variable, denoted by *DV*. In the case of repair cost, one uses unit-cost distributions to simulate the unit cost to restore each type of damageable assembly from each damage state, multiplies by the number of such damaged assemblies, and adds a factor to account for uncertain contractor overhead and profit. In the case of the life-safety *DV*, one compares the vector *DM* with a set of quantitative rules that define whether a facility is life safe, in terms of number and severity of damage to structural elements. In the case of the post-earthquake operability *DV*, one compares the vector *DM* with a set of quantitative rules that define whether a facility is operational, in terms of number and severity of damage to structural, architectural, mechanical, electrical, and plumbing components.

At the end of the analysis, the result is a set of N pairs (w_i, DV_i), where w_i is the weight assigned to simulation i and DV_i is the vector of *DV* calculated for simulation i. The distribution of a *DV* is then given by

$$F_{DV}(dv) = P[DV \le dv] = \sum_{i=0}^{N-1} w_i H(dv - DV_i) \tag{3-1}$$

where the Heaviside function $H(x) = 1$ if $x \ge 0$; and $= 0$ otherwise.

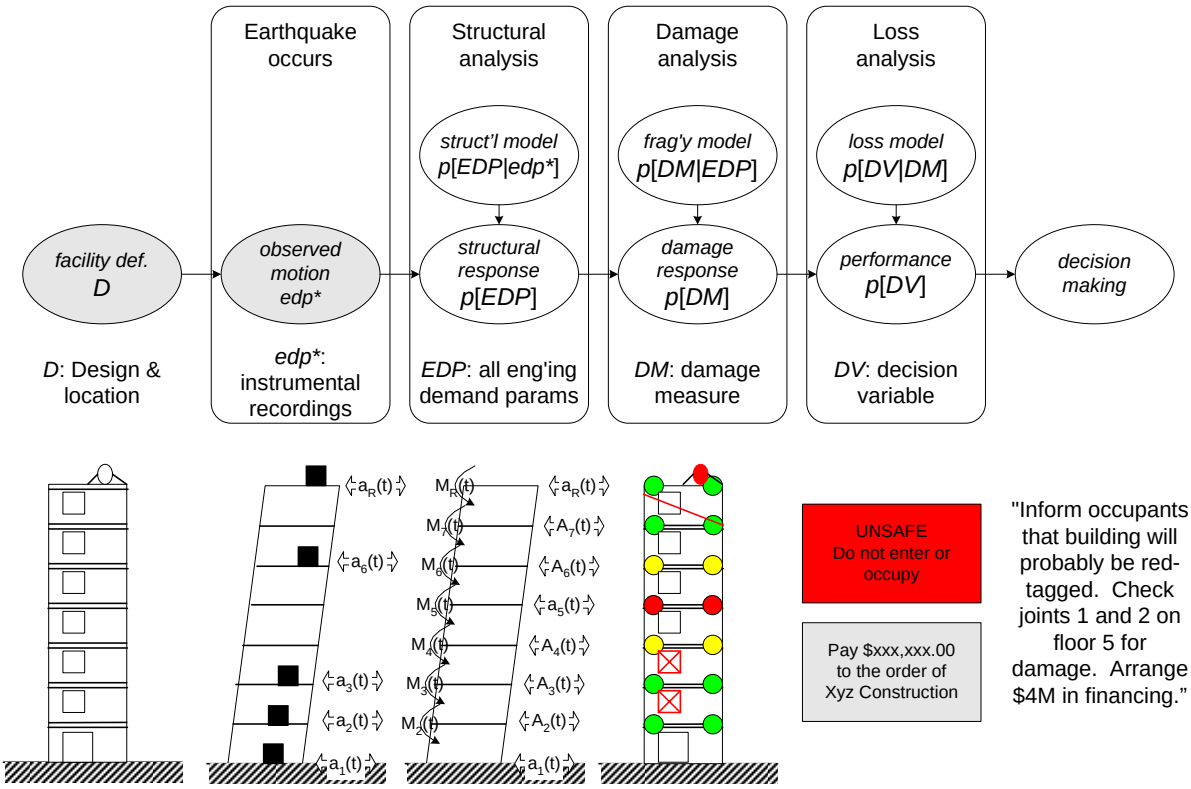

Figure 3-1. Overview of RTLE methodology employed here

3.2 DEFINE THE FACILITY

3.2.1 Data required

The following data are required to define a facility for real-time loss estimation: geotechnical reports; structural drawings; architectural drawings; if possible, mechanical, electrical, and plumbing (MEP) drawings; approximate number of occupants during the day (e.g., 2 PM) and during the night (e.g., 2 AM). These materials are used for three purposes:

(1) To define important summary characteristics of the facility. These characteristics are listed in Table 3-1.

(2) To list the inventory of the facility's damageable assemblies. For the damage and loss analyses, the facility is modeled as comprising a number of damageable assemblies. An assembly is a collection of one or more basic building components, assembled and in place, and defined according to a standard taxonomic system that is based here on the assembly-numbering system of RS Means (1997), extended to account for details of seismic resistance. The inventory is defined using the parameters shown in Table 3-2.

(3) To create a structural model for nonlinear time-history structural analysis.

Table 3-1. Building summary data

Parameter	Comments
Latitude	Decimal degrees N, positive in the U.S.
Longitude	Decimal degrees E, negative in the U.S.
Small-amplitude 1st-mode period	Sec, estimated
Mean damping ratio	Fraction, not percent
Replacement cost	Cost to the owner to rebuild the facility anew at this location, in the year during which the analysis takes place.
Daytime occupancy	Typical number of occupants during the day (e.g., 2 PM)
Nighttime occupancy	Typical number of occupants during the night (e.g., 2 AM)

Table 3-2. Inventory of damageable facility assemblies

Parameter	Meaning
Assembly type	Type of assembly defined according to a standard taxonomic system that determines the assembly's fragility functions and repair costs.
EDP name	Engineering demand parameter to apply to the assembly. An *EDP* is a measure of structural response, such as a member force or deformation to which assembly damage is primarily sensitive. Examples: PADI*m* = modified Park-Ang damage index in (structural) assembly *m* (a reinforced concrete beam-column) = $(\phi-\phi_y)/(\phi_u-\phi_y)$, where ϕ_y = yield curvature ϕ_u = ultimate curvature ϕ = maximum curvature VR*m* = shear force in assembly *m* (a structural element), normalized by nominal ultimate shear capacity V_u for $M = P = 0$, where M denotes bending moment and P denotes axial load in the structural element. PTD*na* = peak transient drift ratio floor *n* along column line *a* PDA*n* = peak diaphragm acceleration, floor *n*, max horiz. dir.
LOS	Line of sight identifier, e.g., the room number that would have to be repainted if the assembly were damaged.
Quantity	Quantity of assemblies of this assembly type, subjected to this *EDP*, in this line of sight.

3.2.2 Monte Carlo and Latin Hypercube simulation

After compiling facility-summary and inventory data, one creates N realizations (simulations) of the structural model, that is, N deterministic models where all parameters are known, and where the samples reflect the joint probability distribution of the uncertain structural characteristics.

One of the simplest ways to simulate the structural model is through Monte Carlo simulation (MCS). In MCS, each variable, denoted generically here by X, has an associated

cumulative distribution function (CDF), denoted by $F_x(x)$, which gives the probability that X will take on a value less than or equal to a particular value x. One can create a sample of X by generating a sample u of a random number uniformly distributed between 0 and 1. The sample of X is then given by

$$x = F_X^{-1}(u) \text{ where } u \sim U(0,1) \tag{3-2}$$

To enhance the efficiency of the analysis, one can take steps to ensure that samples cover the entire support of X, i.e., the tails as well as the body of the distribution. We use Latin Hypercube simulation (LHS), in which we replace u in Equation 3-2 by

$$u = \frac{u_1 + u_2}{N} \tag{3-3}$$

where N is the number of samples desired, u_1 is sampled from $\{0, 1, \ldots N\text{-}1\}$ with equal probability and without replacement, and $u_2 \sim U(0,1)$. (When some of the different components of the uncertain parameters X are correlated, the simulation is more complex. Here, components of X are treated as independent, so the problem of correlated samples is ignored here.) It is sometimes convenient to simulate uncertain X as:

$$X = E[X] \cdot \varepsilon_X \tag{3-4}$$

where $E[X]$ is the expected value of the uncertain parameter X, ε_X is an uncertain parameter with unit mean and standard deviation equal to the coefficient of variation of X, denoted here generically by δ_X.

More generally, X can be a vector of uncertain parameters with a vector coefficient of variation δ_X, $E[X]$ its expected value, and ε_X a vector of uncertain parameters, with unit mean and coefficient of variation equal to δ_X.

In the present study, the uncertain parameters X include structural parameters, assembly damage-resistance parameters, assembly unit-repair-cost parameters, contractor overhead and profit factor, and parameters that define the quantity of damage to building subsystems that would cause the building to fail overall performance levels (e.g., occupiable, life safe, etc.); we refer to these as subsystem-performance parameters. These sets of parameters are discussed next.

3.2.3 Uncertain structural parameters

Five (scalar) parameters of the structural model are treated as uncertain: damping (denoted here by β), structural-component initial stiffnesses (denoted by K_0), post-yield stiffnesses (denoted by K_1), soil spring stiffnesses (denoted by K_S), and structural strengths (denoted generically by F). In Beck et al. (2002), we also included uncertainty in mass, but subsequently found (Porter et al. 2002b) that uncertainty in mass has minimal impact on uncertainty in repair-cost performance. It is therefore necessary to simulate the vector

$$\varepsilon_{Xs} = \left[\varepsilon_\beta, \varepsilon_{K0}, \varepsilon_{K1}, \varepsilon_{KS}, \varepsilon_F \right]^T \tag{3-5}$$

We examined the sensitivity of member stiffness to uncertainties in the material properties of the concrete and reinforcing steel, and the dimensions of the member, for reinforced concrete flexural members in the subject building, and found that the coefficient of variation of initial stiffness was on the order of a few percent. We have conservatively taken the COV of pre- and post-yield stiffness, $\delta_{K0} = \delta_{K1} = 0.05$. As in Beck (2002), we estimate uncertainty in viscous damping as $\delta_\beta = 0.4$, and uncertainty in strength as $\delta_F = 0.11$. Jones et al. (2002) review experimental data by others, and report that the COV of soil shear modulus reduction ratio, G/G_{max}, varies with shearing strain, γ; with values as low as 0.15 at γ = 0.0001%, to nearly 1.0 at γ = 1%. We use the value at γ = 0.03%, $G/G_{max} = 0.35$, as a conservative estimate of δ_{Ks}. Table 3-3 summarizes the foregoing.

Table 3-3. Coefficients of variation of structural model uncertainties

Parameter	δ_{Xs}
Initial structural stiffness, K_0	0.05
Post-yield structural stiffness, K_1	0.05
Foundation stiffness, K_S	0.35
Damping, β	0.40
Structural strength, F	0.11

We take each of these parameters as lognormally distributed. Thus, in a given simulation i: i = 0, 1, … N-1, we simulate ε_X as

$$\varepsilon_{X,i} = \exp\left(\Phi^{-1}(u)\beta + \ln\hat{\varepsilon}\right) \tag{3-6}$$

where u is given by Equation 3-3, β denotes the logarithmic standard deviation of the model parameter and $\hat{\varepsilon}$ denotes the median value of ε, and are given by

$$\hat{\varepsilon} = 1/\sqrt{1+\delta^2} \tag{3-7}$$

$$\beta = \sqrt{\ln\left(1+\delta^2\right)} \tag{3-8}$$

Throughout, the values of u_1 and u_2 in Equation 3-3 are sampled independently for each simulation of each uncertain variable.

3.3 ESTIMATE ENGINEERING DEMANDS (STRUCTURAL ANALYSIS)

A particle filter is used to estimate *EDP*. It is needed for the following reason. When strong motion occurs, sensors at the base and one or more upper stories record acceleration time histories, $a_i(t)$, where i indexes the available channels. One can extract from $a_i(t)$ some but not all of the complete vector of engineering demand parameters (*EDP*) that will be relevant to estimating damage; we denote the subset as *edp**. We have developed two approaches for estimating the complete *EDP* vector from the observed set *edp**, which we call the advanced particle-filter method and the simplified particle-filter method.

Advanced method. Appendix A details a newly developed particle filter that works as follows. One creates a large number of samples of the stochastic structural model, accounting for important uncertainties in mass, damping, force-deformation behavior, and other parameters. One inputs the observed ground motion to these models and predicts *edp** on a

timestep-to-timestep basis. At each timestep, one assesses the degree to which the modeled response at upper levels of the building matches the observed response. When the observed response differs substantially from modeled, one uses Bayesian updating to modify the modeled uncertainties. This detailed approach requires that one can perform a structural analysis that stops at each timestep and restarts with potentially different values of the uncertainties of the structural model. The Kajima team possesses its own structural analysis software and is capable of modifying the software to do this. The CUREE team does not possess such software, and thus employs a second, simpler approach.

Simplified method. In the simpler approach, one creates a large number of equiprobable samples of the stochastic structural model, accounting for important uncertainties in mass, damping, and force-deformation behavior. For each sample of the structural model, one performs a complete nonlinear time-history structural analysis, using the observed base excitation as the ground-motion input. One extracts from the calculated structural response the complete *EDP* vector for each sample, as well as the estimated and observed peak displacements at the location of each sensor above the base. One then uses Bayesian updating to calculate the posterior probability (or weight) of each model based on observed absolute displacements, resamples from these N new equiprobable models based on calculated posterior probabilities, and continues the damage and loss estimate as usual. The algorithm is as follows.

1. Get observed base excitation, denoted by u_k, and observed response (relative displacement) at instrument channel locations, denoted by o. Let o_{jk} denote observed relative displacement at channel j, time step k. Let o_j denote the peak relative displacement at channel j (max over k).

2. Generate N structural realizations ("models") m_i: i=0, 1, N-1, i.e., where i indexes structural model simulation number, and where each realization has equal (prior) probability $P[m_i] = 1/N$.

3. Perform structural analyses using base excitation $u(t)$ and produce estimates of relative displacement at instrument locations $\hat{o}_{ijk}$, where i indexes structural model realization, j indexes instrument channel and k indexes time step.

4. Extract time-max $\hat{o}_{ij} = \max_k[\hat{o}_{ijk}]$.

5. Assume modeling error of estimated observation $\hat{o}_j$ has a constant logarithmic standard deviation denoted by β_j. That is, given a deterministic model of the structure and ground motion, we define error ε as

   $\varepsilon_j = (\ln \hat{o}_j - \ln o_j)$

   and assume ε_j is normally distributed with mean $E[\varepsilon_j] = 0$ and standard deviation $\beta_j = (\mathrm{Var}[\varepsilon])^{1/2} = 0.15$, for all j.

6. Update weights of each model m_i:

$$w_i = P[m_i \mid o] = \frac{p[o \mid m_i] P[m_i]}{\sum_{i=0}^{N-1} p[o \mid m_i] P[m_i]} \tag{3-9}$$

where
$P[m_i|o]$ = posterior probability of model i conditioned on o
$P[m_i]$ = prior probability of model m_i
$= 1/N$
$p[o|m_i]$ = likelihood of observation o
$= \Pi_j[\phi(z_{ij})]$
ϕ = Gaussian probability density function
$z_{ij} = \ln(o_j/\hat{o}_{ij})/\beta_j$

7. Calculate damage and loss for each model i as usual (as described below), but calculate the probability distribution of damage and loss considering that the probability of each sample is $P[m_i|o]$, per Equation 3-9.

3.4 ESTIMATE ASSEMBLY DAMAGE (DAMAGE ANALYSIS)

In the damage analysis, one calculates damage to each damageable assembly via assembly fragility functions. It is assumed that after an assembly is subjected to a certain *EDP*, it will be in an uncertain damage state *DM*, indexed by $dm = 0, 1, 2, \ldots N_{DM}$, where $dm = 0$ indicates the undamaged state. We assume that the damage states can be sorted in increasing order, either because an assembly in damage state $dm = i + 1$ must have passed through damage state i already, or because the effort to restore an assembly from damage state $dm = i + 1$ necessarily restores it from damage state $dm = i$.

The threshold level of *EDP* causing an assembly to reach or exceed damage state *dm* is uncertain (we refer to it as the assembly's capacity or resistance to damage state *dm*), and is denoted by R_{dm}. The cumulative distribution function of capacity is denoted by $F_{R,dm}(x)$; it is the same as the probability that the assembly would reach or exceed damage state *dm* when subjected to $EDP = x$, and is often referred to as the fragility function for the damage state of that assembly. As is often done, we take these fragility functions as cumulative lognormal distribution functions, whose parameters are the median value of the distribution, denoted here by x_m, and logarithmic standard deviation, denoted here by β. Thus,

$$F_{R,dm}(x) = \Phi\left(\frac{\ln(x/x_m)}{\beta}\right) \tag{3-10}$$

where Φ denotes the standard Gaussian cumulative distribution function. Each assembly type and value of *dm* would have its own characteristic median and logarithmic standard deviation, determined by mechanical testing, analytical evaluation, or other means.

One cannot however simply simulate the resistance of each assembly independently for each value of *dm*, because it would be possible that an assembly's simulated resistance to damage state $dm+1$ would be less than simulated resistance to damage state *dm*. Instead, it is necessary to calculate the probability distribution of *DM* conditioned on the value of *EDP* to which the assembly is subjected, and then simulate damage by inverting the conditional cumulative distribution function at a random probability level u. That is, given the response

x to which an assembly is subjected, the cumulative probability distribution of the damage state is

$$\begin{aligned} F_{DM|EDP=x}(dm) &\equiv P[DM \le dm \mid EDP = x] \\ &= 1 - F_{R,dm+1}(x) \qquad 0 \le dm < N_{DM} \\ &= 1 \qquad dm = N_{DM} \end{aligned} \tag{3-11}$$

where $F_{DM|EDP=x}(dm)$ denotes the cumulative probability distribution of damage state DM evaluated at dm, given that $EDP = x$. One simulates the damage to each assembly by inverting Equation 3-11 at a random probability level u, given by Equation 3-3. The simulated damage state of each assembly is then recorded in the vector DM, whose elements are the value of damage measure of each assembly.

3.5 ESTIMATE POST-EARTHQUAKE PERFORMANCE

To measure the qualitative performance of a building after an earthquake, we use an enhanced version of the building performance levels that are in Vision 2000 (SEAOC 1996), FEMA 273 (1997), and FEMA 356 (ASCE 2000). Table 3-4 shows the structural performance levels of FEMA 356: collapse prevention, life safety, and immediate occupancy, denoted by S-5, S-3, and S-1, respectively. It also shows qualitative descriptions of structural damage associated with each performance level (descriptions such as "few," "distributed" and "many"); we refer to those here as damage descriptions, denoted by DD, and indexed by $dd = 1, 2, \ldots N_{DD}$, where N_{DD} denotes the number of qualitative damage descriptions. Table 3-5 shows the nonstructural performance levels and associated damage descriptions for nonstructural assemblies. The overall system performance level (indexed here by pl) is defined in terms of both structural and nonstructural performance levels, as shown in Table 3-6. Note that Table 3-4 refers to structural elements, and Table 3-5 to nonstructural components; we refer to these groups of assemblies generically as "subsystems," i.e., the primary concrete frame subsystem, the cladding subsystem, etc.

Table 3-4. Criteria for assigning structural performance level (ASCE 2000)

Table C1-3 Structural Performance Levels and Damage[1, 2, 3]—Vertical Elements

		Structural Performance Levels		
Elements	**Type**	**Collapse Prevention S-5**	**Life Safety S-3**	**Immediate Occupancy S-1**
Concrete Frames	Primary	Extensive cracking and hinge formation in ductile elements. Limited cracking and/or splice failure in some nonductile columns. Severe damage in short columns.	Extensive damage to beams. Spalling of cover and shear cracking (<1/8" width) for ductile columns. Minor spalling in nonductile columns. Joint cracks <1/8" wide.	Minor hairline cracking. Limited yielding possible at a few locations. No crushing (strains below 0.003).
	Secondary	Extensive spalling in columns (limited shortening) and beams. Severe joint damage. Some reinforcing buckled.	Extensive cracking and hinge formation in ductile elements. Limited cracking and/or splice failure in some nonductile columns. Severe damage in short columns.	Minor spalling in a few places in ductile columns and beams. Flexural cracking in beams and columns. Shear cracking in joints <1/16" width.

Table 3-5. Criteria for assigning nonstructural performance level (ASCE 2000)

Table C1-5 Nonstructural Performance Levels and Damage[1]—Architectural Components				
	Nonstructural Performance Levels			
Component	Hazards Reduced[2] N-D	Life Safety N-C	Immediate Occupancy N-B	Operational N-A
Cladding	Severe distortion in connections. Distributed cracking, bending, crushing, and spalling of cladding elements. Some fracturing of cladding, but panels do not fall in areas of public assembly.	Severe distortion in connections. Distributed cracking, bending, crushing, and spalling of cladding elements. Some fracturing of cladding, but panels do not fall.	Connections yield; minor cracks (<1/16" width) or bending in cladding.	Connections yield; minor cracks (<1/16" width) or bending in cladding.
Glazing	General shattered glass and distorted frames in unoccupied areas. Extensive cracked glass; little broken glass in occupied areas.	Extensive cracked glass; little broken glass.	Some cracked panes; none broken.	Some cracked panes; none broken.
Partitions	Distributed damage; some severe cracking, crushing, and racking in some areas.	Distributed damage; some severe cracking, crushing, and racking in some areas.	Cracking to about 1/16" width at openings. Minor crushing and cracking at corners.	Cracking to about 1/16" width at openings. Minor crushing and cracking at corners.
Ceilings	Extensive damage. Dropped suspended ceiling tiles. Moderate cracking in hard ceilings.	Extensive damage. Dropped suspended ceiling tiles. Moderate cracking in hard ceilings.	Minor damage. Some suspended ceiling tiles disrupted. A few panels dropped. Minor cracking in hard ceilings.	Generally negligible damage. Isolated suspended panel dislocations, or cracks in hard ceilings.

Table 3-6. System performance levels (after ASCE 2000)

pl	**Performance level**	**Max. structural perf. level**	**Max. nonstructural perf. level**
1	Operational	*S*-1	*N-A*
2	Immediate occupancy	*S*-1	*N-B*
3	Life safe	*S*-3	*N-C*
4	Collapse prevention	*S*-5	*N-D*

The authors of FEMA 356 (ASCE 2000) caution the reader not to use these damage descriptions as criteria for determining system performance, but rather to consider these descriptions as what one would be likely to observe if the design meets other criteria not shown in the table. They also caution that the lists of damages are incomplete; that is, the authors feel that the criteria list is not exhaustive because there may be other criteria needed to pin down the performance level, so if any of those listed are violated, that performance level is not satisfied, but if none are violated, then it may still not be satisfied. We note also that the listed structural elements or components are a superset of those that are considered here, so there is no question that the criteria list that we use is incomplete. For present purposes, however, we treat the criteria as a complete list because our primary purpose here is to illustrate an automated procedure for estimating post-earthquake performance level for a facility and we feel that improvements in the defining criteria for each performance level can be readily incorporated if they become available.

We estimate the post-earthquake performance level using an enhanced version of the methodology that we developed in Beck et al. (1999) for the CUREE-Kajima Phase III joint research project. In that work, the performance level is determined first by calculating the fraction of assemblies in each subsystem that are damaged (i.e., the number of assemblies in the subsystem with $dm \geq 1$, divided by the total number of assemblies in the subsystem). We refer to that ratio as the damage fraction (denoted by *DF*) for the subsystem. We then use the calculated *DF* for each relevant subsystem to determine the extent of the damage based on the descriptive terms used in FEMA 356. If the damage extent in a subsystem exceeds that allowed for a given performance level, then the building does not meet the requirements of that performance level.

The allowable damage fractions are based on the description of structural and nonstructural performance levels in Vision 2000 (SEAOC 1996) and FEMA 356 (ASCE 2000, Tables C1-3, C1-4, and C1-5, ignoring the drift levels that the authors judged to correspond to each of these damage levels), which are shown in Tables 3-4 and 3-5. The descriptions of the criteria for these performance levels contain many vague terms that need to be quantified in order to automate the procedure for estimating the post-earthquake performance of a building. For example, for nonductile concrete frame elements, FEMA 356 allows "*extensive* damage to beams; *minor* spalling in nonductile columns; ..." for the life-safety performance level while for the collapse-prevention performance level, it allows "*limited* cracking and/or splice failure in *some* nonductile columns; *severe* damage in short columns, …" where we have italicized the vague terms that need to be quantified.

In Beck et al. (1999), we assigned distinct ranges of *DF* to each *DD*. Here, we enhance the Beck et al. (1999) methodology by relating *DF* to *DD* using the theory of fuzzy sets to more appropriately quantify the vague descriptions in Tables 3-4 and 3-5. Our translation is shown in Table 3-7 and Figure 3-2. We note that the FEMA authors describe damage not in terms of repairs required (as we have done), but somewhat more qualitatively, e.g., "minor spalling." In Table 3-7, we have done our best to map our damage descriptions to theirs, and feel satisfied that the mapping is at least reasonable. We therefore offer our procedure as illustrative of what can be done.

Figure 3-2 illustrates how these translations lead to membership functions for each damage description. For example, if 20% of partitions are damaged in a given simulation, one enters Figure 3-2 with $DF = 20\%$, and observes that the degree of membership that the partition damage can be considered to be "distributed" is 50%, and a 50% degree of membership that one would consider that "many" partitions are damaged, i.e., $\varphi[DD = 3 \mid DF = 0.20] = \varphi\ [DD = 4 \mid DF = 0.20] = 0.5$. From fuzzy set theory, the membership function $\varphi[DD = dd \mid DF = x]$ is to be interpreted as a measure of the degree to which one feels that the damage description *dd* is appropriate for a subsystem if its damage factor $DF = x$. For notational convenience, let

$$\varphi_{dd}(x) = \varphi[DD = dd \mid DF = x] \tag{3-12}$$

and

$$\Phi_{dd}(x) = \varphi[DD \leq dd \mid DF = x] \tag{3-13}$$

which gives the degree to which one feels that the appropriate damage description for the subsystem is at most *dd* when the fraction of elements in the subsystem that are in a prescribed damage state is *x*. From fuzzy set theory,

$$\Phi_{dd}(x) = \max\{\varphi_{dd}(x), \varphi_{dd\text{-}1}(x), \ldots, \varphi_1(x)\} \tag{3-14}$$

Table 3-7. Translations of qualitative performance terminology

dd	Damage description	Damage fraction	Example
1	Negligible, few, little	0 – 5%	"Generally negligible [ceiling] damage:" between 0 and 5% of ceiling area is damaged.
2	Some, minor, limited	1 – 10%	"Some cracked [glazing] panes; none broken:" Between 1% and 10% of lites visibly cracked; no glass fallout.
3	Distributed	5 – 30%	"Distributed [partition] damage:" between 5% and 30% of partitions need patching, painting or repair, measured by lineal feet.
4	Many, extensive	10 – 60%	"Many fractures at [steel moment frame] connections:" between 10% and 60% of connections suffer rejectable damage.
5	Most	50 – 100%	"Most [HVAC equipment] units do not operate:" at least 50% of HVAC components inoperative.

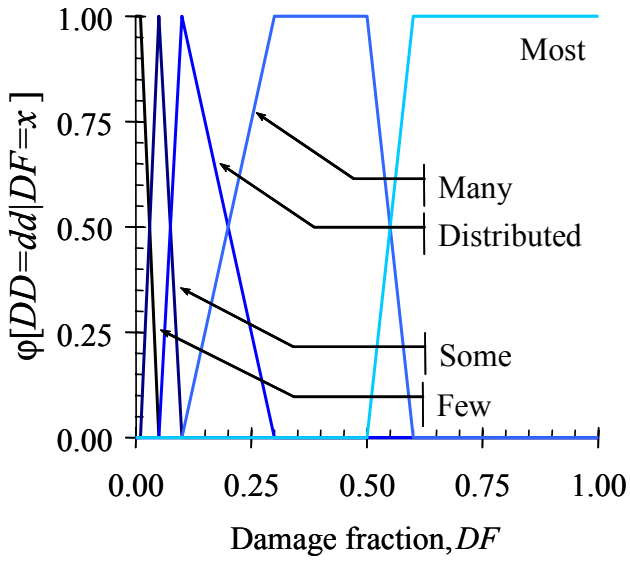

Figure 3-2. Membership functions relating qualitative damage descriptions to damage fraction

As noted previously, we accept the list of criteria for each performance level in Tables 3-4 and 3-5 as complete. Therefore, if all the listed criteria for performance level *pl* are satisfied, then the structure is considered to have satisfied that performance level. Since the

fuzzy set corresponding to the performance level is the intersection of the fuzzy sets corresponding to each criterion that must be satisfied, we take the minimum of the membership values for each criterion.

To briefly illustrate the procedure, during the i^{th} simulation in the ABV method, we determine the degree $\varphi[pl = j \mid \text{simulation } = i\,]$ to which performance level $pl = j$ (j = 1, …, 4) is satisfied for a facility. For example, for immediately occupiable (pl = 2) after the earthquake, we calculate DF for each subsystem involved in the criteria list under *S*-1 and *N*-*B* in Table 3-4 and Table 3-5, respectively, then we evaluate the membership function $\Phi_{dd}(x)$ in Equation (3-14) for the subsystem; finally, we take the minimum value over all relevant subsystems appearing in the criteria for performance level pl = 2. This process is repeated for each performance level in Table 3-6 to get the degree $\varphi[pl = j \mid \text{simulation } = i\,]$ for each j = 1, …, 4.

After all N simulations have been performed, the probability that the facility satisfies performance level $pl = j$ is estimated by the appropriate weighted average of $\varphi[pl = j \mid \text{simulation } = i\,]$ based on the usual Monte Carlo method:

$$P[pl = j] = \sum_{i=0}^{N} w_i \varphi\left[pl = j \mid \text{simulation } = i\right] \tag{3-15}$$

where w_i is given by Equation (3-9). These four probabilities provide a vector decision variable DV_{PL} for the owner and occupants of the building.

Although we have given what we believe is a complete theory for treating the vagueness in the performance level descriptions of FEMA 356, it turns out that in the application presented later, the procedure developed here is not fully exercised; this is because one criterion dominates, namely, in every simulation, there is at least one beam or column in the severe or collapse damage state which we judge to be more in the spirit of the criteria listed for collapse prevention rather than life-safety in Table 3-4. Therefore, regardless of the damage states of all other assemblies, the building does not achieve the life-safety performance level.

3.6 ESTIMATE REPAIR COST (LOSS ANALYSIS)

Each assembly type and damage state is associated with one or more possible repair measures, each with an uncertain repair cost. Let $C_{j,dm}$ denote the uncertain cost to restore an assembly of type j from damage state dm; it can be calculated by standard cost-estimation principles. Let $F_{C,j,dm}(c)$ denote its cumulative distribution function evaluated at c. We take these as lognormally distributed with median values x_m and logarithmic standard deviations β specified for each assembly type and damage state. To simulate $C_{j,dm}$ then, we evaluate

$$C_{j,dm} = \exp\left(\Phi^{-1}\left(u\right)\beta + \ln x_m\right) \tag{3-16}$$

where u is given by Equation 3-3.

Let C_{OP} denote the cost of contractor overhead and profit, as a fraction of the total cost to the contractor to repair damaged assemblies (to which we refer as direct costs). C_{OP} is typically on the order of 15% to 20%. One could simulate C_{OP} as

$$C_{OP} = 0.15 + 0.05 \cdot u \tag{3-17}$$

where u is given by Equation 3-3.

Let RC denote the uncertain repair cost. Let $N_{j,dm}$ denote the number of assemblies of type j in damage state dm. It is calculated by counting the damaged assemblies recorded in the vector DM. Let $C_{j,dm}$ denote the uncertain cost to restore an assembly of type j from damage state dm; it can be calculated by standard cost-estimation principles. We calculate the total repair cost as

$$RC = \left(1 + C_{OP}\right) \sum_{j=1}^{N_j} \sum_{dm=1}^{N_{DM}} N_{j,dm} C_{j,dm} \tag{3-18}$$

Let $F_{C,j,dm}(c)$ denote the cumulative distribution function of $C_{j,dm}$ evaluated at c. Then, for the i^{th} simulation, one draws a sample of $C_{j,dm}$ by inverting $F_{C,j,dm}(c)$ at u, where an independent sample u is calculated using Equation 3-3, then adds up the number of assemblies of each type in each damage state $N_{j,dm}$ from the vector DM, and applies Equation (3-18) to calculate the repair cost RC_i for the simulation.

The cumulative distribution function for the total repair cost $DV_\$$ is calculated from the N simulations of the ABV method by:

$$F_{DV\$}\left(dv\right) = P[DV_\$ \le dv] = \sum_{i=0}^{N} w_i H(dv - RC_i) \tag{3-19}$$

where the Heaviside function $H(x) = 1$ if $x \ge 0$; and $= 0$ otherwise; and w_i is given by Equation (3-9).

4 CUREE SAMPLE APPLICATION

4.1 FACILITY DEFINITION

The CUREE sample facility is the same as that employed in Beck et al. (2002) for the CUREE-Kajima Joint Research Project Phase IV. In summary, the building is a real, 7-story, 66,000 sf (6,200 m^2) hotel located in Van Nuys, CA, at 34.221°N, 118.471°W, in the San Fernando Valley of Los Angeles County. The location is shown in Figure 4-1. It was built in 1966 according to the 1964 Los Angeles City Building Code. The lateral force-resisting system is a perimeter nonductile reinforced-concrete moment frame in both directions. The building was lightly damaged by the M6.6 1971 San Fernando event, approximately 20 km to the northeast, and severely damaged by the M6.7 1994 Northridge Earthquake, whose epicenter was approximately 4.5 km to the southwest. The building has been studied extensively, e.g., Jennings (1971), Scholl et al. (1982), Islam (1996a, 1996b), Islam et al. (1998), and Li and Jirsa (1998). Also, Trifunac et al. (1999) and Browning et al. (2000) provide a detailed account of the physical damage to the structure in the 1994 Northridge earthquake.

In plan, the building is 63 ft by 150 ft, 3 bays by 8 bays, 7 stories tall. The long direction is oriented east-west. The building is approximately 65 ft tall: the first story is 13 ft, 6 in; stories 2 through 6 are 8 ft, 6-½ in; the 7th story is 8 ft. The ground floor, as it existed prior to the 1994 Northridge earthquake, contained a lobby, dining room, tavern, banquet room, and various hotel support services (Figure 4-2). Upper floors are arranged with 22 hotel suites accessed via a central corridor running along the longitudinal axis of the building (Figure 4-3 and Figure 4-4). The hotel is staffed by at most 35 people. Typical staffing is 20 to 22 people during normal business hours, three at night. The average occupancy rate in its 132 suites is 0.70, and the average number of people per occupied room is 1.5. This implies a typical daytime occupancy of 20 to 30, a typical nighttime occupancy of 140 (132 * 0.70 * 1.5 + 3), and a peak occupancy (at night) of 200 (132 * 1.0 * 1.5 + 3). We estimate the replacement cost of the facility to be approximately $7.0M, based on square footage and using RS Means Co., Inc. (2001).

Figure 4-1. Location of the demonstration building: "+" symbol above the "405" shield

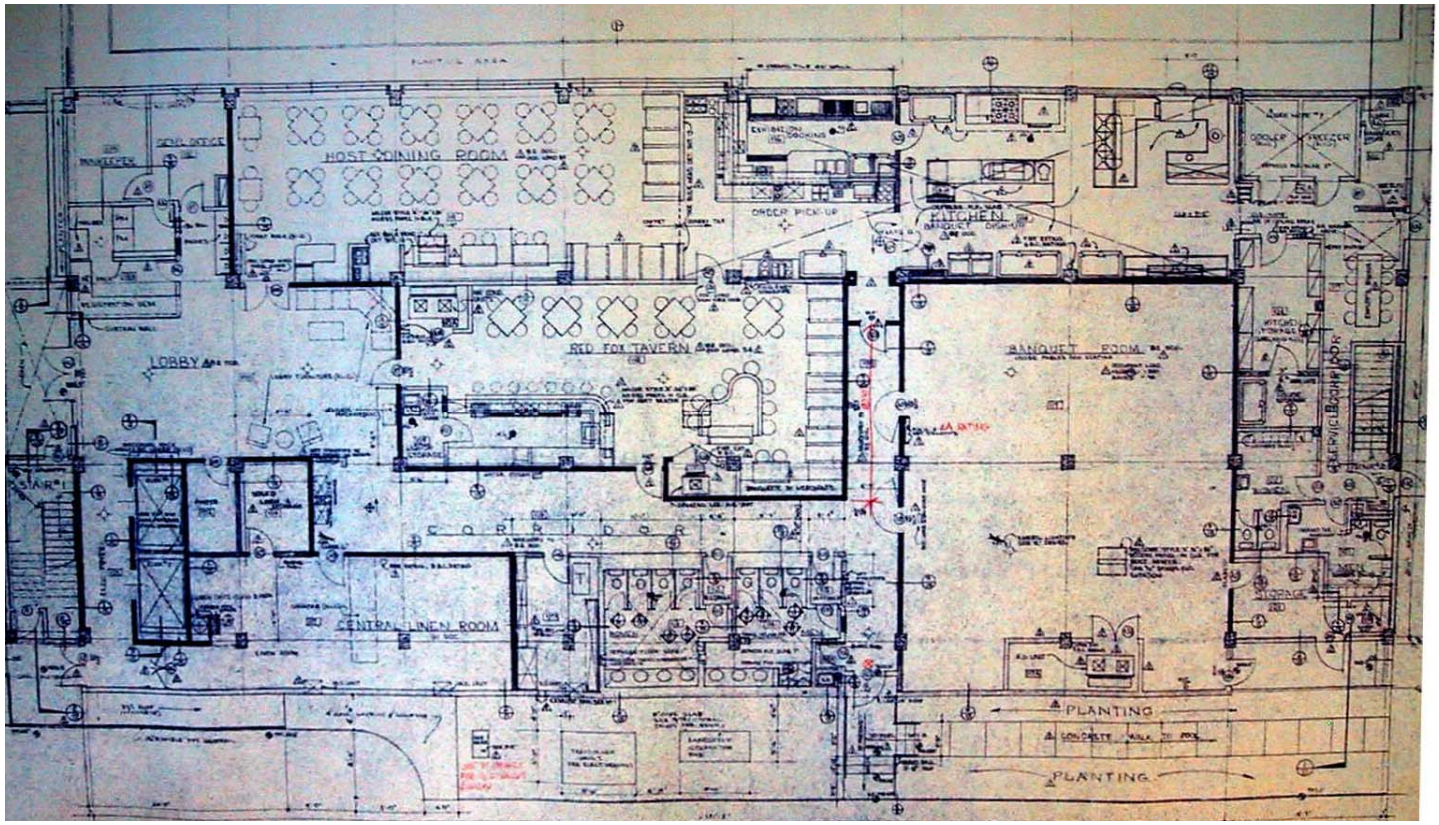

Figure 4-2. First floor architectural plan (Rissman and Rissman Associates, 1965)

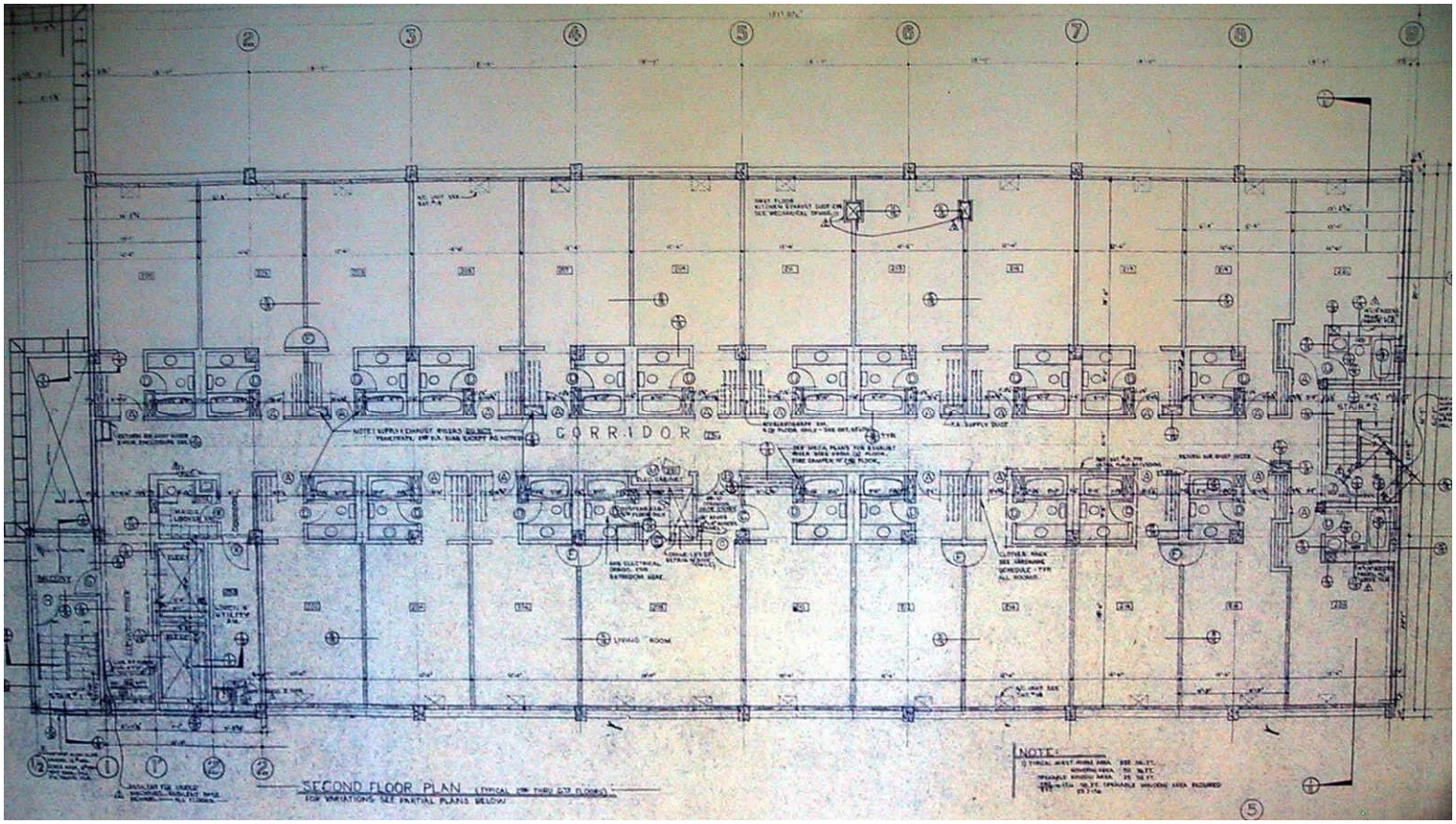

Figure 4-3. Second floor architectural plan (Rissman and Rissman Associates, 1965)

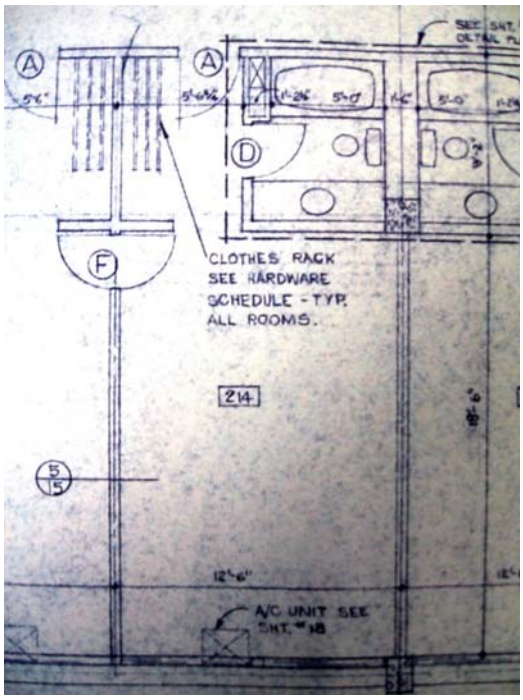

Figure 4-4. Typical hotel suite floor plan (Rissman and Rissman Associates, 1965)

The structural system is a cast-in-place reinforced-concrete moment-frame building with nonductile column detailing. Perimeter moment frames provide the primary lateral force resistance, although the interior columns and slabs also contribute to lateral stiffness. The gravity system comprises 2-way reinforced-concrete flat slabs supported by square columns at the interior and the rectangular columns of the perimeter frame. Slabs are 10-in deep at the 2nd floor, 8½ in at the 3rd through 7th floors, and 8 in at the roof. The roof also has lightweight concrete topping varying in thickness between 3-1/4 in and 8 in. The column plan (with the designer's column numbers) is shown Figure 4-5. As shown in the figure, the building is founded on 24-in diameter drilled piers in groups of two, three, and four piers per pilecap. Pier lengths vary between 31.5 ft and 37 ft.

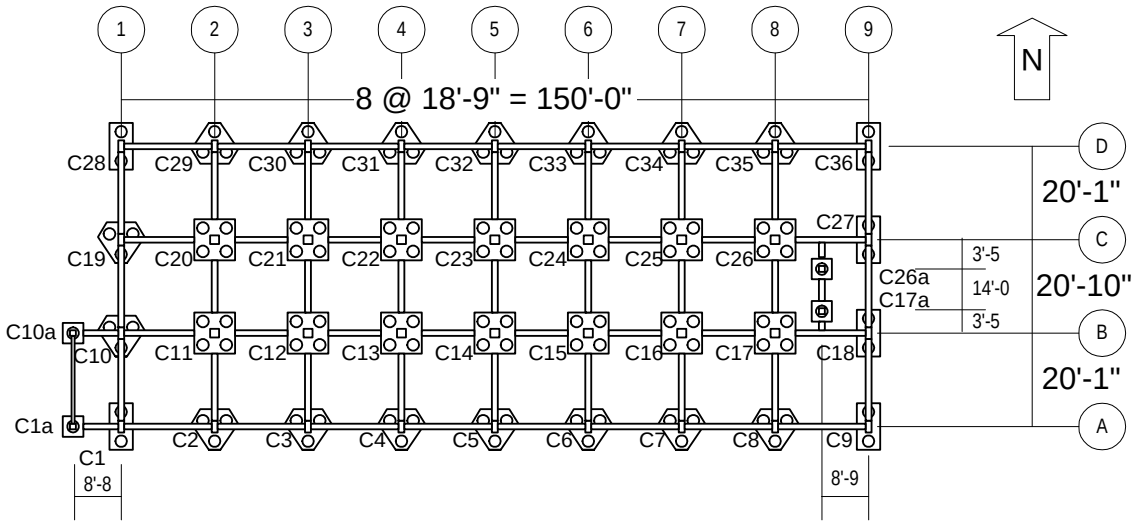

Figure 4-5. Foundation and column plan, showing designer's notation for column numbers

Frames are regular in elevation; the south frame elevation is shown in Figure 4-6. Floor and roof beams and spandrel marks are shown in Figure 4-7. These figures show the designer's notation for beam and column numbering. Floor slabs are flat plates, 10-in thick at the 2nd floor, 8½-in at the 3rd through 7th floors, and 8 in at the roof. The roof also has lightweight concrete topping of varying thickness (3-1/4 in to 8 in). Perimeter columns are 14 in by 20 in, oriented to bend in their strong direction about the east-west axis. Interior columns are 18 in square. Spandrel beams are generally 16 in wide by 30 in deep at the 2nd floor, 16 in wide by 22-½ in deep at the 3rd to 7th floors, and 16 in wide by 22 in deep at the roof. The tops of the spandrel beams are flush with the top of the floor slab.

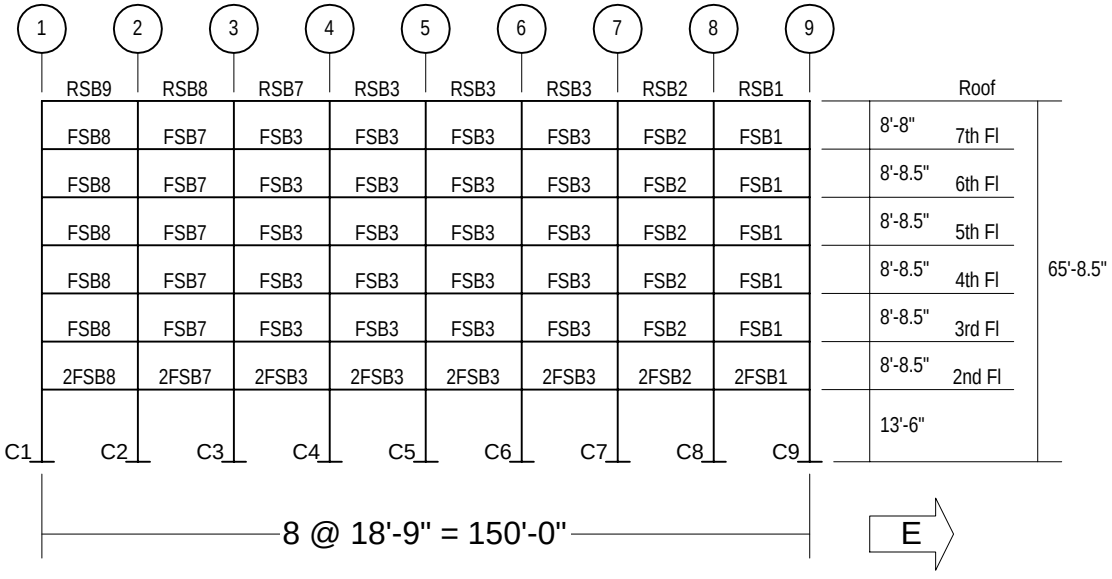

Figure 4-6. South frame elevation, omitting stair tower at west end

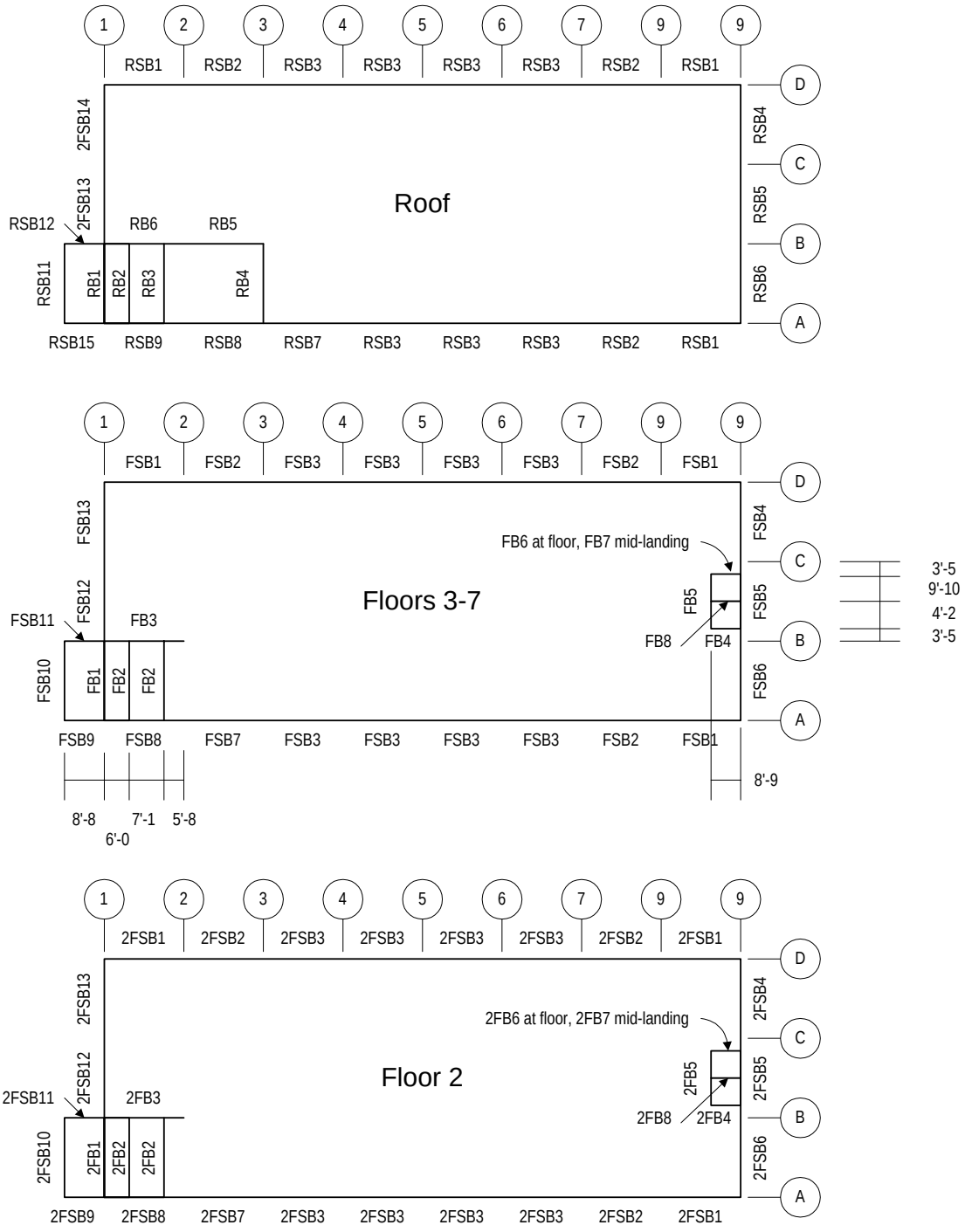

Figure 4-7. Floor beam and floor spandrel beam plans

Column concrete has nominal strength of f'_c = 5 ksi for the first story, 4 ksi for the second story, and 3 ksi from the third to the seventh story. Beam and slab concrete is nominally f'_c = 4 ksi at the second floor and 3 ksi from the third floor to the roof. Table 4-1 provides the column reinforcement schedule. The reinforcement of floor spandrel beams for floors 3 through 7 is shown in Table 4-2. Reinforcement of floor spandrel beams for the 2nd floor and roof is shown in Table 4-3. Column reinforcement steel is A432-62T (Grade 60) for billet bars. Beam and slab reinforcement is ASTM A15-62T and A305-56T (Grade 40) for

intermediate grade, deformed billet bars. Column reinforcement is arranged as shown in Figure 4-8.

Table 4-1. Column reinforcement schedule

		Column mark							
		C13 to C17, C21 to C26	C11, C12, C20	C30 to C34	C10, C18, C19, C27	C2, C3, C8, C29, C35	C1, C9, C28, C36	C1A, C10A	C17A, C26A
Level	Col size	18"x18"	18"x18"	14"x20"	14"x20"	14"x20"	14"x20"	10"x12"	10"x12"
7th floor	Vert. bars	6-#7	6-#7	6-#7	6-#7	6-#7	6-#7	4-#5	
	Ties	#2@12"	#2@12"	#2@12"	#2@12"	#2@12"	#2@12"	#2@10"	
6th floor	Vert. bars	6-#7	6-#7	6-#7	6-#7	6-#7	6-#7	4-#5	4-#5
	Ties	#2@12"	#2@12"	#2@12"	#2@12"	#2@12"	#2@12"	#2@10"	#2@10"
5th floor	Vert. bars	6-#7	6-#8	6-#7	6-#7	6-#7	6-#7	4-#5	4-#5
	Ties	#2@12"	#3@12"	#2@12"	#2@12"	#2@12"	#2@12"	#2@10"	#2@10"
4th floor	Vert. bars	6-#8	8-#9	6-#7	6-#9	6-#7	6-#7	4-#5	4-#5
	Ties	#3@12"	#3@12"	#2@12"	#3@12"	#2@12"	#2@12"	#2@10"	#2@10"
3rd floor	Vert. bars	8-#9	12-#9	6-#9	8-#9	8-#9	6-#7	4-#6	4-#5
	Ties	#3@12"	#3@12"	#3@12"	#3@12"	#3@12"	#2@12"	#2@10"	#2@10"
2nd floor	Vert. bars	10-#9	12-#9	6-#9	8-#9	8-#9	6-#7	4-#6	4-#5
	Ties	#3@12"	#3@12"	#3@12"	#3@12"	#3@12"	#2@12"	#2@10"	#2@10"
1st floor	Col size	20"x20"	20"x20"						
	Vert. bars	10-#9	12-#9	10-#9	12-#9	10-#9	8-#9	4-#8	4-#6
	Ties	#3@12"	#3@12"	#3@12"	#3@12"	#3@12"	#3@12"	#3@10"	#2@10"

Table 4-2. Spandrel beam reinforcement schedule, floors 3 through 7

Beam mark	Width	Height	Top bars					Bottom bars	#3 ties
			7F	6F	5F	4F	3F		
FSB1	16”	22-½”	①⑨ 2#7	2#9	2#9	3#8	3#8	2#7 (2#8 @ 3F, 4F)	①⑨ 3@5”, 5@6”, rest @10”, 3F- 5F
			②⑧ FSB2 top bars						②⑧ 6@4”, 5@6”, 3F-5F
FSB2	16”	22-½”	②⑧ 2#9	3#8	3#8	3#8	3#9	2#6	8@5”, 5@6” ea end
			③⑦ FSB3 top bars						Rest @ 10” 3F-5F
FSB3	16”	22-½”	2#8	2#9	3#8	3#8	3#9	2#6	3@5”, 5@6” ea end
									Rest @ 10” 3F-5F
FSB7	16”	22-½”	③ FSB3 top bars					2#7	3@5”, 5@6” ea end
			② FSB8 top bars						Rest @ 10” 3F-5F
FSB8	16”	22-½”	② 2#8	2#9	2#9	3#8	3#8	2#7 (2#8 @ 5F, 2#9 @ 3F, 4F)	① 3@5”, 5@6”, rest@10” 3F-5F
			① 2#7	2#8	2#9	2#9	3#8		② 6@4”, 5@6” 3F-5F

①, ②, etc.: column lines
3F, 4F, etc: floor levels

Table 4-3. Roof and second-floor spandrel beam reinforcement schedule

Beam mark	Width	Height	Top bars	Bottom bars	#3 ties
RSB1	16”	22”	①⑨ 2#6 ②⑧ 2#8	2#7	#3@10”
RSB2	16”	22”	②⑧ RSB1 top bars ③⑦ RSB3 top bars	2#6	Same
RSB3	16”	22”	2#8	2#6	Same
RSB7	16”	22”	④ RSB3 top bars ③ 2#9	2#6	Same
RSB8	16”	22”	③ 2#9 ② 3#9	2#9	Same
2FSB1	16”	30”	①⑨ 2#9 ②⑧ 2FSB2 top bars	2#8	4 @ 6”, 2 @ 8”, ea end, rest @ 13”
2FSB2	16”	30”	②⑧ 3#8 ③⑦ 2FSB3 top bars	2#6	Same
2FSB3	16”	30”	2#9	2#6	Same
2FSB7	16”	30”	③ 2FSB3 top bars ② 2FSB8 top bars	2#7	Same
2FSB8	16”	30”	② 2#9 ① 2#9	2#8	Same

Drilled piers are reinforced with 4-#6 longitudinal bars, #2 ties at 12-in centers, 3-in cover. Pilecaps are 10’-0” square by 38-in deep (4-pier pilecap), 4’-0” by 10’-0” by 38-in deep (2-pier pilecap), or 2’-6” square by 38-in deep (1-pier pilecap). Triangular pilecaps have edges 2’-0” from pier centers. All piers are spaced at 6’-0” centers. Pier tips are 34.5 to 40 ft below grade, and as shown in the structural drawings.

The ground floor has full-height masonry infill walls in the north frame between column lines 5 and 9, and partial-height masonry walls between column lines 1 and 5. Above the 2nd floor there are no other stiff elements between the columns that might produce a short-column effect. The building is clad on the north and south facades with aluminum window walls, comprising 3/16-in heavy sheet glass in sliding frames, and ¼-in cement asbestos board panels with an ornamental sight-obscuring mesh of baked enamel or colored vinyl. The east and west endwalls are finished on the inside with gypsum wallboard and on the outside with stucco.

Interior partitions are constructed of 5/8-in gypsum wallboard on 3-5/8 in metal studs at 16-in centers. Ceilings in the hotel suites in the 2nd through 7th stories are a textured coating

applied to the soffit of the concrete slab above. At the first floor, ceilings are suspended wallboard or acoustical ceiling tiles (2-ft grid). Upper-story hallway ceilings are suspended ceiling on 2-ft-by-4-ft tee-bar grid, just deep enough to accommodate fluorescent fixtures (approximately 2 in).

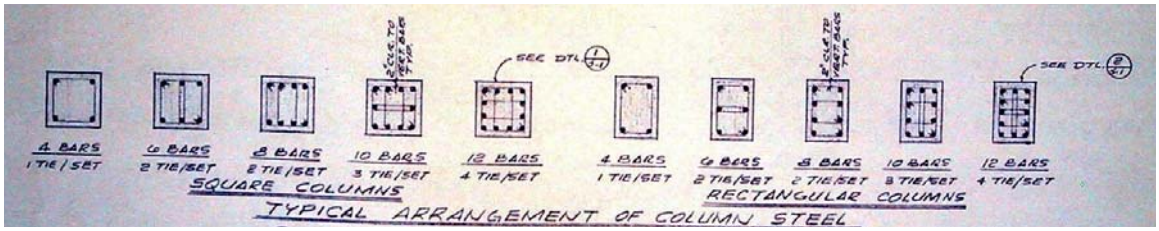

Figure 4-8. Arrangement of column steel (Rissman and Rissman Associates, 1965)

Mechanical, electrical, and plumbing plans are no longer available for this building, either from the City of Los Angeles or the original architect. Equipment conditions were observed in a walkthough in January, 2002. Through-wall air-conditioning units are mounted in the waist panels below the windows and provide ventilation to the suites. Central HVAC is provided only for hallway and ground-floor spaces. Building-service equipment include, on the ground floor: switchgear and transformers (unanchored, unbraced); anchored hot water heater and washing machines; and unanchored dryers and water softener, and on mechanical pads in the parking lot: an unanchored transformer and an anchored diesel backup generator. On the roof, there are two anchored elevator motors, an anchored upright 1000-gal water tank, an anchored cooling tower (for lobby air conditioning) on steel skids, a kitchen fan on possible unanchored 12-in pipe stilts, and two packaged air-condition units on two steel skids each supported by two welded 12-in pipe stilts that do not appear to be anchored to their base.

4.2 INSTRUMENTATION, HISTORIC SHAKING, AND DAMAGE

The building was strongly shaken by the M6.6 1971 San Fernando event, approximately 20 km to the northeast (Figure 4-9). Earth Sciences AR-240 strong-motion accelerometers were located at the southeast corner of the ground floor, middle of the 4th floor, and southwest corner of the roof (Figure 4-10). The instruments recorded peak accelerations at the ground floor of 240 cm/sec^2 in the transverse direction, 130 cm/sec^2 longitudinally, and 170 cm/sec^2 in the vertical direction. Peak roof accelerations were 384 cm/sec^2 transverse and 315 cm/sec^2 longitudinally at the southwest corner of the building (Trifunac *et al.*, 1999). The 5%-damped acceleration response spectra for the ground-floor instruments are shown in Figure 4-11 (calculated using Bispec, Hachem 2000).

Islam (1996) reports building periods of 0.70 sec in the early part of the 1971 earthquake, and 1.5 sec during peak response (Table 4-4). Hart and Vasdevan (1975) performed system identification analysis of the accelerometer records to estimate equivalent viscous damping ratios of 16.4% of critical in the longitudinal direction, 9.7% transverse. McVerry (1979) estimated 17.3% in the longitudinal direction, 19.2% transversely.

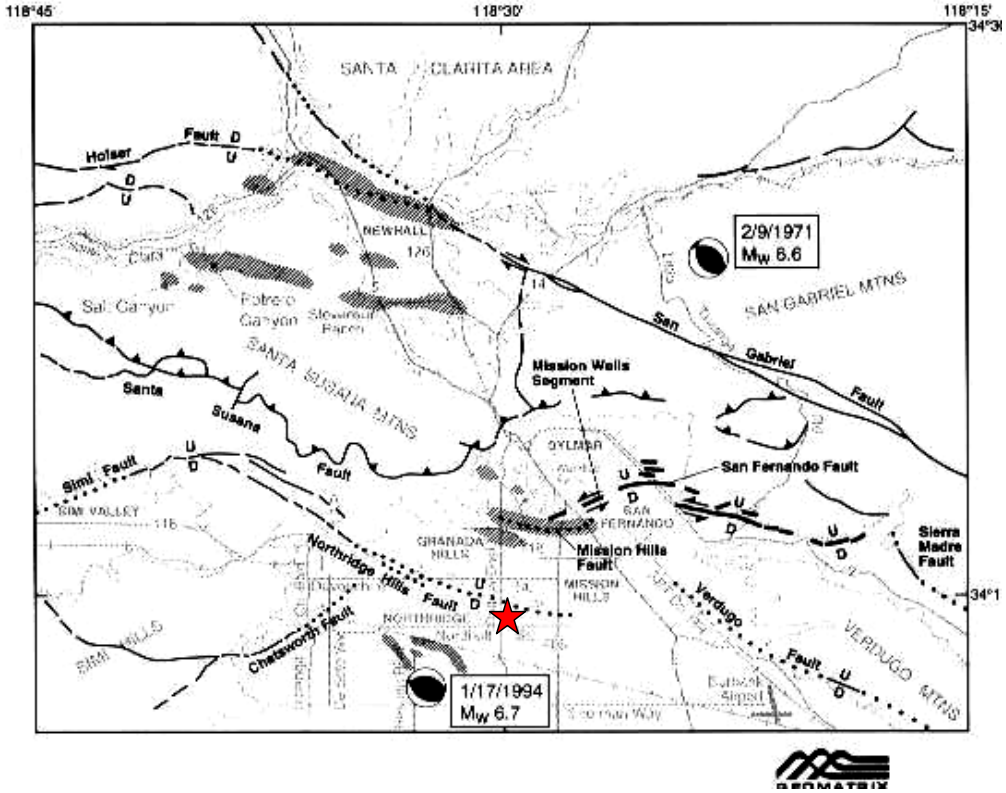

Figure 4-9. Testbed building (star) relative to 1971 and 1994 earthquakes (EERI 1996)

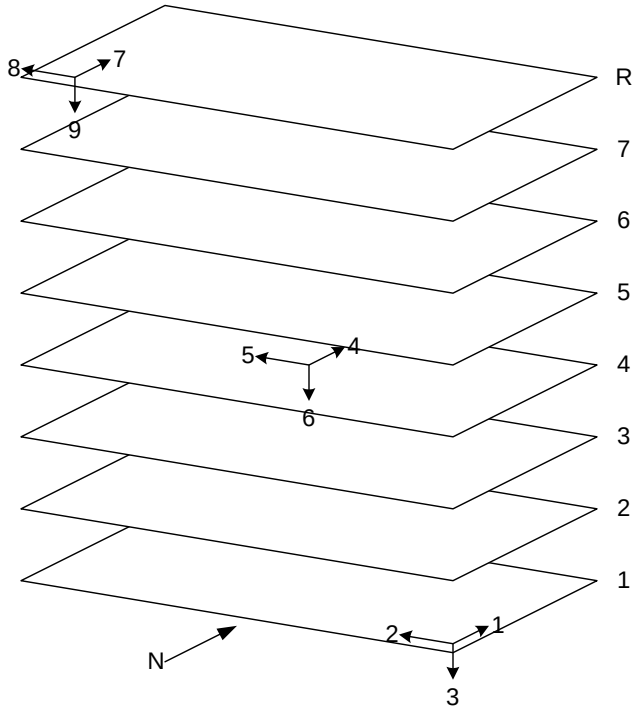

Figure 4-10. Instrument locations in 1971 San Fernando earthquake

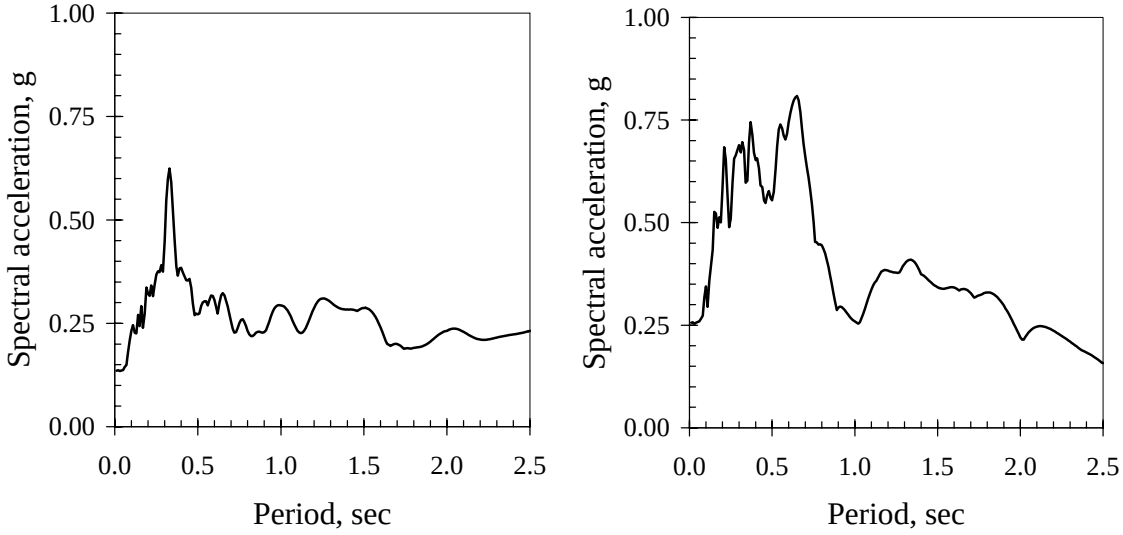

Figure 4-11. Spectral acceleration, 1971 ground-floor motions, longit. (left) and transverse (right)

Table 4-4. Approximate fundamental building periods (Islam, 1996)

	Longitudinal	**Transverse**	**Torsional**
Pre-1971 San Fernando, ambient vibration	0.52 sec	0.40 sec	
1971 San Fernando earthquake			
Early part of earthquake	0.70	0.70	
During peak response	1.5	1.6	
1994 Northridge earthquake			
Early part (0-10 sec)	1.5	2.2	1.4
Middle part (10-20 sec)	2.1	2.2	
Toward the end (>25 sec)	2.4	2.0	

The damage in 1971 mostly required architectural repairs. Jennings (1971) describes "extensive damage to the interior plaster walls, to the plumbing fixtures, etc., on the second, third, and fourth floors. The upper three floors were not damaged severely…. The structural frame received some cracks, indicating strains beyond the elastic limit; the cracks were repaired with epoxy cement." John A. Blume & Associates (1973) report:

> "The structural repair consisted of patching the second-floor beam-column joint on the north side (east end) of the structure…. Some structural distress appeared at some column pour joints located near the exterior beam soffits.… Epoxy repaired the spalled concrete. Paint was applied to areas where only flaking of paint occurred.
>
> Nonstructural damage was extensive. Almost every guest room suffered some damage. About 80 percent of the repair cost was spent on drywall partitions, bathroom tile, and plumbing fixtures. The damage was most severe on the second and third floors and least severe at the sixth and seventh floors.

Some gypsum wallboard had to be replaced. Interior partitions required paint and new vinyl wall covering…. Forty-five bathtubs … and 12 water closets had to be replaced. Bathroom tile had to be patched, grouted, or replaced in over half the bathrooms…. Spalling occurred at architectural concrete attached to structural concrete columns at the ground floor…. Exterior cement plaster spalled and cracked. Windows in every room required some alignment and caulking, although none needed replacing. Doors needed adjustment."

John A. Blume & Associates (1973) report the repair cost as "approximately $145,000," of which $2,000 was for structural repair. Trifunac *et al.* (1999) report the cost of repair as $143,000, while Jennings (1971) estimated repair costs as approximately $250,000.

In 1980, additional accelerometers were installed; their locations are shown in Figure 4-12 (California Strong Motion Instrumentation Program 2001). As of this writing, they have been triggered in 11 subsequent events, whose magnitudes, epicentral distances, intensities are shown in Table 4-5. According to the available literature, and judging by construction permits on file in the Los Angeles Department of Building and Safety, none of these subsequent events other than the Northridge series caused significant damage.

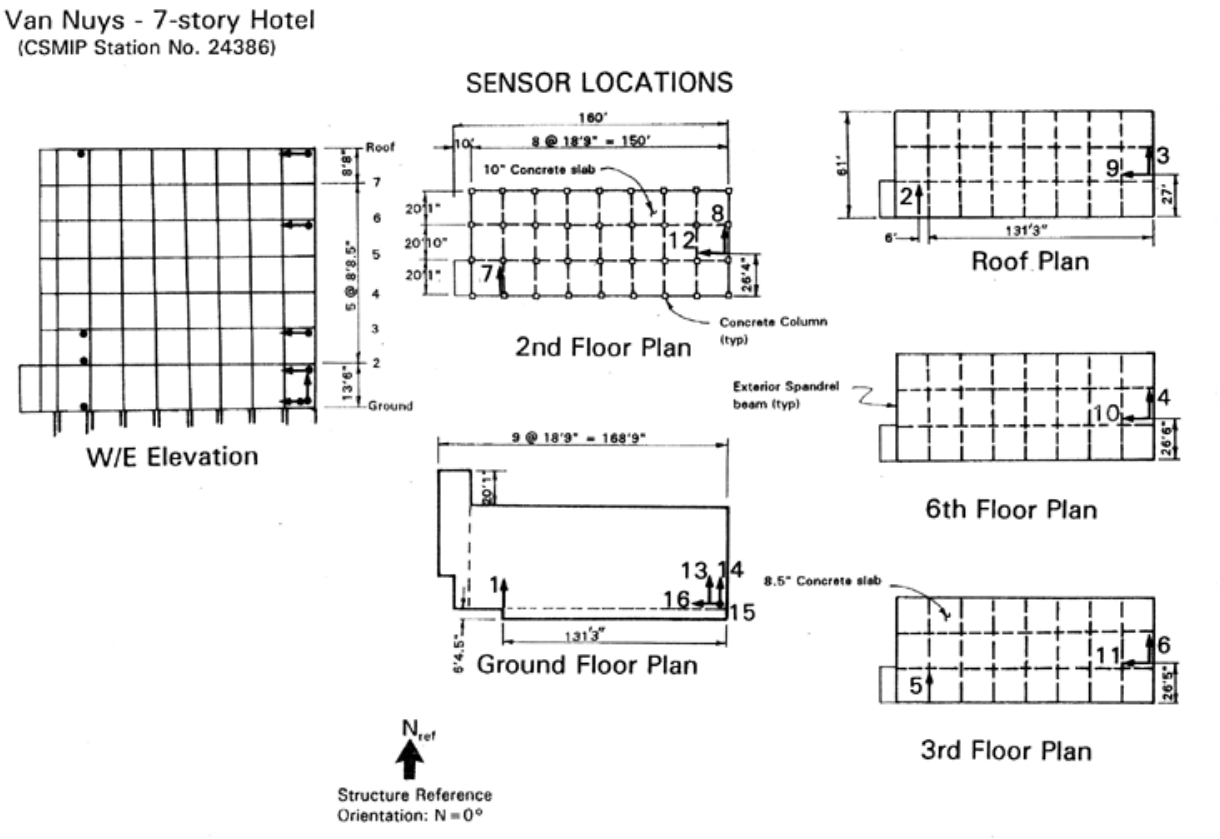

Figure 4-12. Instrument locations after 1980

Table 4-5. Events causing strong motion (Trifunac et al. 1999; CSMIP 1994)

Earthquake	Date	*M*	*R* (km)	*PGA* (cm/sec^2)		*PGV* (cm/sec)		*PGD* (cm)	
				Trans	Long	Trans	Long	Trans	Long
1. San Fernando	9 Feb 1971	6.6	22	240	130	27	23	5.3	9.7
2. Whittier	1 Oct 1987	5.9	41	160		8.7		1.8	
3. Whittier aft.	4 Oct 1987	5.3	38	37	52	1.4	2.2	0.3	0.3
4. Pasadena	3 Oct 1988	4.9	32	54	36	1.6	0.9	0.3	0.2
5. Malibu	19 Jan 1989	5.0	36	15	22	0.9	1.0	0.2	0.2
6. Montebello	12 Jun 1989	4.1	34	21	22	0.8	0.8	0.2	0.2
7. Sierra Madre	28 Jun 1991	5.8	44	56	62	4.6	2.8	1.0	
8. Landers	28 Jun 1992	7.5	190	41	41	12	11	6.1	4.9
9. Big Bear	28 Jun 1992	6.5	150	25	23	3.6	3.6	0.9	1.0
10. Northridge	17 Jan 1994	6.7	7.2	390	440	40	51	12	7.9
11. Northridge aft.	20 Mar 1994	5.2	1.2	270	140	7.5	4.8	0.6	0.6
12. Northridge aft.	6 Dec 1994	4.5	11	57	60	3.0	2.4	0.5	0.2

Shaking, structural response, and damage in the 1994 Northridge earthquake were more severe than in the San Fernando earthquake. As noted in Table 4-5, peak acceleration at the ground floor was 440 cm/sec^2 in the longitudinal direction, 390 cm/sec^2 transversely. The 5%-damped acceleration response spectra for the motion recorded by instruments 16 and 14 are shown in Figure 4-13 (calculated using Bispec [Hachem 2000]). Assuming a fundamental period of 1.5 to 2.0 sec and 5% viscous damping, the building experienced damped elastic spectral acceleration of approximately 0.3 to 0.5g.

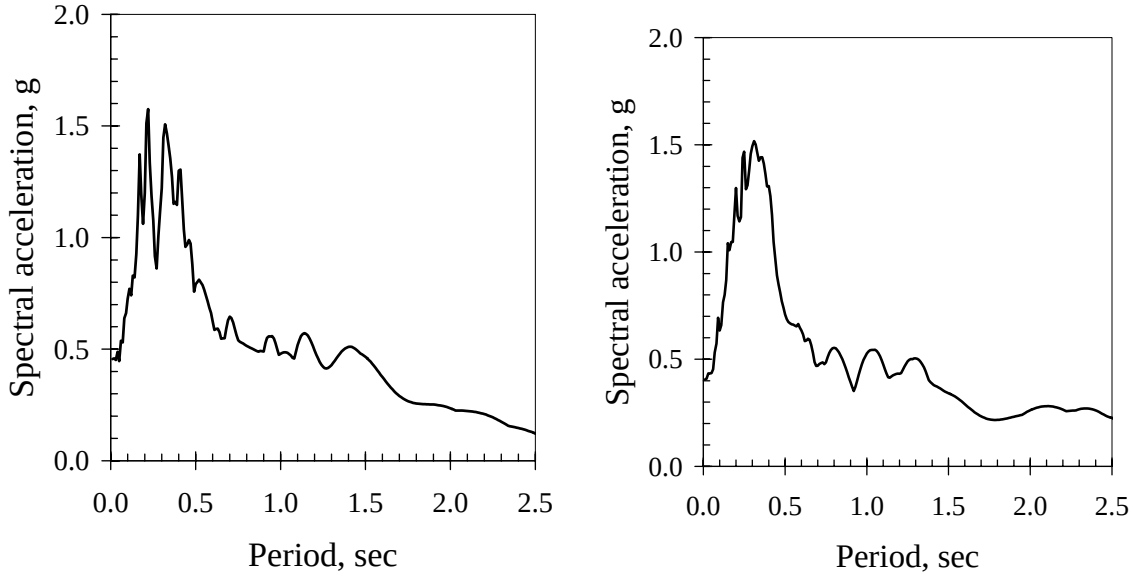

Figure 4-13. Spectral acceleration of ground-floor motions, 1994 longit. (left) and transverse (right)

Islam (1996) reports structural response in the Northridge earthquake in terms of relative displacements and transient interstory drift ratios, as shown in Table 4-6. Several authors have estimated peak responses at the other floors; Table 4-6 shows estimates by Li and Jirsa

(1998) and Browning et al. (2000). The table shows fair agreement among the estimates: transient drift ratios reached approximately 2% in the 1st through 4th stories, decreasing to 0.5% toward the 7th story.

Table 4-6. Recorded peak displacements and story drift ratios

Floor	Max rel. displacement (Islam 1996)	Transient drift ratio relative to floor below		
		Recorded (Islam 1996)	Calc., Li & Jirsa (1998)	Calc., Browning et al. (2000)
Longitudinal				
Roof	9.2 in.		0.3%	0.5%
7			0.6%	0.7%
6	8.2		0.9%	1.3%
5			1.9%	1.9%
4			1.7%	1.9%
3	3.6	1.9%	1.9%	1.0%
2	1.6	1.0%	1.8%	0.4%
Transverse				
R, east	6.9 in.			
R, west	9.0			
6, east	6.0			
3, east	2.9	1.6%		
3, west	3.4	1.3%		
2, east	1.6	1.1%		
2, west	1.9	1.2%		

Trifunac et al. (1999) and Trifunac and Hao (2001) present the results of two thorough damage surveys performed on February 4, 1994, and April 19, 1994. They report extensive structural damage, in the form of shear failure of columns and beam-column joints in the perimeter moment frame. The failures include spalling of the cover concrete over longitudinal bars, buckling of the longitudinal bars and through-cracks up to several inches wide. Damage to the south frame occurred at six locations on the 5th floor (column lines A-3, 4, 5, 7, 8, and 9) and one at the 3rd-floor level (column line A-9), as shown in Figure 4-14. Damage to the north frame occurred in the full-height infill masonry walls at the 1st story, and at the base of the short columns at the 1st story in column lines D-2, D-3, and D-4. Damage to the north frame also occurred at or within the beam-column joint at 12 other locations at the 2nd through 5th floors, as shown in Figure 4-15. The interested reader is referred to Trifunac et al. (1999) and Trifunac and Hao (2001) for additional detail, including photos of the damage.

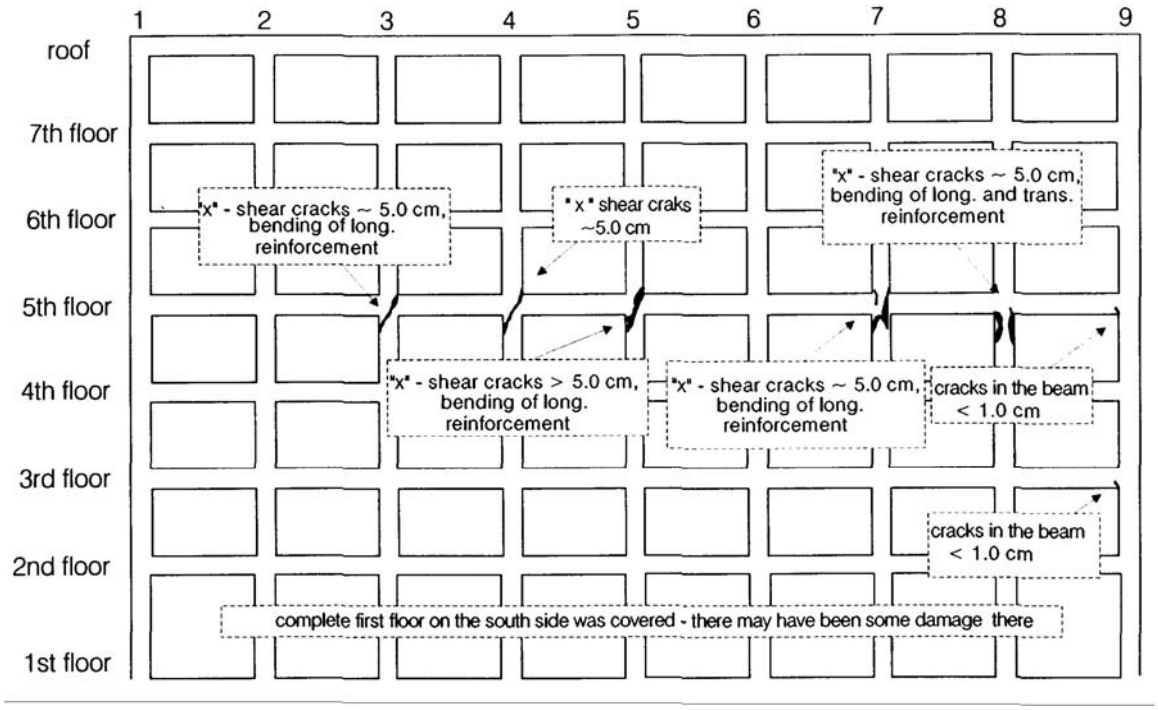

Figure 4-14. Structural damage in 1994 Northridge earthquake, south frame (Trifunac et al. 1999)

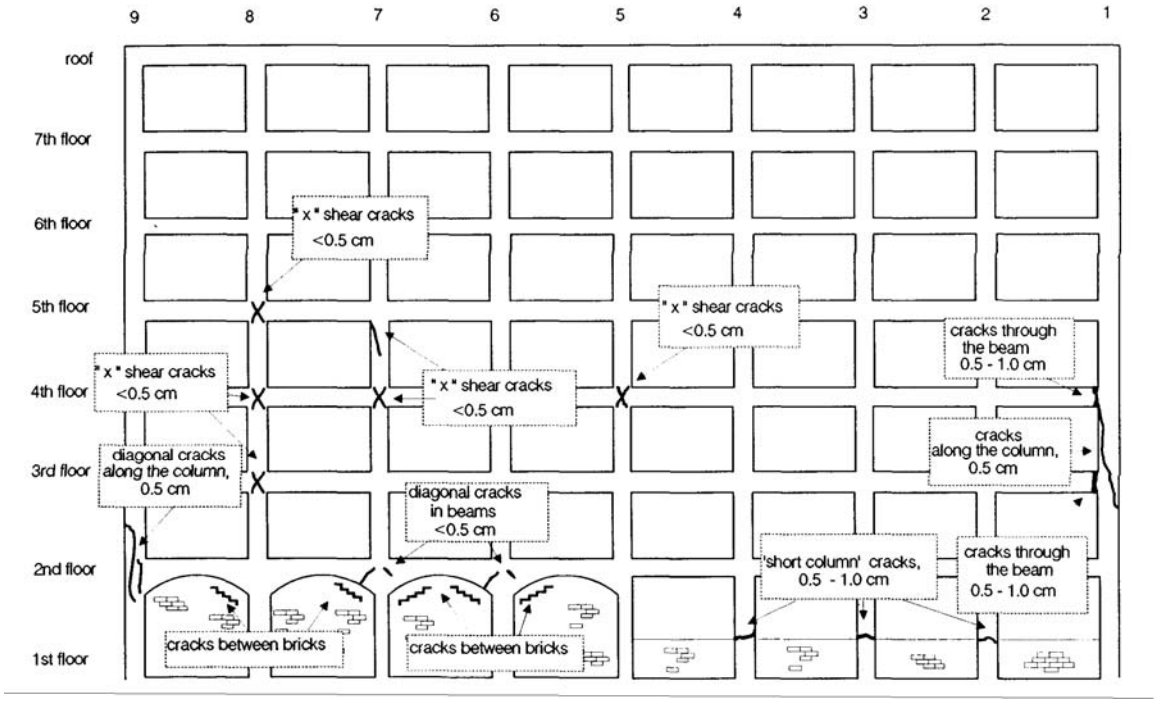

Figure 4-15. Structural damage in 1994 Northridge earthquake, north frame (Trifunac et al. 1999)

Structural repairs after the 1994 Northridge earthquake involved the addition of shearwalls at three columns of the south frame (3, 7, and 8) and four columns of the north frame (3, 5, 7, and 8), and at several interior column lines. Base fixity is provided to the new

shearwalls by the addition of grade beams spanning between pier groups. Figure 4-16 shows the building as it appeared in March 2001. However, consideration of the testbed building after this seismic strengthening effort is beyond the scope of the present project.

Figure 4-16. Shearwalls added to south (left) and north frames (right) after the 1994 Northridge earthquake. (Left: lines A-3, 7 and 8 from near to far. Right: lines D-8, 7, 5, and 3)

Table 4-7 summarizes the inventory of damageable assemblies in the demonstration building. A detailed inventory of assemblies (not shown here) contains information about the particular *EDP* to which each individual assembly is sensitive and the room number of architectural elements (for purposes of repainting-cost calculations).

Table 4-7. Summary of damageable assemblies (south half of demonstration building)

Assembly type	Description	Floor	Unit	Qty
3.5.180.1101.01	Nonductile CIP RC beam-column (column)	1	ea	9
3.5.180.1101.01	Nonductile CIP RC beam-column (column)	2	ea	9
3.5.180.1101.01	Nonductile CIP RC beam-column (column)	3	ea	9
3.5.180.1101.01	Nonductile CIP RC beam-column (column)	4	ea	9
3.5.180.1101.01	Nonductile CIP RC beam-column (column)	5	ea	9
3.5.180.1101.01	Nonductile CIP RC beam-column (column)	6	ea	9
3.5.180.1101.01	Nonductile CIP RC beam-column (column)	7	ea	9
3.5.190.1101.01	Nonductile CIP RC beam-column (beam)	2	ea	8
3.5.190.1101.01	Nonductile CIP RC beam-column (beam)	3	ea	8
3.5.190.1101.01	Nonductile CIP RC beam-column (beam)	4	ea	8
3.5.190.1101.01	Nonductile CIP RC beam-column (beam)	5	ea	8
3.5.190.1101.01	Nonductile CIP RC beam-column (beam)	6	ea	8
3.5.190.1101.01	Nonductile CIP RC beam-column (beam)	7	ea	8
3.5.190.1101.01	Nonductile CIP RC beam-column (beam)	8	ea	8
4.7.110.6700.02	Window, Al frame, sliding, heavy sheet glass, 4'-0x2'-6"x3/16"	2	ea	42
4.7.110.6700.02	Window, Al frame, sliding, heavy sheet glass, 4'-0x2'-6"x3/16"	3	ea	42
4.7.110.6700.02	Window, Al frame, sliding, heavy sheet glass, 4'-0x2'-6"x3/16"	4	ea	42
4.7.110.6700.02	Window, Al frame, sliding, heavy sheet glass, 4'-0x2'-6"x3/16"	5	ea	42
4.7.110.6700.02	Window, Al frame, sliding, heavy sheet glass, 4'-0x2'-6"x3/16"	6	ea	42
4.7.110.6700.02	Window, Al frame, sliding, heavy sheet glass, 4'-0x2'-6"x3/16"	7	ea	42
6.1.500.0001.01	Drywall partition, 5/8-in., 1 side, on metal stud, screws	1	sf	3520
6.1.500.0001.01	Drywall partition, 5/8-in., 1 side, on metal stud, screws	2	sf	3696
6.1.500.0001.01	Drywall partition, 5/8-in., 1 side, on metal stud, screws	3	sf	3696
6.1.500.0001.01	Drywall partition, 5/8-in., 1 side, on metal stud, screws	4	sf	3696
6.1.500.0001.01	Drywall partition, 5/8-in., 1 side, on metal stud, screws	5	sf	3696
6.1.500.0001.01	Drywall partition, 5/8-in., 1 side, on metal stud, screws	6	sf	3696
6.1.500.0001.01	Drywall partition, 5/8-in., 1 side, on metal stud, screws	7	sf	3696
6.1.500.0002.01	Drywall finish, 5/8-in., 1 side, on metal stud, screws	1	sf	3520
6.1.500.0002.01	Drywall finish, 5/8-in., 1 side, on metal stud, screws	2	sf	3976
6.1.500.0002.01	Drywall finish, 5/8-in., 1 side, on metal stud, screws	3	sf	3976
6.1.500.0002.01	Drywall finish, 5/8-in., 1 side, on metal stud, screws	4	sf	3976
6.1.500.0002.01	Drywall finish, 5/8-in., 1 side, on metal stud, screws	5	sf	3976
6.1.500.0002.01	Drywall finish, 5/8-in., 1 side, on metal stud, screws	6	sf	3976
6.1.500.0002.01	Drywall finish, 5/8-in., 1 side, on metal stud, screws	7	sf	3976
6.1.510.1202.02	Stucco finish, 7/8", on 3-5/8” mtl stud, 16"OC, typ quality	1	sf	512
6.1.510.1202.02	Stucco finish, 7/8", on 3-5/8” mtl stud, 16"OC, typ quality	2	sf	512
6.1.510.1202.02	Stucco finish, 7/8", on 3-5/8” mtl stud, 16"OC, typ quality	3	sf	512
6.1.510.1202.02	Stucco finish, 7/8", on 3-5/8” mtl stud, 16"OC, typ quality	4	sf	512
6.1.510.1202.02	Stucco finish, 7/8", on 3-5/8” mtl stud, 16"OC, typ quality	5	sf	512
6.1.510.1202.02	Stucco finish, 7/8", on 3-5/8” mtl stud, 16"OC, typ quality	6	sf	512
6.1.510.1202.02	Stucco finish, 7/8", on 3-5/8” mtl stud, 16"OC, typ quality	7	sf	512

4.3 STRUCTURAL RESPONSE MODEL

4.3.1 Structural model using Ruaumoko

The structural model employed here is an enhancement of the one we used in the CUREE-Kajima Joint Research program Phase IV (Beck et al. 2002), with the addition of soil springs in place of the fixed-based columns assumed in our prior study. Furthermore, we use a Latin Hypercube method to simulate 100 realizations of the structural model (as opposed to 20 simulations using simple Monte Carlo methods in Beck et al. 2002). Finally, as mentioned in Chapter 3 and justified in Porter et al. (2002b), we take mass as deterministic and stiffnesses (initial, post-yield, and soil-spring), damping, and strengths as uncertain. Coefficients of variation for uncertain parameters are as described in Chapter 3.

Hutchinson (2003) provides a model of soil-spring stiffness for this building. The three-pile groups at column lines 2 through 8 are assigned vertical stiffness of 9000 k/in, horizontal stiffness of 290 k/in, and rotational stiffness about the N-S axis (perpendicular to the plane of the south frame) of 8 x 10^6 k-in/rad. The vertical stiffness of the two-pile groups at column lines 1 and 9 are assigned a value of 6000 k/in and horizontal stiffness of 300 k/in. These piles are arranged along the N-S axis, so the rotational stiffness they provide the base of these columns about the N-S axis is likely to be modest, and for simplicity is ignored here.

4.3.2 Application of simplified particle filter

Base excitation u_k is taken from channel 16 as shown in Figure 4-12. Observed relative displacements o_{jk} are taken from channels 9, 10, 11, and 12 (roof, 6th, 3rd, and 2nd floors, respectively). The values o_j are taken as the peak response over time:

$o_j = \mathrm{Max}_k(o_{jk})$

4.4 DAMAGE AND REPAIR-COST MODEL

Parameters of fragility functions and unit-repair costs used here are shown in Table 4-8 and Table 4-9, respectively. Contractor overhead and profit is taken as 17.5% of total repair costs to the contractor.

Table 4-8. Summary of assembly fragility parameters

Assembly type	Description	*DM*	Damage	*EDP*	R_m	R_β
6.1.510.1202.02	Stucco finish, 7/8", 3-5/8" mtl stud, 16"OC, typ quality	1	Cracking	PTD	0.012	0.5
6.1.500.0002.01	Drywall finish, 5/8-in., 1 side, on metal stud, screws	1	Visible dmg	PTD	0.0039	0.17
6.1.500.0002.01	Drywall finish, 5/8-in., 1 side, on metal stud, screws	2	Signif dmg	PTD	0.0085	0.23
6.1.500.0001.01	Drywall partition, 5/8-in., 1 side, on metal stud, screws	1	Visible dmg	PTD	0.0039	0.17
6.1.500.0001.01	Drywall partition, 5/8-in., 1 side, on metal stud, screws	2	Signif dmg	PTD	0.0085	0.23
3.5.180.1101.01	Nonductile CIP RC beam-column	1	Light	PADI	0.080	1.36
3.5.180.1101.01	Nonductile CIP RC beam-column	2	Moderate	PADI	0.31	0.89
3.5.180.1101.01	Nonductile CIP RC beam-column	3	Severe	PADI	0.71	0.8
3.5.180.1101.01	Nonductile CIP RC beam-column	4	Collapse	PADI	1.28	0.74
4.7.110.6700.02	Window, Al frame, sliding, hvy sheet glass, …	1	Cracking	PTD	0.023	0.28

DM: damage measure
EDP: type of engineering demand parameter to which the assembly is sensitive. PTD = peak transient drift ratio; PADI = Park-Ang damage index (displacement portion)
R_m = median capacity; R_β = logarithmic standard deviation of capacity

Table 4-9. Summary of unit repair costs

Assembly type	Description	*DM*	Repair	Unit	C_m	C_β
6.1.510.1202.02	Stucco finish, 7/8", on 3-5/8" mtl stud, 16"OC, typ	1	Patch	64	125	0.2
6.1.500.0002.01	Drywall finish, 5/8-in., 1 side, on metal stud, screws	1	Patch	64	88	0.2
6.1.500.0002.01	Drywall finish, 5/8-in., 1 side, on metal stud, screws	2	Replace	64	253	0.2
6.1.500.0001.01	Drywall partition, 5/8-in., 1 side, on metal stud, screws	1	Patch	64	88	0.2
6.1.500.0001.01	Drywall partition, 5/8-in., 1 side, on metal stud, screws	2	Replace	64	525	0.2
3.5.180.1101.01	Nonductile CIP RC beam-column	1	Epoxy	ea	8,000	0.42
3.5.180.1101.01	Nonductile CIP RC beam-column	2	Jacketed repair	ea	20500	0.4
3.5.180.1101.01	Nonductile CIP RC beam-column	3,4	Replace	ea	34300	0.37
4.7.110.6700.02	Window, Al frame, sliding, hvy sheet glass, 4'-0x2'-	1	Replace	ea	180	0.2
09910.700.1400	Paint on exterior stucco or concrete	1	Paint	sf	1.45	0.2
09910.920.0840	Paint on interior concrete, drywall, or plaster	1	Paint	sf	1.52	0.2

C_m: median unit repair cost

C_β: logarithmic standard deviation of unit repair cost

4.5 HINDCAST OF DAMAGE, SYSTEM PERFORMANCE, AND LOSS

The demonstration building was analyzed using the motion recorded at the base during the 1994 Northridge earthquake. We used N = 100 simulations of the structural model and *EDP*. The structural analyses took approximately 4 hr on an ordinary desktop computer, i.e., approximately 2.4 minutes per analysis. Because the subsequent damage, performance, and loss analyses could be performed much more quickly, we performed 1,000 simulations of these, using each *EDP* vector 10 times. The increased number of simulations is appropriate because there is much more uncertainty in the results of the damage analysis compared with the results of the structural analysis.

4.5.1 Damage locations

Table 4-10 shows the ten most-likely-damaged columns and ten most-likely-damaged beams, according to the posterior damage distributions. Comparing the results with Figure 4-14 shows very poor prediction of actual damage locations. Our model predicts extensive damage in 3rd-story columns and roof beams, whereas the actual damage was concentrated at the top of the 4th-story columns and in their joints with 5th-floor beams. None of the predicted most-likely damage locations actually experienced damage in the Northridge earthquake. The implication is that either (a) actual structural conditions in the building differed in some important way from those shown on the construction documents, (b) the fragility functions employed here are incorrect or inappropriate for the beam-columns in the case-study building, or (c) both are true. In any case, since actual damage was due to shear, and since the fragility functions used here are based on flexure, it seems that our fragility functions need reconsideration.

Table 4-10. Most-likely damage locations for beams and columns

Location*	$P[DM = \text{light}]$	$P[DM = \text{moderate}]$	$P[DM \geq \text{severe}]$
Col 3A1	0.022	0.060	0.91
Col 3A2	0.033	0.16	0.78
Col 2A8	0.037	0.18	0.76
Col 3A8	0.038	0.18	0.76
Col 2A3	0.044	0.20	0.74
Col 2A1	0.055	0.20	0.72
Col 4A1	0.061	0.20	0.70
Col 3A3	0.051	0.21	0.71
Col 5A1	0.093	0.20	0.66
Col 3A4	0.054	0.22	0.70
Beam 7A7	0.056	0.22	0.69
Beam 8A1	0.068	0.25	0.65
Beam 8A2	0.072	0.26	0.64
Beam 8A6	0.073	0.26	0.63
Beam 8A3	0.073	0.26	0.63
Beam 8A4	0.073	0.26	0.63
Beam 8A5	0.073	0.26	0.63
Beam 8A8	0.122	0.28	0.54
Beam 3A3	0.44	0.23	0.054
Beam 2A3	0.46	0.19	0.031

* "Col *x*A*y*" means the column at story *x*, column line A-*y*. "Beam *x*A*y*" means the beam at floor *x*, from column line *y* to column line *y*+1

4.5.2 System performance level

In every simulation, damage to beam and column elements exceeded that allowed under the life-safety performance level. This implies near-certainty that the building would not be in the life-safety performance level when exposed to the 1994 Northridge earthquake. Since that is in fact what did happen in Northridge, our model merely implies that, had such a real-time loss estimation system been in place at the time of the 1994 Northridge earthquake, it would have accurately and with near certainty predicted the system performance level.

4.5.3 Repair costs

The prior and posterior probability distributions of repair cost are shown in Figure 4-17. The distributions were almost perfectly lognormally distributed, with median values of $2.5 and $2.6 million, respectively, and logarithmic standard deviations of 0.06 and 0.08, respectively. (We have no information about the actual repair cost of the building after the 1994 Northridge earthquake; only that the repairs were costly enough to cause a several-year closure of the building.)

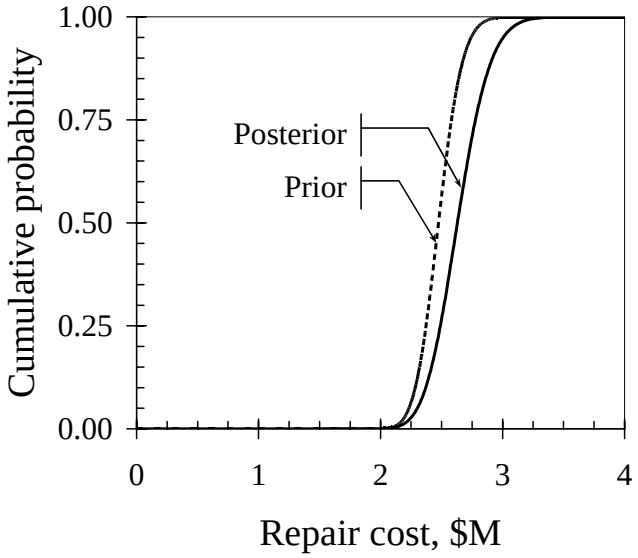

Figure 4-17. Hindcast repair cost distributions for the 1994 Northridge earthquake

Note that reduced uncertainty about damping and stiffness that comes from the earthquake response records does not produce reduced uncertainty regarding *DV*. This observation can perhaps be explained by noting that one expects to reduce uncertainty regarding an uncertain variable *X* when one observes samples of *X*, but not necessarily when one observes samples of another variable *Y* related in some nonlinear fashion to *X*. For example, a more accurate fundamental period can put the structural model closer to a spectral peak in the base motion.

A second, and more important, observation from the similarity of the prior and posterior $DV_{\$}$ distributions is that Bayesian updating of $DV_{\$}$ is almost immaterial, at least in the present case study. That is, observing structural response and comparing it with the calculated value does not add much information at the level of the repair cost. In hindsight, this is a predictable result. We observed in Porter et al. (2002b) that the greatest contributors to uncertainty in $DV_{\$}$ were the intensity measure (denoted by *IM*, and measured, for example, by damped elastic spectral acceleration), detailed ground-motion time history, denoted by a(*t*), and assembly capacity, with structural parameters contributing only modestly to uncertainty in $DV_{\$}$. In the case of real-time loss estimation, *IM* and a(*t*) are known, and the Bayesian updating using observed *edp** provides no information about assembly capacity, and thus cannot affect the uncertainty associated with it. The minor change in the *DV* distribution observed here is due primarily to reduced uncertainty about damping and stiffness.

We conclude from this observation that perhaps it is not much help to perform Bayesian updating of *EDP* in real-time loss estimation, or even to consider uncertainty in the structural model, when the structural uncertainties seem to contribute so little to overall uncertainty in *DV*. To ignore structural uncertainty would be a valuable timesaver. There would be no need to simulate the structural model and no need to perform numerous nonlinear time-history structural analyses. One need only perform a single deterministic nonlinear time-history structural analysis using the input ground motion recorded at the building base, and then

perform the (much faster) damage and loss-analyses of ABV as usual. In addition, ignoring structural uncertainties would save time and money in that there would be no need to install instruments on upper floors: structural analysis with a best-estimate structural model appears to provide a good-enough estimate of upper-story response so that the instruments are irrelevant for purposes of real-time loss estimation (but, of course, are of interest for the purpose of investigating the structural properties and response).

5 KAJIMA SAMPLE APPLICATION

5.1 OUTLINE OF DEMONSTRATION

This chapter deals with a sample demonstration for an office building designed according to the Japanese earthquake-resistance design code. The building was damaged by the Great Hanshin Earthquake (1995), and its damage was investigated in detail. However, it was not instrumented, nor is there any recorded structural response to directly show its behavior during the earthquake available. Thus, in this demonstration, we apply the particle filter to simulated data from a non-linear time history analysis of a model of the building as a substitute for measurement of the true response.

At first, the seismic response and damage is simulated to create an earthquake scenario by performing a 3D nonlinear time history analysis along with the assembly-based vulnerability (ABV) method for the damage analysis. These analyses are informed by structural drawings, the damage description from a post-earthquake investigation and they use a ground motion acceleration time history recorded near the site. Then, assuming that only a part of the response is available as output of imaginary installed sensors, the rest of response is estimated using the particle filter, and damage is estimated by the ABV method. It should be noted that, in this demonstration, the vulnerability and fragility curves are the same when creating the earthquake damage scenario as when estimating it, which means we assume no errors exist in the assembly model and in the vulnerability and fragility curves. When the real-time loss-estimation system moves to the practical stage, such kinds of errors, never negligible, must be taken into account.

5.2 FACILITY DEFINITION

Figures 5-1 and 5-2 show a photograph and an elevation drawing of the model building. It is a mid-rise (7-story above-ground and 2 stories below) reinforced concrete building constructed in 1969, whose total floor area is 3,900 m^2. The features are summarized in Table 5-1. It should be noted that the replacement cost shown in Table 5-1 is simply calculated by multiplying the total floor area by the unit cost, which is based on statistics by the Ministry of Land, Infrastructure and Transport of the Japanese government; i.e. it does not represent an actual replacement cost.

The stories below the fourth floor are used as a commercial complex, and there is an open well space from the ground floor to the third floor. The fourth story and higher are offices, and

with typical floor area of 430 m^2. The first and typical office floor plans are shown in Figures 5-3 and 5-4, respectively. The structural system consists of a reinforce concrete frame and seismic-resistant reinforced concrete walls. The foundation system is a monolithic mat foundation, supported by relatively good soil layers which are classified in the second hard soil type by the current seismic resistance design code of Japan. The soil profile of the site is shown in Table 5-2.

Table 5-1. Summary of model building features

Year Built	1969
Stories	7F/B2
Use	Complex (Office/Commercial)
Typical Floor Area	430 m^2
Total Floor Area	3900 m^2
Site Area	420 m^2
Construction	Reinforced Concrete
Replacement Cost	U.S.$7.4M*

*The value was calculated by multiplying total floor area by unit cost (based on the statistics by Ministry of Land Infrastructure and Transport of the Government of Japan)

Figure 5-1. Model building

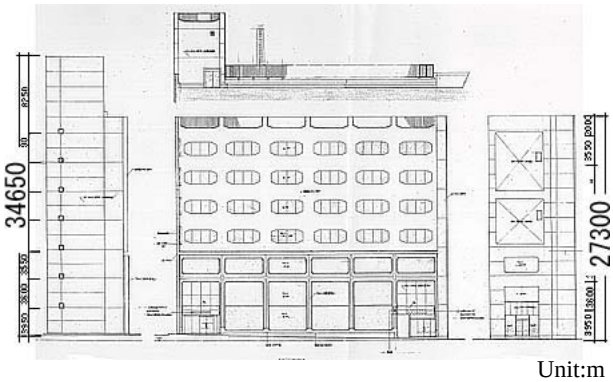

Unit:m

Figure 5-2. Elevation

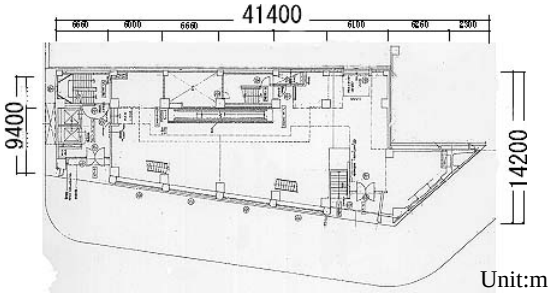

Unit:m

Figure 5-3. First floor plan

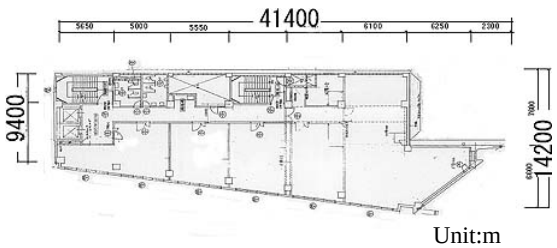

Unit:m

Figure 5-4. Typical floor plan

Table 5-2. Soil profile of subject site

Soil profile	Depth (m)	N-value
Fill	GL-1	2
Silt and mud	GL-2	5
	GL-3	4
	GL-4	8
Coarse sand	GL-5	8
Sand gravel	GL-6	21
	GL-7	32
	GL-8	12
	GL-9	34
	GL-10	50
Silt	GL-11	22
Fine sand	GL-12	22
	GL-13	37
Sand gravel	GL-14	50
	GL-15	50
	GL-16	50
	GL-17	40
	GL-18	50
	GL-19	50
	GL-20	50
	GL-21	36

As shown in Figure 5-5, the site is in Nagata district, Kobe city, and belongs to the so-called “damaged belt,” where a number of buildings and structures were heavily damaged in the Great Hanshin Earthquake of 1995. What is more, the building had been designed according to a former seismic resistant code, which was altered in 1980. Nevertheless, it was in the “moderate” damage state after the earthquake. The most significant damage was: damage of a corner column in the first story, an inclined cooling tower on the roof, breaks in the plumbing, overturning of power supply equipment on the seventh floor, and many cracks in the finish. Figure 5-6 shows some of this damage.

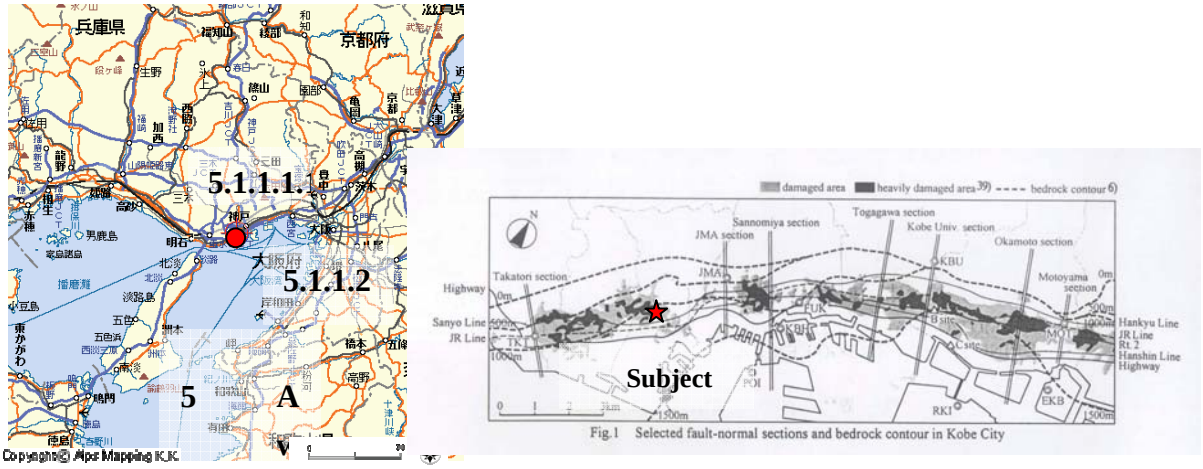

Figure 5-5. Subject site (Nagano et al. 1998)

Damaged column

Cracked exterior wall panels

Inclined cooling

Crashed gravity tank

Power facility room on the 7th floor

Figure 5-6. Damages by the Kobe Earthquake

5.3 SEISMIC RESPONSE ANALYSIS

5.3.1 Structural model

To create simulated earthquake response data, a nonlinear time history analysis was executed using Kajima's in-house structural analysis code. In the analysis, the building was modeled as a 3-D frame model shown in Figure 5-7. For simplicity, the structure below grade was omitted, and it was assumed that the ground motion acted on the fixed first floor. The

building has earthquake-resisting walls to resist lateral loads, which were modeled using brace elements whose restoring force characteristics consisted of a tri-linear backbone curve and origin-oriented hysteresis. A typical backbone curve is shown in Figure 5-8. To model columns, flexure, shear, and axial deformation were each modeled with a tri-linear backbone curve and origin-oriented hysteresis. For beams, flexure and shear were treated the same, but axial deformation was assumed rigid.

Table 5-3 summarizes the result of the eigenvalue analysis of the structural model. The first three modes are shown in Figure 5-9. They correspond to the fundamental modes for two horizontal (EW-direction, NS direction), and rotational motions, respectively. Mass was modeled as a concentrated mass at each floor centroid and rotational inertia about a vertical axis through each floor centroid as shown in Table 5-4. Damping was assumed as 3% of critical.

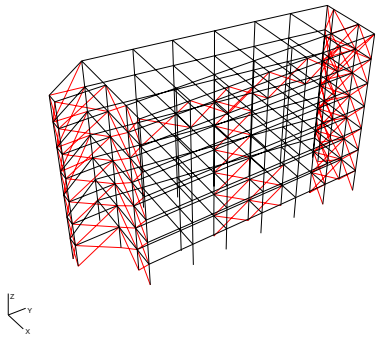

Figure 5-7. Analytical model

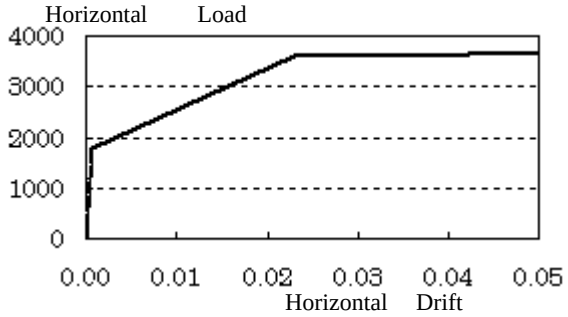

Figure 5-8. Horizontal load-drift relationship of brace element (origin-oriented trilinear)

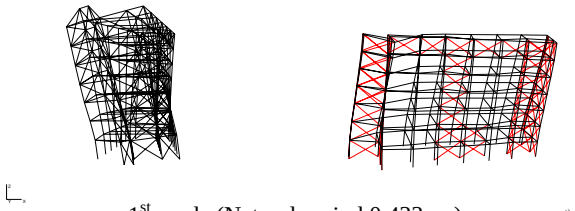

1st mode (Natural period 0.433sec)

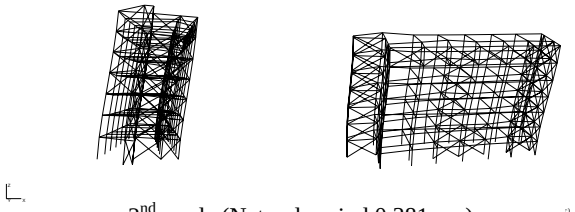

2nd mode (Natural period 0.381 sec)

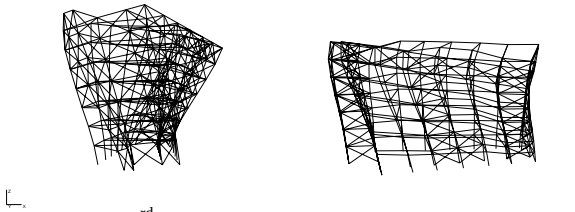

3rd mode (Natural period 0.266 sec)

Figure 5-9. Fundamental modes

Table 5-3. Summary of eigenvalue analysis

	Period	Participation factor		
Mode	**(sec)**	**NS**	**EW**	**Rotation**
1st	0.433	-0.422	0.653	-6.454
2nd	0.381	0.995	0.576	-0.411
3rd	0.266	0.132	-0.304	-6.499
4th	0.122	0.447	-0.502	4.174
5th	0.104	0.350	0.273	-1.563

Table 5-4. Mass and rotational inertia

	Floor Height	Weight	Rotational Inertia
Floor	**cm**	**kN**	**kN*m2**
Roof	355.0	7800	1.40E+06
7	355.0	5900	9.70E+05
6	355.0	5200	8.93E+05
5	355.0	5500	9.15E+05
4	355.0	5400	8.94E+05
3	360.0	5600	9.27E+05
2	360.0	5700	9.42E+05

5.3.2 Input ground motion

As an input ground motion for this demonstration, we selected a ground motion record from NTT Kobe (NTT Facilities 2004), whose acceleration time histories and response acceleration spectra are shown in Figures 5-10 and 5-11, respectively. The Kobe Japan Meteorological Agency, at which very strong motion was recorded with more than 800 Gal of peak ground acceleration (PGA), is just three kilometers distant from the subject site. Nevertheless, we chose the NTT Kobe record because the damage level of the building was moderate, as described before, despite the structure being designed according to a former seismic resistant code, and because ground motion accelerations with a PGA of around 350 Gal were recorded at a very close observation station (this record was not used since some of its local maxima were truncated.)

We calculated three cases of response with both the NS- and EW-direction motions acting at the same time, and with each of them acting alone, respectively. However, the rest of this chapter deals only with the case where the NS direction ground motion acts alone. One reason is for simplicity and another is that the building response due to the NS-direction ground motion on its own was not much different from that due to both ground motions at once.

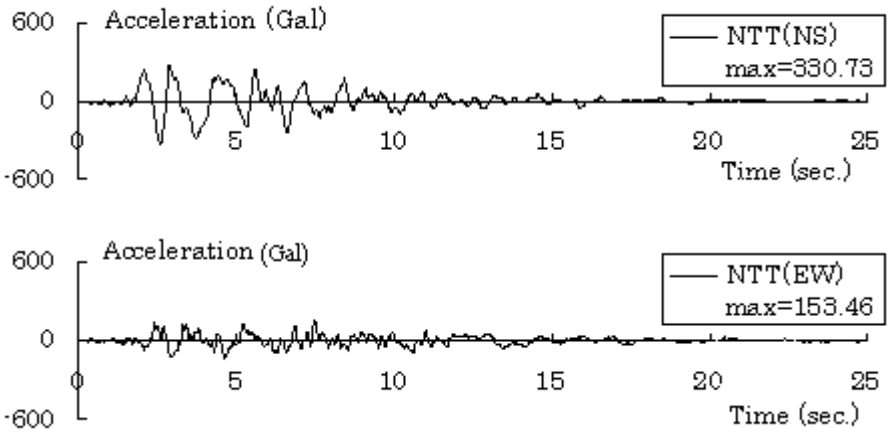

Figure 5-10. Input ground motion (acceleration time history)

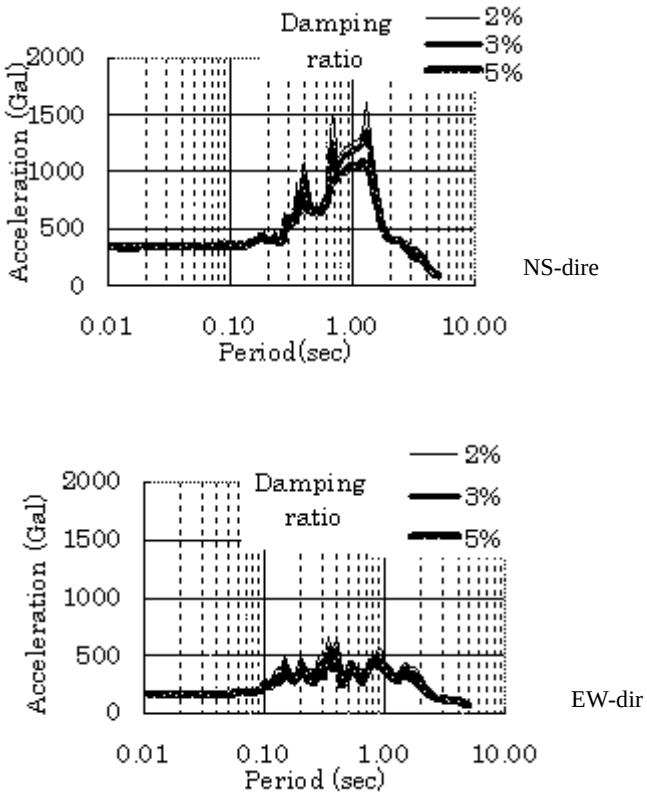

Figure 5-11. Input ground motion (response acceleration spectrum)

5.3.3 Damage and repair-cost model

In calculating the damage amount by the ABV method, the building was not disassembled

into tangible units, such as a single column, a single air-conditioner etc., but the whole building replacement cost was divided into the following eight element groups according to the cost distribution of a common office building: structure, exterior wall, partition wall, ceiling and finishing sensitive to acceleration, electric equipment, plumbing and tank, HVAC, and elevator. Then, they were divided into each floor equally, after that they were adjusted as shown in Table 5-5 considering the facts that: machine rooms were on the 7th story, a well hole was built in from the ground floor to the third floor, the cost of the 7th story includes that of a penthouse on the roof, and the cost of the first floor includes those of partitions, equipment, etc. on underground floors. It should be noted that the sum of all figures in Table 5-5 is not 100 % because the table does not contain some costs such as those of earthwork and temporary work, which do not exist as tangible objects, and that of underground structure, which is regarded as not subject to damage by earthquake vibration.

Table 5-5. Cost distribution

Floor	**Structural**	**Non-structural**						
		Cladding	**Partition**	**Ceiling**	**Electrical**	**Plumbing**	**HVAC**	**Elevator**
7	3.1%	3.1%	0.5%	0.2%	3.1%	0.8%	2.4%	1.5%
6	2.5%	1.8%	0.6%	0.2%	0.9%	0.8%	1.0%	0.2%
5	2.5%	1.8%	0.6%	0.2%	0.9%	0.8%	1.0%	0.2%
4	2.5%	1.8%	0.6%	0.2%	0.9%	0.8%	1.0%	0.2%
3	2.5%	2.2%	0.6%	0.2%	0.9%	0.8%	1.3%	0.2%
2	2.5%	2.2%	0.6%	0.2%	0.9%	0.8%	1.3%	1.8%
1	2.5%	2.6%	1.9%	0.7%	2.3%	5.0%	3.0%	3.4%

The damage factor (ratio of the mean repair cost to replacement cost) of each assembly was determined using vulnerability curves (Figure 5-12) and engineering demand parameters (*EDP*s) calculated by time history analysis. The vulnerability curves except for structural elements were based on the results of the former research phase (Beck et al. 2002).

For structural elements designed according to the former earthquake resistant code, appropriate vulnerability curves had not been developed in the former phase of research. We therefore developed some fragility curves based on the results of a series of structural tests conducted from 1973 to 1977 (BRI 1977). Background material related with the project (BRI 1978), includes about 240 structural test records. Among them, we selected 78 tests using the following criteria: specimens were ordinarily designed according to the former code, crack

growing sketches were obtained, and at least some shear failure could be found. Then, we showed some of the cracking sketches to several structural engineers and research engineers and asked them to judge the damage levels, without telling them the deformations of the test specimens, according to a post-earthquake safety assessment standard (Japan Building Disaster Prevention Association 1991). Based on the engineers' judgments and on the test records, we determined deformation capacities for the damage state (minor, moderate, and major[1]) for every specimen and calculated their mean and standard deviation. Figure 5-13 shows the fragility curves, which are plotted assuming that the capacities have lognormal probability distributions.

We also showed crack sketches depicting each of typical three damage states to a construction engineer, who was an expert on renewal work, and also asked him to estimate the cost to repair that damage. His estimation for repair cost of minor, moderate and major damage was 16%, 43% and 100% of replacement cost, respectively. Figure 5-12(a) shows the resulting vulnerability curve of the structural elements, which is plotted as a sum of the products of damage probabilities, easily calculated using fragility curves, and the cost rate.

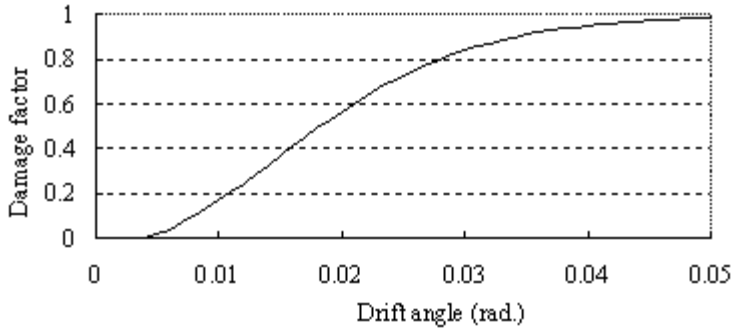

Figure 5-12(a). Vulnerability curve (structural components)

[1] We read damage level III, IV and V as minor, moderate, and major, respectively. Damage level I and II are regarded as not needing any restoration.

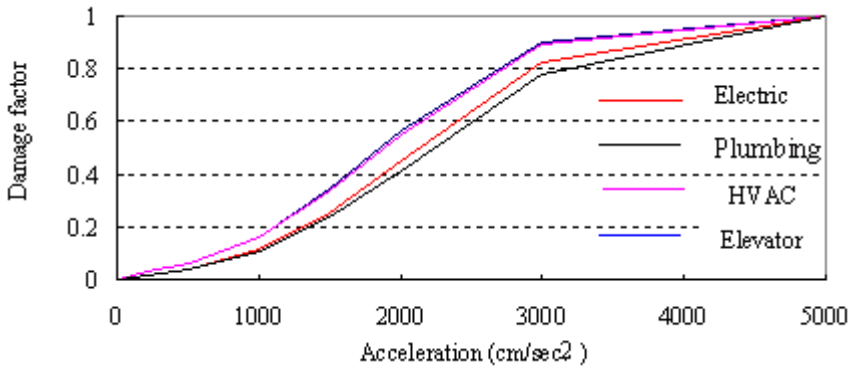

Figure 5-12(b). Vulnerability curve (equipment)

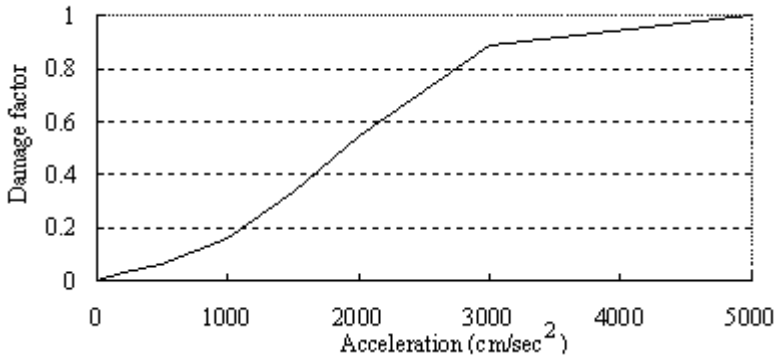

Figure 5-12(c). Vulnerability curve (acceleration-sensitive element)

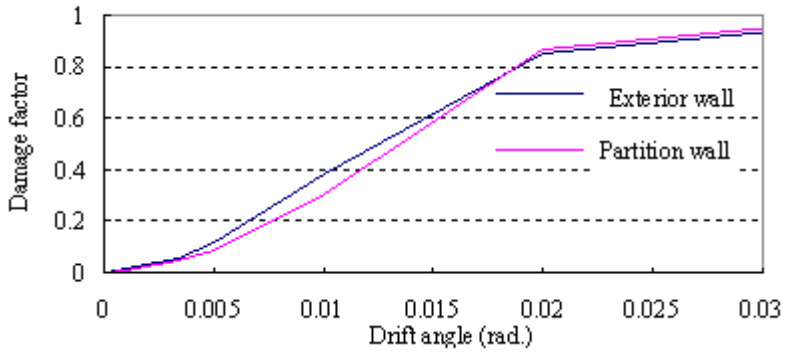

Figure 5-12(d). Vulnerability curve (deformation-sensitive element)

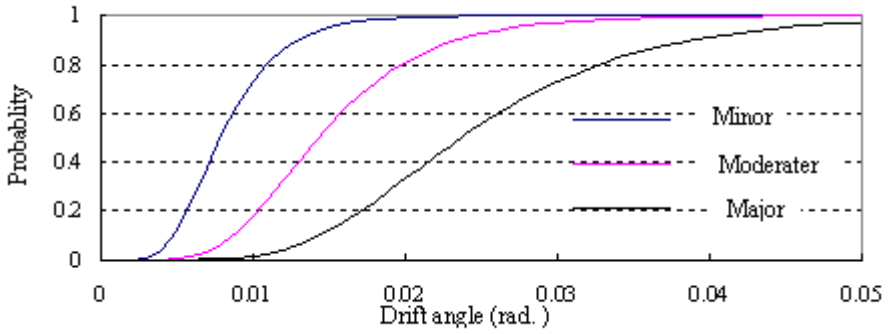

Figure 5-13. Fragility curves for structural element

5.3.4 Results

Figures 5-14 and 5-15 show time histories of inter-story drift angle and acceleration at the floor centroids. The histories after 10 seconds are omitted since the amplitudes are relatively small. The maximum inter-story drift angle and the maximum acceleration of each story or floor are shown in Figure 5-16. The maximum inter-story drift angle was 0.016 rad at the third story, and the maximum acceleration was 626 Gal at the roof.

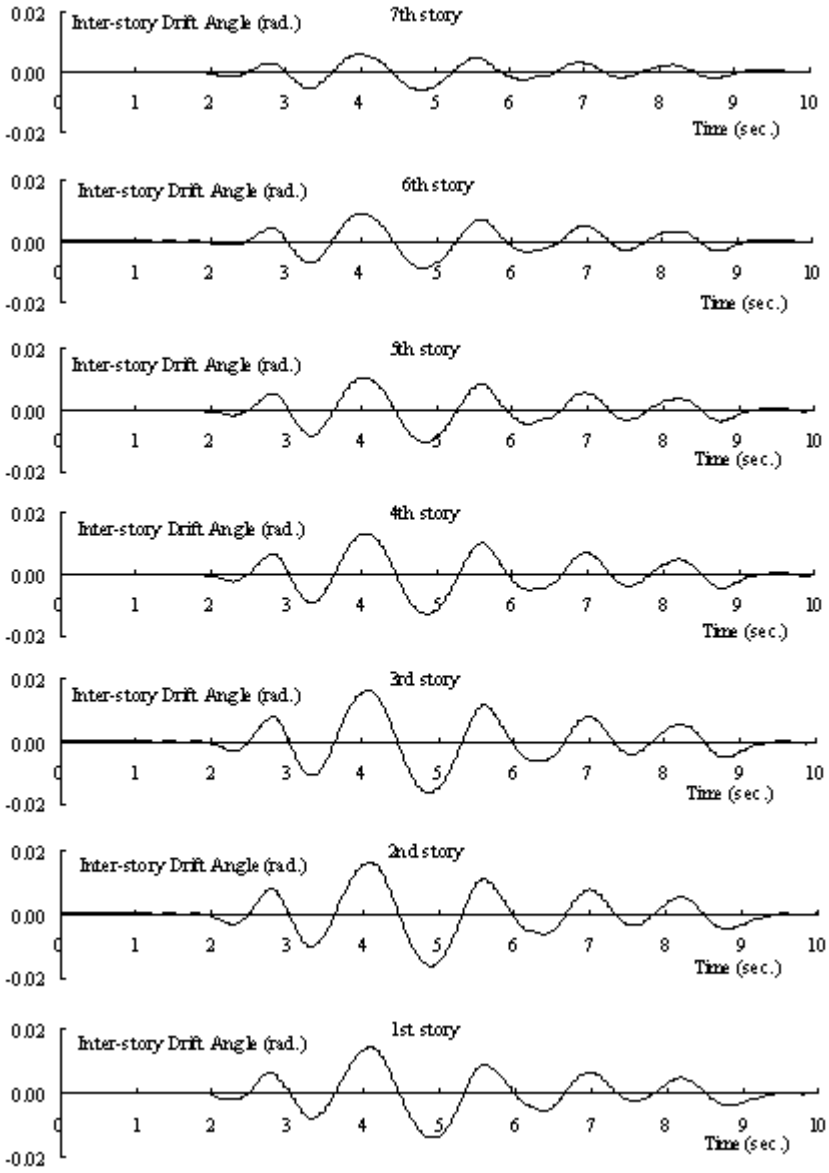

Figure 5-14. Time-history of inter-story drift angle

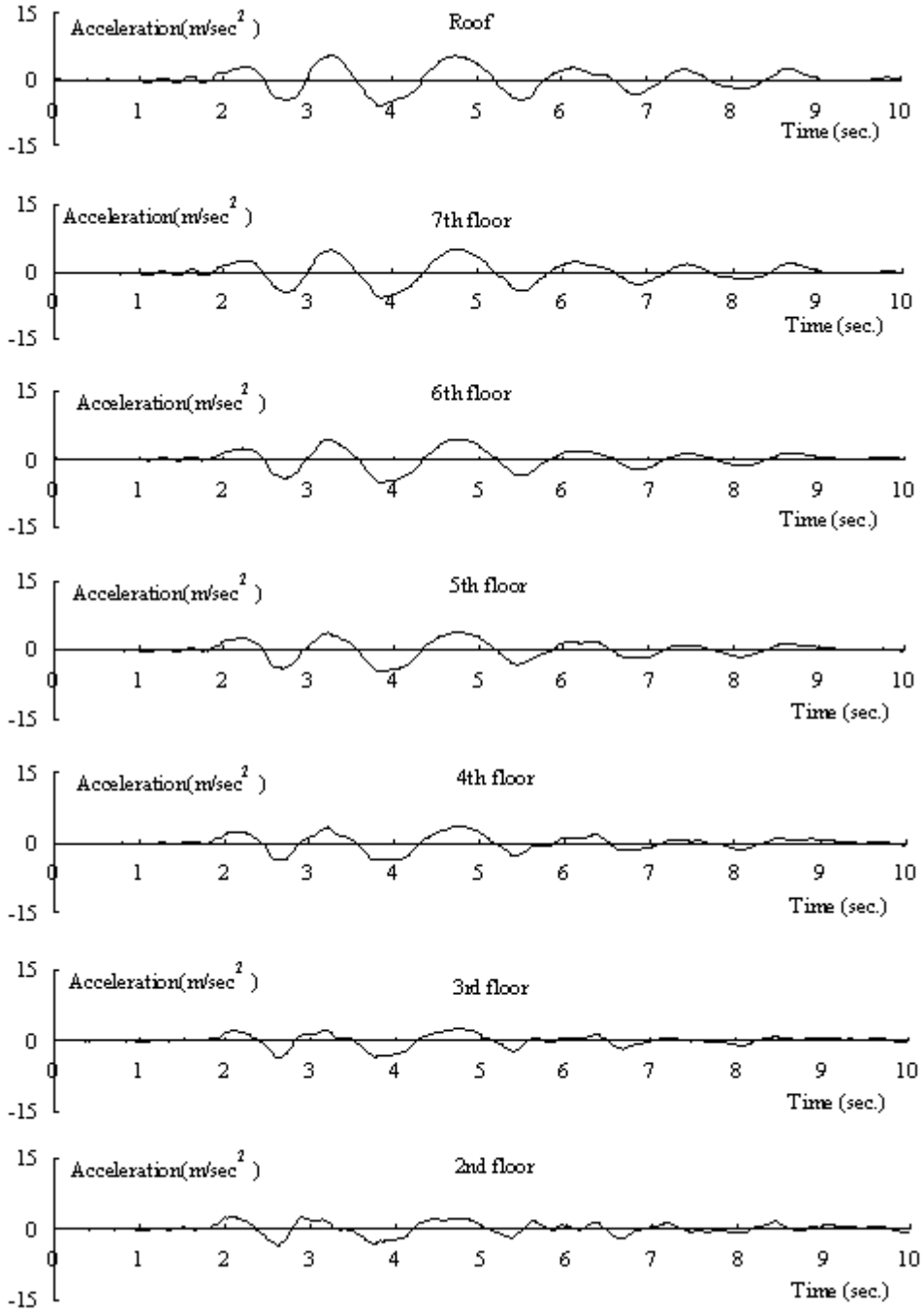

Figure 5-15. Time-history of floor response acceleration

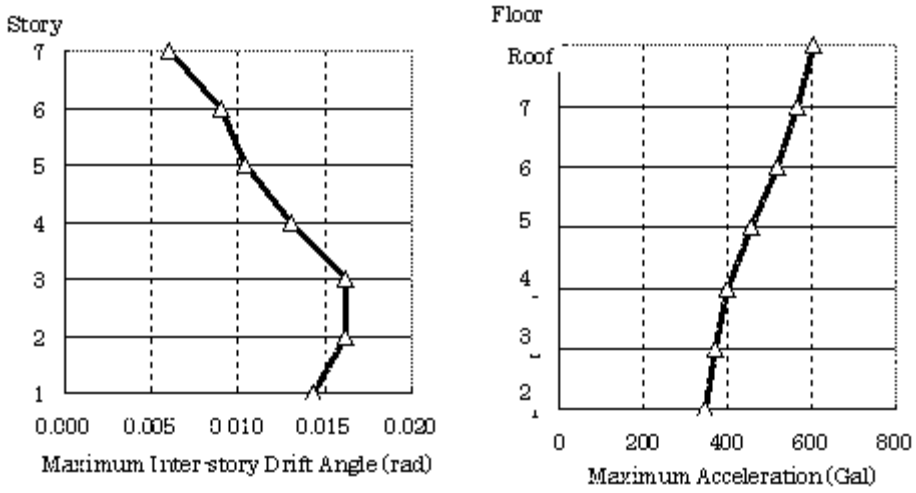

Figure 5-16. Distribution of maximum response

Damage factors were calculated using the damage and repair model already described, with EDPs shown in Figure 5-16. Table 5-6 summarizes those for each assembly. Summing up the products of the damage factors in Table 5-6 and the cost distribution in the corresponding cells of Table 5-5 produces the total direct repair cost rate as 20.2% of replacement cost. Assuming 10% for the overhead and profit of contractors, the repair cost rate of the building is 22.2%

Table 5-6. Damage factor of each assembly element

Floor	Structural	Non-structural elements						
		Cladding	Partitions	Ceiling	Electrical	Plumbing	HVAC	Elevator
7	4.2%	20.7%	30.2%	8.3%	5.9%	5.6%	8.3%	8.4%
6	13.7%	39.0%	56.3%	7.7%	5.4%	5.1%	7.7%	7.7%
5	19.0%	47.2%	66.3%	6.6%	4.6%	4.4%	6.6%	6.6%
4	28.9%	60.3%	75.3%	5.8%	4.0%	3.9%	5.8%	5.8%
3	41.7%	76.3%	86.4%	5.2%	3.6%	3.5%	5.2%	5.2%
2	41.9%	76.6%	86.6%	5.0%	3.4%	3.3%	5.0%	4.9%
1	34.1%	66.8%	79.8%	4.7%	3.2%	3.1%	4.7%	4.6%

In contrast with this analytical result, the damage inspection report after the Great Hanshin earthquake implies that the repair cost rate would be around 10% of the replacement cost,

which is substantially smaller than our calculation. This difference comes from the fact that we did not consider the anisotropy of the assembly fragilities, namely, exterior walls and partitions usually have much larger capacity for out-of-plane deformation than that for in-plane deformation. This means the EDPs for those assembly elements should be the in-plane drift angle. Turning our attention to the inspection report again, exterior walls parallel to NS direction (short direction of the building) were heavily damaged; however, almost no damage was observed in the exterior walls in the longitudinal direction. This fact is in agreement with the recorded ground motions where the PGA in the NS-direction was more than twice that in the EW-direction, shown in Figures 5-10 and 5-11.

Therefore, supposing that there was no damage in the exterior walls and partitions that are perpendicular to the NS-direction, we calculated the damage factor again after altering the cost distribution factors in Table 5-5. That is, we changed the cost factors for exterior walls into 22% of the original, and for partitions into half, respectively. The decreased amounts were determined with the rate of the building perimeter, ((9.4+14.2)/(9.4+14.2+41.4+41.4) = 0.22) and supposing that partitions were equally distributed in both directions. The re-calculated direct repair cost was 10.6%, which agrees well with the inspection after the earthquake.

As we saw above, it is important to consider the direction of vibration in order to follow get agreement with the post-earthquake observations. However, in the following section, we take the result that the total direct repair cost ratio was 20.2 %, since the purpose of this demonstration is verification of the particle filter approach, not clarification of the damage that occurred in the Great Hanshin earthquake.

5.4 APPLICATION OF PARTICLE FILTER

This section deals with an example application of the particle filter to estimate damage location and severity. In this application, it is assumed that only the input ground acceleration and roof response acceleration are available though accelerometers, and that the rest of the response and all of the damage are to be estimated. The approach follows that presented in Ching et al (2004).

5.4.1 Identification model

In applying the particle filter, the building was modeled with a 1-D 7-DOF lumped-mass, shear-spring model. The equation of the motion can be written as

$$M\ddot{x}_t + C_t\dot{x}_t + K_t x_t = Fu_t \tag{5-1}$$

where

$x_t = [x_{7,t}, x_{6,t} \cdots, x_{1,t}]^T$, $F = [-m_7, -m_6, \cdots, -m_1]^T$

$$M = \begin{bmatrix} m_7 & 0 & \cdots & 0 \\ 0 & m_6 & \cdots & 0 \\ \vdots & \vdots & \ddots & \vdots \\ 0 & 0 & \cdots & m_1 \end{bmatrix} \qquad K_t = \begin{bmatrix} k_{7,t} & -k_{7,t} & 0 & \cdots & 0 \\ -k_{7,t} & k_{7,t}+k_{6,t} & -k_{6,t} & \cdots & 0 \\ 0 & -k_{6,t} & k_{6,t}+k_{5,t} & \cdots & 0 \\ \vdots & \vdots & \vdots & \ddots & \vdots \\ 0 & 0 & 0 & \cdots & k_{2,t}+k_{1,t} \end{bmatrix}$$

$$C_t = \begin{bmatrix} c_{7,t} & -c_{7,t} & 0 & \cdots & 0 \\ -c_{7,t} & c_{7,t}+c_{6,t} & -c_{6,t} & \cdots & 0 \\ 0 & -c_{6,t} & c_{6,t}+c_{5,t} & \cdots & 0 \\ \vdots & \vdots & \vdots & \ddots & \vdots \\ 0 & 0 & 0 & \cdots & c_{2,t}+c_{1,t} \end{bmatrix}$$

$\dot{x}$: derivative of x with respect to time

$x_{i,t}$: displacement of i-th degree of freedom

m_i : mass of i-th degree of freedom

The hysteresis characteristics of the shear springs are modeled by a nonlinear system with four independent parameters as:

$$k_{i,t} = k_{i,0} \exp\left\{-\exp(\gamma) \cdot \mu_{i,t}^{\exp(\rho)}\right\} \tag{5-2}$$

where

$$c_{i,t} = k_{i,0} \cdot \delta\left\{1 + \exp(\lambda) \cdot \mu_{i,t}\right\}$$

$$\mu_{1,t} = \max_{0 \le k \le t}\left(\left|x_{1,k}\right| / h_1\right) \quad \mu_{i,t} = \max_{0 \le k \le t}\left(\left|x_{i,k} - x_{i-1,k}\right| / h_i\right) \qquad \text{For } i = 2,3,\cdots,7$$

Structural parameters for the system are shown in Table 5-7. The initial values of the four independent model parameters and their standard deviations for the "random-walk" model used at each time step to generate samples are summarized in Table 5-8. The number of parallel filters was ten, and two hundred samples were generated for each filter.

Table 5-7. Parameters of 1D-7D lumped-mass model

Floor	Height (m)	Weight (kN)	Initial stiffness (kN)
Roof	3.55	7,800	1,600,000
7	3.55	5,900	2,300,000
6	3.55	5,200	2,800,000
5	3.55	5,500	3,200,000
4	3.55	5,400	3,800,000
3	3.6	5,600	4,400,000
2	3.6	5,700	7,300,000

Table 5-8. Parameters of particle filter

	Initial mean	Standard deviation at each time step
γ	1.8	0.3
ρ	-1.6	0.1
δ	0.0036387	0.001
λ	3.9	0.5
ν	0.1	0.1

5.4.2 Damage and repair-cost estimation

To estimate repair cost, we used ABV for each sample of the particle filter. The ABV approach requires fragility curves for each assembly. We possessed the ones shown in Figure 5-13 for structural assemblies, but lacked fragility curves for the remaining assemblies. We did however have the vulnerability curves shown in Figures 5-12 (b), (c) and (d). (Fragility curves give the probability of exceeding some undesirable limit state as a function of input excitation. Vulnerability curves give a measure of loss, such as repair cost, as a function of some excitation.) To create the required fragility curves, we converted each vulnerability curve into a fragility curve, where the limit state is the damage requiring repairs that cost the full replacement-cost of the component, i.e., causing a damage factor equal to one. That is, we assumed only a single relevant damage state, in which the corresponding assembly element was totally damaged, and took its probability of occurrence given the input excitation as the mean damage factor at the same level of excitation. This avoids bias in estimating repair-cost

using the new fragility curves.

Then, the damage factor of the whole building C_R can be calculated as:

$$C_R = (1 + C_{OP}) \sum_{i=1}^{n_a} \sum_{j=1}^{n_D^i} URC_{i,j} \cdot I(DM_i = j) \tag{5-3}$$

where

C_{OP} : uncertain overhead and profit

$URC_{i,j}$: uncertain repair cost for the i-th assembly in the j-th damage state

$I(DM_i = j)$: indicator function which equals to one if the statement in parentheses is true and 0 otherwise.

When calculating the mean and variance of equation (5-3), we make the following three assumptions on random variables C_{OP}, $URC_{i,j}$, and $I(DM_i = j)$.

Assumption 1. Different types of random variables are statistically independent.

Assumption 2. Each capacity for each damage state is statistically independent between different assembly elements even if they are of the same assembly type.

Assumption 3 Repair costs are perfect correlated between the same assembly types, but statistically independent between different assembly types (e.g., structural components and electrical equipment)

Using these assumptions, the mean and variance are calculated using samples generated in the particle filter algorithm as:

(a) For the mean,

$$E[RC] = E\left[E[1 + C_{OP}] \sum_{k=1}^{N_S} \left\{ \sum_{i=1}^{N_m} \sum_{j=1}^{N_D^i} E[RC_{ij}] P\left(DM_i = j \middle| edp_{i,k}\right) \right\} w_k \right] \tag{5-4}$$

In the right-hand side of equation (5-4), the most external expectation represents taking the expectation using the filter samples; E[RC_{ij}] is the expectation of repair cost for the damage state j of assembly i; P($DM_i = j|edp_{i,k}$) is the probability that assembly i suffers damage state j on the condition that the corresponding engineering demand parameter is $edp_{i,k}$; subscript k means the quantity comes from the k-th sample of the particle filter; the parameter w_k is the weight of the k-th sample; N_s, N_m, and N^i_D are the number of samples in a single filter, elements in the estimated structure, and damage states assumed in the i-th assembly, respectively.

(b) For the variance,

$$Var[RC] = E[RC^2] - \{E[RC]\}^2 \tag{5-5}$$

$$E[RC^2] = E\left[\{E[(1+C_{OP})^2]\} \sum_{k=1}^{N_S} \left\{ \sum_{i=1}^{N_m} \sum_{j=1}^{N_D^i} \left(E^2[RC_{ij}] + \sigma_{RC_{ij}}^2 \right) + E[RC \cdot RC]_k \right\} w_k \right] \tag{5-6}$$

where

$$E[RC \cdot RC]_k = \sum_{i=1}^{N_m} \sum_{j=1}^{N_D^i} \sum_{\substack{P=1 \\ (\neq i)}}^{N_m} \sum_{q=1}^{N_D^p} \left[E[RC_{ij} \cdot RC_{pq}] P(DM_i = j | edp_{i,k}) P(DM_p = q | edp_{p,k}) \right]$$

$$E[RC_{ij} \cdot RC_{pq}] = E[RC_{ij}] E[RC_{pq}] + \rho_{RC_{ij}, RC_{pq}} \cdot \sigma_{RC_{ij}} \cdot \sigma_{RC_{pq}}$$

σ_{RCij} is the standard deviation of RC_{ij} and $\rho_{RCij,RCpq}$ is the coefficient of correlation between RC_{ij} and RC_{pq}. When assembly i and p are the same type assembly, $\rho_{RCij,RCpq} = 1$, otherwise $\rho_{RCij,RCpq} = 0$.

5.4.3 Results

To show the estimate of *EDP* from the particle filter, the maximum values up to time t are plotted against t in Figures 5-15 and 5-16 for the inter-story drift angle and response acceleration, respectively. In these figures, bold lines are the target (simulated "measured" response), and the three thin lines are the statistics of the EDP estimates. The central line is the mean and the top and bottom lines are the mean plus and minus one standard deviation, respectively. The figures show that the particle filter works well because at most time steps, except near the beginning of response, the measured response lies in the range between two standard deviations around the mean.

For calculating the values in equations (5-5) and (5-6), E[RC_{ij}] was taken as the same value as used in the deterministic analysis; σ_{RCij}, the coefficient of variation (quotient of the standard deviation by the mean), was taken as 0.2. The mean and standard deviation of the damage factor of each assembly and each story were calculated as shown in Tables 5-9 and 5-10, respectively. In Table 5-9, the figures in parentheses show the standard deviations. Substituting them into equations (5-4) and (5-6), we got 21.5% and 15.4% for the mean and standard deviation of the direct repair cost rate of the whole building, respectively. Given the mean and standard deviation of C_{OP} as 0.1 and 0.02, respectively, the mean and standard deviation of the whole repair cost rate was calculated as 23.6% and 18.6 %.

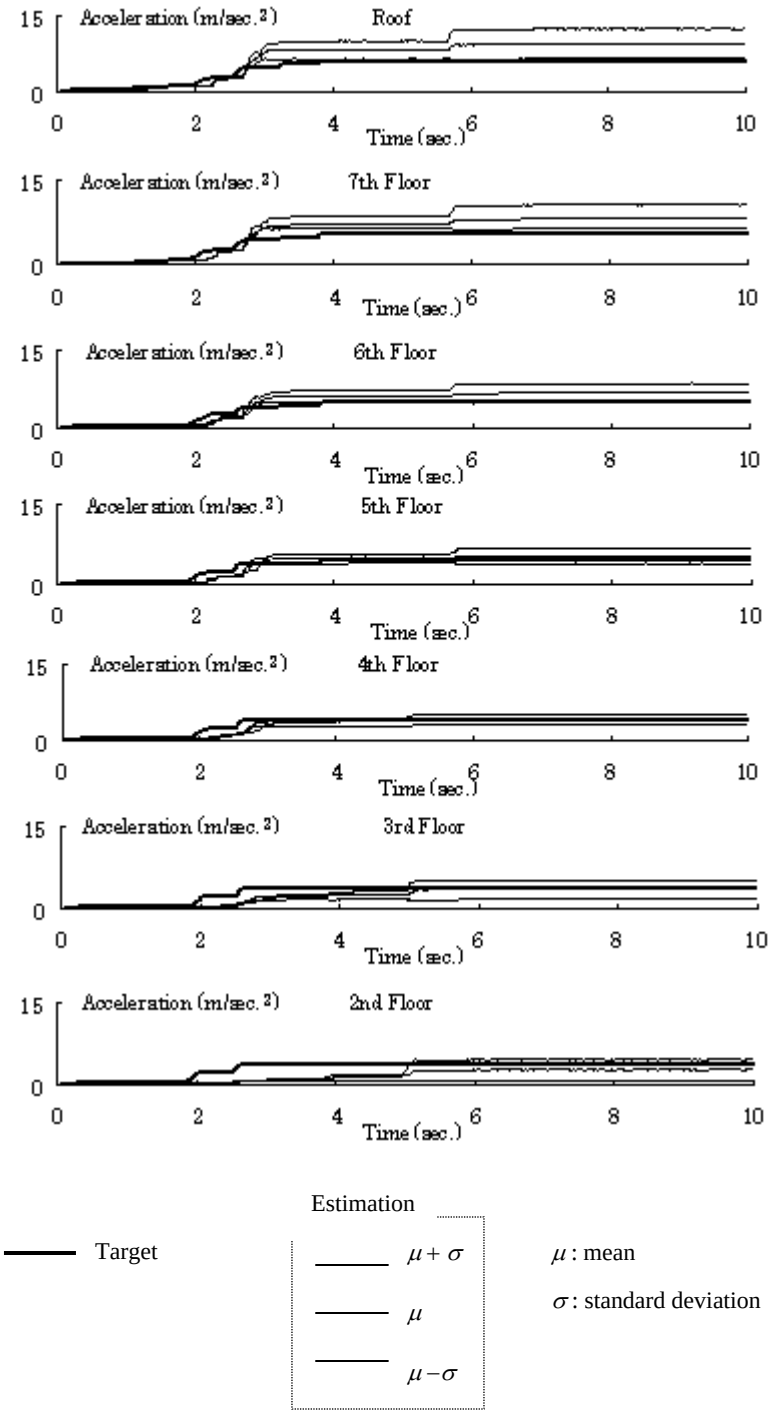

Figure 5-17. Estimation of maximum inter-story drift angle

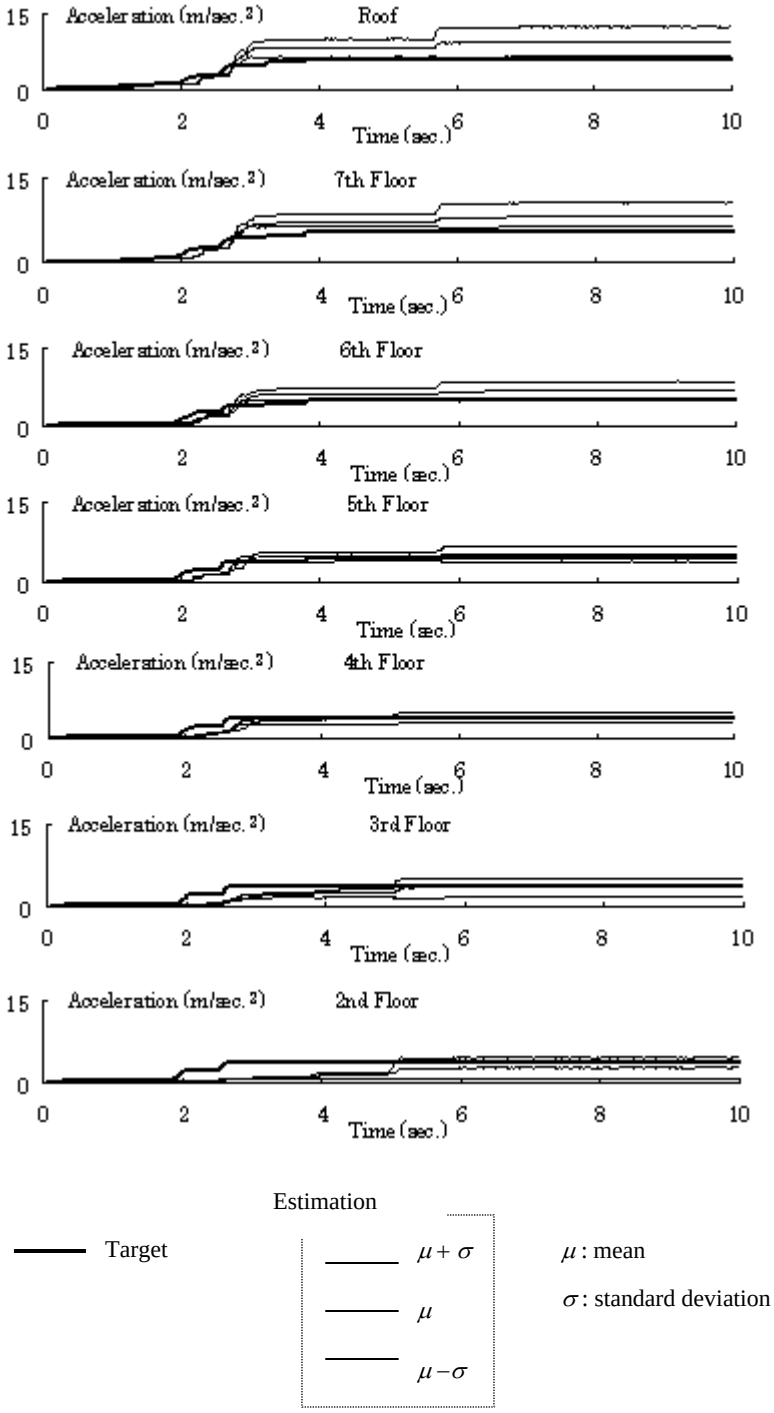

Figure 5-18. Estimation of maximum acceleration

Table 5-9. Mean and standard deviation* of damage factors for each assembly

Floor	Structural	Non structural						
		Cladding	Partitions	Ceiling	Electrical	Plumbing	HVAC	Elevator
7	25.2%	47.7%	54.2%	16.0%	11.8%	11.0%	16.0%	16.3%
	(31.8%)	(51.8%)	(52.0%)	(37.5%)	(33.0%)	(32.0%)	(37.5%)	(37.8%)
6	35.1%	58.1%	61.5%	13.0%	9.5%	8.9%	13.0%	13.2%
	(39.6%)	(51.6%)	(51.1%)	(34.4%)	(29.9%)	(29.0%)	(34.4%)	(34.7%)
5	41.2%	60.4%	63.1%	10.0%	7.1%	6.7%	10.0%	10.1%
	(43.4%)	(51.3%)	(50.8%)	(30.6%)	(26.3%)	(25.6%)	(30.6%)	(30.8%)
4	44.0%	60.9%	63.4%	7.2%	5.1%	4.8%	7.2%	7.3%
	(44.9%)	(51.2%)	(50.7%)	(26.4%)	(22.4%)	(21.9%)	(26.4%)	(26.5%)
3	43.8%	60.8%	63.4%	5.6%	3.9%	3.7%	5.6%	5.6%
	(44.8%)	(51.2%)	(50.7%)	(23.5%)	(19.7%)	(19.4%)	(23.5%)	(23.5%)
2	42.9%	60.7%	63.3%	5.0%	3.5%	3.3%	5.0%	5.0%
	(44.4%)	(51.3%)	(50.8%)	(22.3%)	(18.7%)	(18.4%)	(22.3%)	(22.2%)
1	23.3%	45.0%	52.2%	3.7%	2.6%	2.5%	3.7%	3.7%
	(30.3%)	(51.5%)	(52.0%)	(19.3%)	(16.1%)	(15.9%)	(19.3%)	(19.2%)

*Values in parentheses show standard deviations

Table 5-10. Damage factor distribution in each story

Floor	Mean	Standard deviation
7	12.0%	11.2%
6	23.4%	19.6%
5	27.3%	22.7%
4	27.4%	22.8%
3	27.3%	22.6%
2	26.2%	21.8%
1	20.5%	16.9%

5.5 DISCUSSION

Since the mean of the direct repair cost rate 21.5% agrees with that of the target value of the simulated earthquake damage scenario, this particle filter works well to estimate the

damage as a whole. However, examining the estimated results for each assembly, it is not always satisfying from the viewpoint of practical use. For instance, the repair-cost rate of the structural element on the 7th floor was estimated as 25.2% for the mean and 31.8% for the standard deviation, compared with the target value of 4.2%. In this demonstration, the gaps between the estimated and target values came from the fact that the particle filter could estimate *EDP*s only with a relatively large variation, which can be observed in Figures 5-15 and 5-16. In order to estimate the details more precisely, we may adopt more refined identification models such as using a more realistic nonlinear restoring-force model instead of the chosen nonlinear springs, or by increasing the number of independent parameters, or both. However, considering the accuracy of the fragility curves at present, which have a substantial influence on the uncertainty of damage estimates (Porter et al. 2002c), it may not be justified to simply make the identification model more complicated. When it is used in practice, it is important to consider the purpose of the estimation and to select a model that will be able to keep appropriate accuracy for that purpose.

In closing this chapter, we outline future work needed to bring the system into practical use. The first matter is concerned with determining the parameters shown in Table 5-8. A characteristic of the algorithm is that the initial values are rather irrelevant. The important value is the standard deviation used in the "random-walk" to generate samples at each time step. The values shown in Table 5-8 were determined by trial and error; however, there will be no room to apply a trial-and-error method in a practical application. It is necessary to perform a prior sensitivity analysis to examine the values and their valid limitations.

The second consideration for future work is to examine the minimum number of sensors required for good damage and loss estimation, as well as their appropriate installation points. Although they have become cheaper in recent years, the installation and maintenance cost of sensors can never be negligible. However, based on the study of the CUREE sample building, it is clear that more work is needed to reduce the uncertainty in the existing fragility functions, if possible, before the information from the sensors above the base can be successfully utilized to improve the accuracy of the damage and loss estimation. Alternatively, consideration could be given to sensors that relate more closely to the damage itself such as strain gauges at connections or on wall partitions, so that the particle filter receives information that is more closely linked to the damage state.

6 CONCLUSIONS AND FUTURE DIRECTIONS

Macroscopic versus component-level accuracy. In both the CUREE and Kajima case studies, we found that hindcasting of the overall system performance was very good, but prediction of detailed damage was poor. We infer that either (a) as-built conditions tend to differ substantially from those shown on the structural drawings, (b) inappropriate fragility functions were employed, or (c) both. It is noteworthy that in both case studies the estimated damage locations were systematically wrong, with models suggesting likely damage concentrated at one floor while actual damage occurred at another, which might in general lend weight to hypothesis (a).

Is a stochastic structural model needed? In the CUREE case study, we used a simplified particle filter to update EDP and found that the above-base sensor data adds little information to the performance prediction, probably because structural uncertainties are relatively unimportant compared with the uncertainties regarding assembly damageability. The implications are that real-time loss estimation may be insensitive to structural uncertainties; that costly simulations of structural response may be avoided; and that real-time loss estimation does not benefit significantly from instruments other than those at the base of the building.

Additional work required to prescribe particle-filter parameters. In the Kajima case study, we used the detailed particle filter, and found that it was necessary to tune the particle-filter parameters corresponding to the standard deviations in the "random-walk" models of the structural model parameters. Since practical applications to real-time loss estimation would not allow such tuning, additional study is required, either to prescribe appropriate particle-filter parameters for general use, or to try to sequentially estimate them as the data is processed in real time.

Opportunities for implementation. Because much of the cost of applying this RTLE algorithm results from the cost of instrumentation and the effort of setting up a structural model, the readiest application would be to instrumented buildings whose structural models are already available, e.g., those designed by Kajima. Furthermore, the methodology might produce the most value when applied to important facilities such as those required for emergency response, and buildings with high cost of testing for concealed damage, such as steel-frame structures.

Opportunities for further research. It would be interesting to follow up on the CUREE-Kajima Phase-V RTLE project with a study to determine under what conditions (location, structure type, time value, etc.) RTLE would be desirable from a building-owner's perspective. The value to Kajima is marketing and sales information. On the other hand, from an academic viewpoint, the study could explore (1) Bayesian updating of RTLE-produced damage states using observed damage or using sensors that are more closely related to the damage state (e.g., strain gauges at vulnerable connections); and (2) the value of information for expensive inspections. For example, if one inspects a connection with a modeled 50% failure probability and finds that the connection is undamaged, is it necessary to examine one with 10% failure probability?

7 REFERENCES CITED

Alspach, D.L. and H.W. Sorenson, 1972, Nonlinear Bayesian estimation using Gaussian sum approximations, *IEEE Transactions on Automatic Control*, **17**(4), 439-448.

American Society of Civil Engineers (ASCE), 2000, *FEMA-356: Prestandard and Commentary for the Seismic Rehabilitation of Buildings*, Washington, DC, 490 pp.

Applied Technology Council (ATC), 1985, *ATC-13: Earthquake Damage Evaluation Data for California*, Redwood City, CA, 492 pp.

Applied Technology Council (ATC), 1989, 1991, 1996, *ATC-20: Procedures for Postearthquake Safety Evaluation of Buildings*, Redwood City, CA, 144 pp.

Beck, J.L., 1978, *Determining Models of Structures from Earthquake Records*, EERL Report 78-01, Earthquake Engineering Research Laboratory, California Institute of Technology, Pasadena, California. http://resolver.caltech.edu/CaltechEERL:1978.EERL-78-01

Beck, J.L., A. Kiremidjian, S. Wilkie, A. Mason, T. Salmon, J. Goltz, R. Olson, J. Workman, A. Irfanoglu, and K. Porter, 1999, *Decision Support Tools for Earthquake Recovery of Businesses, Final Report, CUREe-Kajima Joint Research Program Phase III*, Consortium of Universities for Earthquake Engineering Research, Richmond, CA.

Beck, J.L., K.A. Porter, R. Shaikhutdinov, S. K. Au, K. Mizukoshi, M. Miyamura, H. Ishida, T. Moroi, Y. Tsukada, and M. Masuda, 2002, *Impact of Seismic Risk on Lifetime Property Values, Final Report*, Consortium of Universities for Research in Earthquake Engineering, Richmond, CA, http://resolver.caltech.edu/caltechEERL:2002.EERL-2002-04

Browning, J., Li, Y., Lynn, A., and Moehle, J.P., 2000, Performance assessment for a reinforced concrete frame building, *Earthquake Spectra*, **16** (3), 541-555.

Building Research Institute (BRI), 1977, *General Technology Development Project, New Earthquake Resistant Design Code (Draft)*, BRI report No. 70 (in Japanese.)

Building Research Institute (BRI), 1978, *Background Data about Deformation Capacity of Reinforced Concrete Columns Under Large Deformation (Part III)*, BRI Background Data No.21 (in Japanese.)

California Geological Survey, 2002a, *About CSMIP*, Sacramento, CA, http://www.consrv.ca.gov/cgs/smip/about.htm

California Geological Survey, 1999, *Strong Motion Data Center*, Sacramento, CA, http://docinet3.consrv.ca.gov/csmip/

California Institute of Technology (Caltech), 2002, *Caltech Civil Engineering and Applied Mechanics, Research*, Pasadena, CA, http://www.ce.caltech.edu/resources.html

California Strong Motion Instrumentation Program, 2001, *Van Nuys 7-Story Hotel, CSMIP Station No. 24386*, California Division of Mines and Geology, Sacramento, CA, ftp://ftp.consrv.ca.gov/pub/dmg/csmip/BuildingPages/BLD24386.HTM

Celebi, M., A. Sanli, M. Sinclair, S. Gallant, and D. Radulescuc, 2004, "Real-time seismic monitoring needs of a building owner—and the solution: a cooperative effort" *Earthquake Spectra*, 20 (2), 333–346.

Ching, J. and J.L. Beck, 2003, *Two-Step Bayesian Structural Health Monitoring Approach for IASC-ASCE Phase II Simulated and Experimental Benchmark Studies*, Earthquake Engineering Research Laboratory, California Institute of Technology, Pasadena, CA

Ching, J., J.L. Beck, K.A. Porter, and R.V. Shaikhutdinov, 2004, *Real-Time Bayesian State Estimation of Uncertain Dynamical System*, Earthquake Engineering Research Laboratory, California Institute of Technology, Pasadena, CA

CISN, 2001, *Welcome to the California Integrated Seismic Network*, http://www.cisn.org/index.html

Czarnecki, R.M., 1973, *Earthquake Damage to Tall Buildings, Structures Publication 359,* Massachusetts Institute of Technology, Cambridge, MA, 125 pp.

Doebling, S.W., C.R. Farrar, M.B. Prime, and D.W. Shevitz, 1996, *Damage Identification and Health Monitoring of Structural and Mechanical Systems From Changes in Their Vibration Characteristics: A Literature Review*, Los Alamos National Laboratory Report LA-13070-MS.

Doucet, A. and S. Godsill, 1998, *On Sequential Simulation-based Methods for Bayesian Filtering*, Report CUED/F-INFENG/TR310, Department of Engineering, Cambridge University.

Earthquake Engineering Research Institute (EERI), 1996, Supplement C to Volume 11, April 1995, Northridge Earthquake Reconnaissance Report, vol. 1-2, *Earthquake Spectra*.

Farhat, C. and F.M. Hemez, 1993, Updating finite dynamics models using an element-by element sensitivity methodology, *AIAA Journal*, **31**(9), 1702-1711.

Federal Emergency Management Agency, 1997, *FEMA-273: NEHRP Guidelines for the Seismic Rehabilitation of Buildings,* Washington, DC, 386 pp.

Federal Emergency Management Agency, 1999, *HAZUS99,* Washington, D.C., http://www.fema.gov/hazus

Gordon, N.J., D.J. Salmond, and A.F.M. Smith, 1993, Novel approach to nonlinear/non-Gaussian Bayesian state estimation, *IEEE Proceedings-F*, **140**(2): 107-113.

Hachem, M.M., 2000, *BiSpec Version 1.1.2*, University of California, Berkeley, California.

Hart, G.C., and Vasdevan, R., 1975, Earthquake Design of Buildings: Damping, *Journal of the Structural Division*, 101 (ST1), Jan 1975, 11-29.

Hoshiya, M and E. Saito, 1984, Structural identification by extended Kalman filter, *Journal of Engineering Mechanics*, **110**(12), p. 1757.

Hutchinson, T., 2003, Analytical Modeling of Foundation, in Krawinkler, H., ed., *PEER Performance-Based Earthquake Engineering Methodology: Structural and Architectural Aspects*, Pacific Earthquake Engineering Research (PEER) Center, Richmond, CA

Islam, M.S., 1996a, Analysis of the response of an instrumented 7-story nonductile concrete frame building damaged during the Northridge Earthquake, *Proceedings of the 1996 Annual Meeting of the Los Angeles Tall Buildings Structural Council, May 10, 1996, Los Angeles, CA.*

Islam, M.S., 1996b, Holiday Inn, *1994 Northridge Earthquake Buildings Case Study Project Proposition 122: Product 3.2*, Seismic Safety Commission, Sacramento CA, 189-233.

Islam, M.S., M. Gupta, and S. Kunnath, 1998, Critical review of the state-of-the-art analytical tools and acceptance criterion in light of observed response of an instrumented nonductile concrete frame building, *Proceedings, Sixth US National Conference on Earthquake Engineering, Seattle, Washington, May 31-June 4, 1998,* Earthquake Engineering Research Institute, Oakland CA, 11 pp.

Japan Building Disaster Prevention Association, 1991, *Standard of Damage Level Judgment for Earthquake-Damaged Buildings and Restoring Guideline* (in Japanese)

Jaynes, E.T., 2003, *Probability Theory: The Logic of Science*. Cambridge, United Kingdom: Cambridge University Press.

Jazwinski, A.H., 1970, *Stochastic Processes and Filtering Theory*, Academic Press, New York.

Jennings, P.C., 1971, *Engineering Features of the San Fernando Earthquake of February 9, 1971, Report EERL 71 – 02*, California Institute of Technology, Pasadena, CA.

John A. Blume & Associates, 1973, "Holiday Inn (29)" *San Fernando, California, Earthquake of February 9, 1971, vol. 1, part a,* National Oceanographic and Aviation Administration, Washington, DC, 359-393

Jones, A.L., S.L. Kramer, and P. Arduino, 2001, *Estimation of Uncertainty in Geotechnical Properties for Performance-Based Earthquake Engineering*, Report PEER 2002/16, Pacific Earthquake Engineering Research (PEER), Center, Richmond, CA

Julier, S.J., J.K. Uhlmann, and H.F. Durrant-Whyte, 2000, A new method for the nonlinear transformation of means and covariances in filters and estimators, *IEEE Transactions on Automatic Control*, **45**(3), 477-482.

Kalman, R.E., 1960, A new approach to linear filtering and prediction problems, *J. Basic Engr.*, **82**D, 35-45.

Kalman, R.E. and R.S. Bucy, 1961, New results in linear filtering and prediction problems, *J. Basic Engr.*, **83**D.

Kim, H.M. and T.J. Bartkowicz, 1993, Damage detection and helath monitoring of large space structures, *Sound and Vibration*, **27**(6), 12-17.

Kitagawa, G., 1996, Monte Carlo filter and smoother for non-Gaussian nonlinear state space models, *Journal of Computational and Graphical Statistics*, **5**, 1-25.

Koh, C.G. and S.M. See, 1994, Identification and uncertainty estimation of structural parameters. *J. Engng. Mech.*, **120**(6), p. 1219.

Kustu, O., D.D. Miller, and S.T. Brokken, 1982, *Development of Damage Functions for Highrise Building Components*, for the US Department of Energy, URS/John A Blume & Associates, San Francisco, CA

Lam, H.F. and J.L. Beck, 2001-2004, *Caltech Online Monitoring and Evaluation Testbeds (COMET)*, California Institute of Technology, Pasadena, CA, http://comet.caltech.edu

Levy, M. and M. Salvadori, 1992, *Why Buildings Fall Down*. W.W. Norton and Company, New York, NY.

Li, Y.R. and J.O. Jirsa, 1998, Nonlinear analyses of an instrumented structure damaged in the 1994 Northridge Earthquake, *Earthquake Spectra*, **14** (2), 245-264.

Lizundia, B., W. Dong, W.T. Holmes, and R. Reitherman, 1993, *Analysis of Unreinforced Masonry Building Damage Patterns in the Loma Prieta Earthquake and Improvement of Loss Estimation Methodologies: Technical Report to the USGS*, USGS Award 14-08-001-G1951, Rutherford & Chekene, Consulting Engineers, San Francisco, CA, 247 pp.

Martel, R.R., 1936, A report on earthquake damage to type III buildings, *Earthquake Investigations in California, 1934-1935*, Special Publication No. 201, U.S. Department of Commerce Coast and Geodetic Survey, Washington, DC, 143-160

McClure, F.E., 1973, *Performance of Single-Family Dwellings in the San Fernando Earthquake of February 9, 1971*, National Oceanic and Atmospheric Administration, Washington, D.C., 95 pp.

McVerry, G.H., 1979, *Frequency Domain Identification of Structural Models for Earthquake Records, Report No. EERL 79-02*, California Institute of Technology, Pasadena, CA, http://caltecheerl.library.caltech.edu/documents/disk0/00/00/02/23/00000223-00/7902.pdf, 221 pp.

Nagano, M., S. Ohno, K. Koyamada, and K. Kato, 2001, Bedrock motions and site amplifications in Kobe city during the 1995 Hyogo-ken Nanbu Earthquake, *Journal of Structure and Construction Engineering*, AIJ, No. 511, 77-84, Sep. 1998. (In Japanese)

NTT Facilities 2004, *NTT Facilities*, http://www.ntt-f.co.jp/rd/jisikan/jisikan01.html

Porter, K.A., 2000, *Assembly-Based Vulnerability of Buildings and its Uses in Seismic Performance Evaluation and Risk-Management Decision-Making*, Doctoral Dissertation, Stanford University, Stanford, CA, and ProQuest Co., Ann Arbor, MI, pub. 99-95274, 196 pp., http://wwwlib.umi.com/dissertations/preview/9995274

Ott, J. and R.G. O'lone, 1988, 737 fuselage separation spurs review of safeguards, *Aviation Week and Space Technology*, 92-95.

Pacific Earthquake Engineering Center (PEER), 2004, http://peer.berkeley.edu

Porter, K.A., and A.S. Kiremidjian, 2001, *Assembly-Based Vulnerability and its Uses in Seismic Performance Evaluation and Risk-Management Decision-Making*, Report No. 139, John A.

Blume Earthquake Engineering Center, Stanford, CA, 214 pp., http://keithp.caltech.edu/publications.htm

Porter, K.A., J.L. Beck, H.A. Seligson, C.R. Scawthorn, L.T. Tobin, and T. Boyd, 2002a, *Improving Loss Estimation for Woodframe Buildings*, Consortium of Universities for Research in Earthquake Engineering, Richmond, CA, 136 pp., http://resolver.caltech.edu/caltechEERL:2002.EERL-2002-01 (main report) http://resolver.caltech.edu/caltechEERL:2002.EERL-2002-02 (appendices)

Porter, K.A., J.L., Beck, and R.V., Shaikhutdinov, 2002b, *Investigation of Sensitivity of Building Loss Estimates to Major Uncertain Variables for the Van Nuys Testbed*, Pacific Earthquake Engineering Research Center, Richmond, CA.

Porter, K.A., J.L. Beck, and R.V. Shaikhutdinov, 2002c, Sensitivity of building loss estimates to major uncertain variables, *Earthquake Spectra*, **18** (4)

Rissman and Rissman Associates, 1965, *Holiday Inn Van Nuys Structural Drawings*, Pacific Palisades, CA.

RS Means Co., Inc., 1997, *Means Assemblies Cost Data*, Kingston, MA.

RS Means Co., Inc., 2001, *Means Square Foot Costs*, Kingston, MA.

Rutherford & Chekene, 1990, *Seismic Retrofitting Alternatives for San Francisco's Unreinforced Masonry Buildings: Estimates of Construction Cost & Seismic Damage*, San Francisco, CA, 360 pp.

SAC Joint Venture, 2000, *FEMA 352, Recommended Postearthquake Evaluation and Repair Criteria for Welded Steel Moment-Frame Buildings*, Federal Emergency Management Agency, Washington, D.C., http://www.fema.gov/hazards/earthquakes/fema352.shtm

Schierle, G.G., 2002a, *Northridge Earthquake Field Investigations: Statistical Analysis of Woodframe Damage*, Consortium of Universities for Research in Earthquake Engineering, Richmond, CA, 151 pp.

Scholl, R.E., O. Kustu, C.L. Perry, and J.M. Zanetti, 1982, *Seismic Damage Assessment for High-Rise Buildings, URS/JAB 8020*, URS/John A. Blume & Associates, Engineers, San Francisco, CA, 321 pp.

Sohn, H., Farrar, C.R. Farrar, F.M. Hemez, D.D. Shunk, D.W. Stinemates, B.R. Nadler, and J.J. Czarnecki, *A Review of Structural Health Monitoring Literature: 1996-2001*, Los Alamos National Laboratory Report LA-13976-MS, January 2004.

Structural Engineers Association of California (SEAOC), 1996, Vision 2000, conceptual framework for performance-based seismic design, *Recommended Lateral Force Requirements and Commentary, 1996, 6th Edition*, Sacramento, CA, 391-416

Trifunac, M.D., S.S. Ivanovic, and M.I. Todorovska, 1999, *Instrumented 7-Storey Reinforced Concrete Building in Van Nuys, California: Description of the Damage from the 1994 Northridge Earthquake and Strong Motion Data*, Report CE 99-02, University of Southern California Department of Civil Engineering, Los Angeles, CA

Trifunac, M.D., and T.Y. Hao, 2001, *7-Storey Reinforced Concrete Building in Van Nuys, California: Photographs of the Damage from the 1994 Northridge Earthquake, Report CE 01-05*, University of Southern California Department of Civil Engineering, Los Angeles, CA, 91 pp, http://www.usc.edu/dept/civil_eng/Earthquake_eng/CE_Reports/01_05/01_05_ALL.PDF

TriNet, 2001, *TriNet ShakeMap: About the Maps*, California Institute of Technology and U.S. Geological Survey, Pasadena, CA, http://www.trinet.org/shake/about.html

TriNet, 2002, *TriNet, The Seismic System for Southern California*, California Institute of Technology and U.S. Geological Survey, Pasadena, CA, http://www.trinet.org

U.S. Geological Survey, 2000, *Advanced National Seismic System-ANSS*, http://www.anss.org/

van der Merwe, R. and E.A. Wan, 2003, Gaussian mixture sigma-point particle filters for sequential probabilistic inference in dynamic state-space models, *Proceedings of IEEE International Conference on Acoustics, Speech and Signal Processing (ICASSP)*, Hong Kong.

van der Merwe, R., N. de Freitas, A. Doucet, and E.A. Wan, 2000, *The Unscented Particle Filter*, Report CUED/F-INFENG/TR380, Department of Engineering, Cambridge University.

Vanik M.W., J.L. Beck, and S.K. Au, 2000, A Bayesian probabilistic approach to structural health monitoring, *Journal of Engineering Mechanic*s, **126**, 738-745.

Wan, E.A. and R. van der Merwe, 2000, The unscented Kalman filter for nonlinear estimation, *Proceedings of Symposium 2000 on Adaptive Systems for Signal Processing, Communication and Control*, IEEE, Lake Louise, Alberta, Canada.

Yun, C.B. and M. Shinozuka, 1980, Identification of nonlinear dynamic systems, *Journal of Structural Engineering*, **8**(2), 187-203.

APPENDIX A: CHING ET AL. 2004

A BAYESIAN STATE ESTIMATION METHOD FOR NONLINEAR SYSTEMS AND ITS APPLICATION TO RECORDED SEISMIC RESPONSE

JIANYE CHING[1], JAMES L. BECK[2], KEITH A. PORTER[3] AND RUSTEM SHAIKHUTDINOV[4]

ABSTRACT

The focus of this paper is to demonstrate the application of a recently developed Bayesian state estimation method to the recorded seismic response of a building and to discuss the issue of model selection. The method, known as the particle filter, is based on stochastic simulation. Unlike the well-known extended Kalman filter, it is applicable to highly nonlinear systems with non-Gaussian uncertainties. Recently developed techniques that improve the convergence of the particle filter simulations are also introduced and discussed.

The particle filter is applied to strong motion data recorded in the 1994 Northridge earthquake in a 7-story hotel whose structural system consists of non-ductile reinforced-concrete moment frames, two of which were severely damaged during the earthquake. We address the issue of model selection. Two identification models are proposed: a time-varying linear model and a simplified time-varying nonlinear degradation model. The latter is derived from a nonlinear finite-element model of the building previously developed at Caltech. For the former model, the resulting performance is poor since the parameters need to vary significantly with time in order to capture the structural degradation of the building during the earthquake. The latter model performs better because it is able to characterize this degradation to a certain extent even with its

[1] George W. Housner Postodoctoral Fellow, Dept. of Civil Engineering, California Institute of Technology, Pasadena, CA 91125, USA. Email: jyching@netzero.net
[2] Professor of Applied Mechanics and Civil Engineering, Dept. of Civil Engineering, California Institute of Technology, Pasadena, CA 91125, USA. Email: jimbeck@its.caltech.edu
[3] Senior George W. Housner Researcher, Dept. of Civil Engineering, California Institute of Technology, Pasadena, CA 91125, USA. Email: keithp@its.caltech.edu
[4] Graduate student, Dept. of Civil Engineering, California Institute of Technology, Pasadena, CA 91125, USA. Email: rustem@its.caltech.edu

parameters fixed. For this case study, the particle filter provides consistent state and parameter estimates, in contrast to the extended Kalman filter, which provides inconsistent estimates. It is concluded that for a state estimation procedure to be successful, at least two factors are essential: an appropriate estimation algorithm and a suitable identification model.

Key words: Bayesian analysis, Monte Carlo simulation, Stochastic simulation, Importance sampling, Particle filter, Model selection, Seismic response, State estimation, System identification

1. INTRODUCTION

1.1 Applications of state estimation in civil engineering

State estimation is the process of using dynamic data from a system to estimate quantities that give a complete description of the system state according to some representative model of it. State estimation has the potential to be widely applied in civil engineering. For instance, real-time structural health monitoring techniques that detect changes of dynamical properties of structural systems during earthquakes can be cast into a real-time state estimation problem. More generally, real-time system identification is useful to understand better the nonlinear behavior of structures subject to seismic loading. A real-time state-estimation methodology can be used for this purpose. For structural control, the ability to estimate the system state in real time can help to accomplish an efficient control strategy.

Because of their wide applicability, real-time state-estimation and identification methods have been studied in civil engineering for various purposes. Beck (1978) used an invariant-embedding filter for modal identification. Yun and Shinozuka (1980) used an extended Kalman filter to study nonlinear fluid-structure interaction. Hoshiya and Saito (1984) used the extended Kalman filter for structural system identification. Lin *et al.* (1990) developed a real-time identification methodology for better understanding of the degrading behavior of structures subject to

dynamic loads. Ghanem and Shinozuka (1995) presented several different adaptive estimation techniques (e.g. extended Kalman filter, recursive least squares, recursive prediction error methods) and verified them using experimental data (Shinozuka and Ghanem 1995). Glaser (1996) used the Kalman filter to identify the time-varying natural frequency and damping of a liquefied soil to get insight into the liquefaction phenomenon. Sato and Qi (1998) derived an adaptive H_∞ filter and applied it to time-varying linear and nonlinear structural systems in which displacements and velocities of the floors are measured. Smyth *et al.* (1999) formulated an adaptive least-squares algorithm for identifying multi-degree of freedom nonlinear hysteretic systems for control and monitoring.

1.2 Development of Bayesian state-estimation algorithms

Among state-estimation methodologies, those founded on the Bayesian framework are powerful because of the following facts: (1) they are rigorously based on the probability axioms and therefore preserve information; (2) they give the probability density function (PDF) of the system state conditioned on the available information, which can then be used for any probability-based structural health monitoring, system identification, reliability assessment or control technique. With the PDF available, one can estimate the state and also give a description of the associated uncertainties. The first Bayesian state-estimation algorithm was formulated by Kalman for linear systems with Gaussian uncertainties; it is well known as the Kalman filter (KF) (Kalman 1960; Kalman and Bucy 1961). Later, the KF was modified to give the extended Kalman filter (EKF, Jazwinski 1970) to accommodate lightly nonlinear systems. The EKF has been the dominant Bayesian state-estimation algorithm for nonlinear systems and non-Gaussian uncertainties for the last 30 years.

Although the EKF has been widely used, it is only reliable for systems that are almost linear on the time scale of the updating intervals (Julier *et al.* 2000; Wan and van der Merwe 2000). However, civil-engineering systems are often highly nonlinear when subject to severe loading events, in which the applicability of the Kalman filter and extended Kalman filter is questionable. These older techniques have been used by civil engineering researchers for decades (Beck 1978; Yun and Shinozuka 1980; Hoshiya and Saito 1984; Koh and See 1994) although their applicability for nonlinear systems and non-Gaussian uncertainties is seldom verified either empirically or theoretically.

Several important breakthroughs (Alspach and Sorenson 1972; Gordon *et al.* 1993; Kitagawa 1996; Doucet *et al.* 2000; Julier *et al.* 2000) have produced Bayesian state-estimation algorithms that are applicable to highly nonlinear systems. State estimation for general nonlinear dynamical systems is still an active research area, and novel techniques (e.g., van der Merwe *et al.* 2000; van der Merwe and Wan 2003) can be found in the most recent signal-processing literature. Although these breakthroughs have had significant impact in the area of signal processing, they are rarely seen in the civil-engineering literature. Exceptions include Yoshida and Sato (2002) and Maruyama and Hoshiya (2003), who have implemented an improved version of Kitagawa's approach for system identification and damage detection.

1.3 Scope of this paper

In this paper, we investigate the application to recorded seismic response of a Bayesian state estimation method called the particle filter (PF) that employs stochastic simulation. The PF technique has the following advantages: 1) it is applicable to highly nonlinear systems with non-Gaussian uncertainties; 2) it is not limited to the first two moments as in the KF and EKF; and 3) as the sample size approaches infinity, the resulting state estimates converge to their expected

values. However, the simulation is usually computationally expensive. Sometimes the state estimates can be inaccurate because of insufficient samples. We introduce several recent developments that address these difficulties and present new techniques that are useful to improve the convergence. We also compare the performance of the EKF with that of the the PF using a case study.

We explicitly address the issue of model selection in this paper using two different identification models: a time-varying linear structural model and a simplified nonlinear model. The former has been popular for system identification involving degrading structural systems (e.g., Lin *et al.* 1990). However, we show that the linear time-varying model does not perform well for the real-data case study. We discuss the drawbacks of the linear time-varying model and develop the simplified nonlinear model that works better.

This paper has the following structure: In Section 2, we define the general problem of Bayesian state estimation for nonlinear dynamical systems. In Section 3, we review the KF and EKF algorithms. In Section 4, we introduce importance-sampling filter techniques. In Section 5, we present a case study of the recored seismic response of a building to demonstrate the application of the different methods and models.

2. STATE ESTIMATION

Consider the following discrete-time state-space model of a dynamical system:

$$x_k = f_{k-1}(x_{k-1}, u_{k-1}, w_k) \qquad y_k = h_k(x_k, u_k, v_k) \qquad k = 1, 2...T \qquad (1)$$

The two equations in (1) are called, from left to right, state transition (evolution or predictor) and observation (output or corrector) equations, respectively. In this equation, $x_k \in R^n$, $u_k \in R^p$ and $y_k \in R^q$ are the system state, input (known excitation) and observed output at time k; $w_k \in R^l$ and $v_k \in R^m$ are introduced to account for unknown disturbances, model errors and measurement

noise; f_k is the prescribed state transition function at time k; and h_k is the prescribed observation function at time k. The values of the variables x_k, y_k, w_k and v_k are uncertain and so are modeled as random variables, while u_k is considered to be a known excitation.

For each time k, the dynamical system input u_k and output $\hat{y}_k$ are measured. (In order to avoid confusion, we denote the observed output value by $\hat{y}_k$). We denote $\{\hat{y}_1, \hat{y}_2, ..., \hat{y}_k\}$ and $\{u_1, u_2, ..., u_k\}$ by $\hat{Y}_k$ and U_k, respectively. Our goal is to evaluate the conditional PDF $p(x_k \mid \hat{Y}_k)$ for the state x_k at every time k in a Markovian fashion, i.e., to update this conditional sequentially PDF using the observed system input and output up to the current time, using only the oformation produced at the end of the previous timestep and observation data from the current timestep, based on prescribed probabilistic models for w_k and v_k. From this conditional PDF, some important features of the state, such as the conditional expectation $E(x_k \mid \hat{Y}_k)$ and conditional covariance matrix $Cov(x_k \mid \hat{Y}_k)$, can be estimated. Note that the conditioning of every PDF on U_k is implicit.

The basic equations for updating $p(x_{k-1} \mid \hat{Y}_{k-1})$ to $p(x_k \mid \hat{Y}_k)$ are the predictor and updater (or corrector) equations that follow from the Theorem of Total Probability and Bayes Theorem, respectively:

$$
\begin{aligned}
p(x_k \mid \hat{Y}_{k-1}) &= \int p(x_k \mid x_{k-1}) p(x_{k-1} \mid \hat{Y}_{k-1}) dx_{k-1} \\
p(x_k \mid \hat{Y}_k) &= \frac{p(\hat{y}_k \mid x_k) p(x_k \mid \hat{Y}_{k-1})}{\int p(\hat{y}_k \mid x_k) p(x_k \mid \hat{Y}_{k-1}) dx_k} = \frac{p(\hat{y}_k \mid x_k) p(x_k \mid \hat{Y}_{k-1})}{p(\hat{y}_k \mid \hat{Y}_{k-1})}
\end{aligned}
\tag{2}
$$

where $\hat{Y}_{k-1}$ is dropped in $p(x_k \mid x_{k-1})$ and $p(\hat{y}_k \mid x_k)$ because the models for the state transition and observation PDFs make it irrelevant. The main challenge in Bayesian state estimation for

nonlinear systems is that these basic equations cannot be readily evaluated because they involve high-dimensional integrations.

3. KALMAN FILTER

When f_k and h_k in (1) are both linear in u_k, x_k, w_k and v_k, i.e.

$$f_k(x_k, u_k, w_k) = A_k x_k + B_k u_k + G_k w_k \qquad h_k(x_k, u_k, v_k) = C_k x_k + D_k u_k + H_k v_k \tag{3}$$

and w_k and v_k are zero-mean independent Gaussian random variables, the conditional PDF is also Gaussian and can be updated analytically. Furthermore, it is sufficient to update the first two moments because they completely specify this conditional PDF. The updating algorithm is the well-known Kalman filter (KF). It comprises two steps, the predictor (uncertainty-propagation) and updater (estimation) steps.

In the uncertainty-propagation step, the goal is to compute $p(x_k, y_k \mid \hat{Y}_{k-1})$ from $p(x_{k-1} \mid \hat{Y}_{k-1})$. First, $p(x_k \mid \hat{Y}_{k-1})$ is computed based on $p(x_{k-1} \mid \hat{Y}_{k-1})$ using the following moment equations:

$$\begin{aligned} x_{k|k-1} &\equiv E(x_k \mid \hat{Y}_{k-1}) = A_{k-1} x_{k-1|k-1} + B_{k-1} u_{k-1} \\ P_{k|k-1} &\equiv Cov(x_k \mid \hat{Y}_{k-1}) = A_{k-1} P_{k-1|k-1} A_{k-1}^T + G_{k-1} G_{k-1}^T \end{aligned} \tag{4}$$

Note that the values $x_{0|0}$ and $P_{0|0}$ have to be given prior to the initialization of the algorithm. Second, $p(y_k \mid \hat{Y}_{k-1})$ is computed based on $p(x_k \mid \hat{Y}_{k-1})$ and u_k using the following moment equations:

$$\begin{aligned} y_{k|k-1} &\equiv E(y_k \mid \hat{Y}_{k-1}) = C_k x_{k|k-1} + D_k u_k \\ P^y_{k|k-1} &\equiv Cov(y_k \mid \hat{Y}_{k-1}) = C_k P_{k|k-1} C_k^T + H_k H_k^T \end{aligned} \tag{5}$$

and finally, the conditional covariance between x_k and y_k is the $n \times q$ matrix computed as follows:

$$P_{k|k-1}^{xy} \equiv Cov(x_k, y_k \mid \hat{Y}_{k-1}) = P_{k|k-1} C_k^T \tag{6}$$

This completes the computation of all the moments needed to specify the Gaussian PDF $p(x_k, y_k \mid \hat{Y}_{k-1})$.

In the estimation step, $p(x_k \mid \hat{Y}_k)$ is updated based on (2):

$$\begin{aligned} p(x_k \mid \hat{Y}_k) &= \frac{p(\hat{y}_k \mid x_k) p(x_k \mid \hat{Y}_{k-1})}{p(\hat{y}_k \mid \hat{Y}_{k-1})} \\ &= const \cdot e^{\frac{-1}{2}\left[\left(\hat{y}_k - C_k x_k - D_k u_k\right)^T \left(H_k H_k^T\right)^{-1} \left(\hat{y}_k - C_k x_k - D_k u_k\right)\right]} \cdot e^{\frac{-1}{2}\left[\left(x_k - x_{k|k-1}\right)^T \left(P_{k|k-1}\right)^{-1} \left(x_k - x_{k|k-1}\right)\right]} \end{aligned} \tag{7}$$

where *const* is a quantity not depending on x_k. Because $p(x_k \mid \hat{Y}_k)$ is Gaussian, differentiating $p(x_k \mid \hat{Y}_k)$ with respect to x_k and solving for zero, we obtain $x_{k|k}$; on the other hand, $P_{k|k}$ is equal to the negative of the inverse of the Hessian of $\log\left[p(x_k \mid \hat{Y}_k)\right]$:

$$\begin{aligned} x_{k|k} &= x_{k|k-1} + \left[I + P_{k|k-1} C_k^T \left(H_k H_k^T\right)^{-1} C_k\right]^{-1} \cdot P_{k|k-1} C_k^T \left(H_k H_k^T\right)^{-1} \cdot \left(\hat{y}_k - y_{k|k-1}\right) \\ P_{k|k} &= \left[P_{k|k-1}^{-1} + C_k^T \left(H_k H_k^T\right)^{-1} C_k\right]^{-1} \end{aligned} \tag{8}$$

Making use of the following lemmas

$$\left(I + PQ\right)^{-1} P = P\left(I + QP\right)^{-1} \qquad \left(A^{-1} + VC^{-1}V^T\right)^{-1} = A - AV\left(C + V^T AV\right)^{-1} V^T A \tag{9}$$

where P and Q are conformable matrices, A and C are positive definite, we conclude with the following equations for the estimation step:

$$\begin{aligned} x_{k|k} &= x_{k|k-1} + P_{k|k-1}^{xy} \cdot (P_{k|k-1}^{y})^{-1} \cdot (\hat{y}_k - y_{k|k-1}) \\ P_{k|k} &= P_{k|k-1} - P_{k|k-1}^{xy} \cdot (P_{k|k-1}^{y})^{-1} \cdot P_{k|k-1}^{xy\ T} \end{aligned} \tag{10}$$

3.1 Extended Kalman filter

Many dynamical systems exhibit nonlinear behavior, and the direct use of KF is prohibited. However, if f_k and h_k are only slightly nonlinear, an approximation for KF can be derived by linearizing the uncertainty propagation and estimation steps. The resulting filter is the well-known extended Kalman filter (EKF). To explain the linearization (LN) technique for the uncertainty propagation step, we consider the following general uncertainty propagation problem:

$$Y = f(X) \tag{11}$$

where $X \in R^n$ and $Y \in R^m$ are uncertain vectors. Using Taylor series expansion around $X = EX$, we have

$$f(X) = f(EX) + \nabla_x f \cdot (X - EX) + HOT \tag{12}$$

where $\nabla_x f$ is the Jacobian matrix evaluated at $x = EX$; HOT denotes the higher order terms. As a result, the first two moments of Y are

$$EY = f(EX) + HOT \tag{13}$$

and

$$Cov(Y) = (\nabla_x f) \cdot Cov(X) \cdot (\nabla_x f)^T + HOT \tag{14}$$

Under the assumption that $f(x)$ is nearly linear near $x = EX$, all higher order terms are relatively small; therefore, EY and $Cov(Y)$ are approximated by

$$EY_{LN} = f(EX) \qquad Cov(Y)_{LN} = (\nabla_x f) \cdot Cov(X) \cdot (\nabla_x f)^T \tag{15}$$

where EY_{LN} and $Cov(Y)_{LN}$ denote the approximations of the LN technique for EY and $Cov(Y)$. The approximations EY_{LN} and $Cov(Y)_{LN}$ are accurate estimates of EY and $Cov(Y)$ if $f(x)$ is almost linear on the support region of the PDF of X and become exact when $f(x)$ is linear in

x. On the other hand, the approximations are poor if $f(x)$ is highly nonlinear on the support region of the PDF of X.

For the uncertainty propagation step in EKF, the goal is to find the LN approximations of $x_{k|k-1}$, $P_{k|k-1}$, $y_{k|k-1}$, $P^{y}_{k|k-1}$ and $P^{xy}_{k|k-1}$ based on $x_{k-1|k-1}$ and $P_{k-1|k-1}$. To simplify the notation, we define $z_k = [x_k^T \quad w_k^T \quad v_k^T]^T$ and $z_{k|k} = [x_{k|k}^T \quad 0^T \quad 0^T]^T \in R^{n+l+m}$, so $f_k(x_k, u_k, w_k) = f_k(z_k, u_k)$.

When propagating from $[x_{k-1|k-1}, P_{k-1|k-1}]$ to $[x_{k|k-1}, P_{k|k-1}]$, we expand $f_{k-1}(z_{k-1}, u_{k-1})$ in the neighborhood of $z_{k-1|k-1}$. With the LN approximation, we get

$$x_{k|k-1} = E[f_{k-1}(z_{k-1}, u_{k-1})] \approx f_{k-1}(z_{k-1|k-1}, u_{k-1}) \equiv x^{LN}_{k|k-1} \tag{16}$$

and

$$\begin{aligned} P_{k|k-1} &\approx (\nabla_z f_{k-1}) \cdot E\left\{(z_{k-1} - z_{k-1|k-1})(z_{k-1} - z_{k-1|k-1})^T \mid D_{k-1}\right\} \cdot (\nabla_z f_{k-1})^T \\ &= (\nabla_z f_{k-1}) \cdot Cov\left\{z_{k-1} \mid D_{k-1}\right\} \cdot (\nabla_z f_{k-1})^T \equiv P^{LN}_{k|k-1} \end{aligned} \tag{17}$$

where $\nabla_z f_{k-1} \in R^{n\times(n+l+m)}$ is the Jacobian matrix evaluated at $z_{k-1} = z_{k-1|k-1}$. It can be seen that

$$P^{LN}_{k|k-1} = \left(A^{LN}_{k-1}\right) \cdot P_{k-1|k-1} \cdot \left(A^{LN}_{k-1}\right)^T + \left(G^{LN}_{k-1}\right) \cdot \left(G^{LN}_{k-1}\right)^T \tag{18}$$

where $A^{LN}_{k-1} \equiv \nabla_x f_{k-1}\big|_{z_{k-1}=z_{k-1|k-1}} \in R^{n\times n}$ and $G^{LN}_{k-1} \equiv \nabla_w f_{k-1}\big|_{z_{k-1}=z_{k-1|k-1}} \in R^{n\times l}$ are the Jacobian matrices. Similarly, h_k is also linearized to get the approximations for $y_{k|k-1}$, $P^{y}_{k|k-1}$ and $P^{xy}_{k|k-1}$:

$$\begin{aligned} y_{k|k-1} &\approx h_{k-1}(x^{LN}_{k|k-1}, u_k, 0) \equiv y^{LN}_{k|k-1} \\ P^{y}_{k|k-1} &\approx \left(C^{LN}_k\right) P^{LN}_{k|k-1} \left(C^{LN}_k\right)^T + \left(H^{LN}_k\right)\left(H^{LN}_k\right)^T \equiv P^{y,LN}_{k|k-1} \\ P^{xy}_{k|k-1} &\approx P^{LN}_{k|k-1} \left(C^{LN}_k\right)^T \equiv P^{xy,LN}_{k|k-1} \end{aligned} \tag{19}$$

where $C^{LN}_k \equiv \nabla_x h_k\big|_{x_k = x_{k|k-1}, v_k = 0} \in R^{q\times n}$ and $H^{LN}_k \equiv \nabla_v h_k\big|_{x_k = x_{k|k-1}, v_k = 0} \in R^{q\times m}$.

For the estimation step, (10) can still be used as an approximation. If f_k and h_k are indeed linear, EKF is identical to KF. The degree of accuracy of EKF relies on the validity of the linear approximation. Notice that EKF is not suitable for tracking multi-modal or highly non-Gaussian conditional PDFs due to the fact that it only updates the first two moments.

When the system parameters are unknown, it is important to also estimate them. Uncertain parameters can be augmented into system states and estimated using EKF. However, since the augmented state-space model is always nonlinear (even if the original model had linear dynamics), the EKF may perform poorly. Also, the EKF algorithm is not suitable for estimating unknown parameters used to parameterize the amplitudes of the uncertainty terms w_k and v_k. We have discussed this issue and provided solutions in Ching *et al.* (2004).

4. PARTICLE FILTERS

We have seen that EKF can only propagate and estimate the first two moments of the conditional PDF. For systems with non-Gaussian uncertainties, it is often desirable to propagate and estimate the conditional PDF itself; however, doing so thoroughly requires an infinite number of parameters to represent the functional form of the conditional PDF. An alternative is to conduct stochastic simulation by drawing samples from the conditional PDF so that the conditional expectation of any function of x_k can be consistently estimated. We focus on the stochastic simulation techniques in this section and use the term particle filters (PF) to denote the resulting algorithms (following van der Merwe *et al.* 2000; Doucet and Andrieu 2000). Similar PF algorithms have been called Monte Carlo filters by Kitagawa (1996) and sequential Monte Carlo Bayesian filters by Doucet and Godsill (1998) and Doucet *et al.* (2000).

4.1 Basic equations

We first present some basic equations that are useful throughout this section. Let $X_k = \{x_0, x_1, ..., x_k\}$, then according to Bayes rule,

$$p(X_k \mid \hat{Y}_k) = \frac{p(X_k, \hat{Y}_k)}{p(\hat{Y}_k)} = \frac{p(X_{k-1}, x_k, \hat{Y}_{k-1}, \hat{y}_k)}{p(\hat{Y}_k)}$$
$$= \frac{p(X_{k-1}, \hat{Y}_{k-1}) \cdot p(x_k, \hat{y}_k \mid X_{k-1}, \hat{Y}_{k-1})}{p(\hat{Y}_k)} = \frac{p(X_{k-1} \mid \hat{Y}_{k-1}) \cdot p(x_k, \hat{y}_k \mid X_{k-1}, \hat{Y}_{k-1})}{p(\hat{y}_k \mid \hat{Y}_{k-1})}$$
$$= p(X_{k-1} \mid \hat{Y}_{k-1}) \cdot \frac{p(\hat{y}_k \mid x_k, X_{k-1}, \hat{Y}_{k-1}) \cdot p(x_k \mid X_{k-1}, \hat{Y}_{k-1})}{p(\hat{y}_k \mid \hat{Y}_{k-1})} = p(X_{k-1} \mid \hat{Y}_{k-1}) \cdot \frac{p(\hat{y}_k \mid x_k) \cdot p(x_k \mid x_{k-1})}{p(\hat{y}_k \mid \hat{Y}_{k-1})} \qquad (20)$$

where we have used the fact that $p(\hat{y}_k \mid x_k, X_{k-1}, \hat{Y}_{k-1}) = p(\hat{y}_k \mid x_k)$ and that $p(x_k \mid X_{k-1}, \hat{Y}_{k-1}) = p(x_k \mid x_{k-1})$ based on (1) and the fact that the PDFs for v_k and w_k are prescribed. Evaluating the recursive equation in (20), we get

$$p(X_k \mid \hat{Y}_k) = p(x_0) \cdot \prod_{m=1}^{k} \frac{p(\hat{y}_m \mid x_m) \cdot p(x_m \mid x_{m-1})}{p(\hat{y}_m \mid \hat{Y}_{m-1})} = \frac{p(x_0)}{p(\hat{Y}_k)} \cdot \prod_{m=1}^{k} p(\hat{y}_m \mid x_m) \cdot p(x_m \mid x_{m-1}) \qquad (21)$$

4.2 Stochastic simulation for state estimation

Our interest is to develop a simulation algorithm for the conditional PDF $p(X_k \mid \hat{Y}_k)$ that is Markovian, in that information is required only from timesteps *k*-1 and *k*; earlier state and observation data can be forgotten. In other words, if $\hat{X}_{k-1}$ is a sample from $p(X_{k-1} \mid \hat{Y}_{k-1})$, the sample from $p(X_k \mid \hat{Y}_k)$ must have the form $\hat{X}_k = \{\hat{X}_{k-1}, \hat{x}_k\}$, where $\hat{x}_k$ is the new sample and $\hat{X}_{k-1}$ is the previous sample from $p(X_{k-1} \mid \hat{Y}_{k-1})$. However, such an algorithm is incomplete because it ignores the information $\hat{y}_k$, i.e., because $p(X_{k-1} \mid \hat{Y}_{k-1})$ is different from $p(X_{k-1} \mid \hat{Y}_k) = p(X_{k-1} \mid \hat{Y}_{k-1}, \hat{y}_k)$.

Importance-sampling technique

We can however sample from an importance-sampling PDF $q(X_k \mid \hat{Y}_k)$ that admits a sampling procedure by choosing $q(X_{k-1} \mid \hat{Y}_{k-1})$ so that it is identical to $q(X_{k-1} \mid \hat{Y}_k)$. In other words, the structure of $q(X_k \mid Y_k)$ is such that X_{k-1} is independent of y_k conditioned on Y_{k-1}. Drawing N samples $\left\{\hat{X}_k^i : i = 1,...,N\right\}$ randomly from $q(X_k \mid \hat{Y}_k)$ (selected so that it is readily sampled), the expectation conditioned on $\hat{Y}_k$ of any function of the state X_k, denoted by $r(X_k)$, can be estimated using the importance-sampling technique as follows:

$$E[r(X_k) \mid \hat{Y}_k] \approx \frac{1}{N}\sum_{i=1}^{N} \hat{\beta}_k^i \cdot r(\hat{X}_k^i) \equiv \hat{r}_{k,N}^1 \tag{22}$$

where $\hat{\beta}_k^i = p(\hat{X}_k^i \mid \hat{Y}_k) \big/ q(\hat{X}_k^i \mid \hat{Y}_k)$ is the non-normalized importance weight of the *i*-th sample.

Any quantity of interest can be estimated with the appropriate $r(\cdot)$ function in (22); for instance, if $r(X_k) = X_k$, $E[r(X_k) \mid \hat{Y}_k]$ is simply the conditional expectation $E[X_k \mid \hat{Y}_k]$; if $r(X_k) = X_k X_k^T$, $E[r(X_k) \mid \hat{Y}_k]$ is the conditional second moment $E[X_k X_k^T \mid \hat{Y}_k]$. In practice, the quantity of interest might be any facility-performance metric such as repair cost, repair duration, casualties, occupancy, or operability.

Let $\left\{X_k^i : i = 1,...,N\right\}$ denote the state variables corresponding to N random samples from $q(X_k \mid \hat{Y}_k)$ (before drawing the actual samples). It is readily shown that the estimator $r_{k,N}^1 = \frac{1}{N}\sum_{i=1}^{N} \beta_k^i \cdot r(X_k^i)$ is an unbiased estimator of $E[r(X_k) \mid \hat{Y}_k]$ if the support region for $p(X_k \mid \hat{Y}_k)$ is a subset of that for $q(X_k \mid \hat{Y}_k)$:

$$E\left[r_{k,N}^1\right]=\frac{1}{N}\sum_{i=1}^{N}E_q\left[\beta_k^i\cdot r(X_k^i)\right]=E_q\left[\beta_k\cdot r(X_k)\right]=\int\left[p(X_k\mid\hat{Y}_k)\big/q(X_k\mid\hat{Y}_k)\right]r(X_k)\cdot q(X_k\mid\hat{Y}_k)dX_k$$
$$=\int r(X_k)\cdot p(X_k\mid\hat{Y}_k)dX_k=E\left[r(X_k)\mid\hat{Y}_k\right] \tag{23}$$

According to the Central Limit Theorem, $r_{k,N}^1$ converges (as N approaches infinity) to a Gaussian random variable with mean equal to $E[r(X_k)\mid\hat{Y}_k]$ and with variance that decays as $1/N$. Therefore, $r_{k,N}^1$ is a consistent estimator of $E[r(X_k)\mid\hat{Y}_k]$.

Although $r_{k,N}^1$ is unbiased and consistent, it is not a feasible estimator because the non-normalized importance weights $\beta_k^i=p(X_k^i\mid\hat{Y}_k)\big/q(X_k^i\mid\hat{Y}_k)$ depend on $p(X_k^i\mid\hat{Y}_k)$, which cannot be computed easily since in order to evaluate $p(X_k^i\mid\hat{Y}_k)$, we have to evaluate $p(\hat{Y}_k)$, as shown by (21), which is a difficult task. Nevertheless, we show that the following estimator is computable while it is asymptotically unbiased and consistent:

$$r_{k,N}^2\equiv\left(\frac{1}{N}\sum_{i=1}^{N}\beta_k^i\cdot r(X_k^i)\right)\Bigg/\left(\frac{1}{N}\sum_{j=1}^{N}\beta_k^j\right)=r_{k,N}^1\big/\bar{\beta}_k^N \tag{24}$$

where

$$\bar{\beta}_k^N=\left(\sum_{j=1}^{N}\beta_k^j\right)\Big/N \tag{25}$$

Note that $\hat{r}_{k,N}^2$, unlike $\hat{r}_{k,N}^1$, can be computed conveniently from samples $\left\{\hat{X}_k^i:i=1,...,N\right\}$:

$$\hat{r}_{k,N}^2=\sum_{i=1}^{N}\left[\beta_k^i\Big/\left(\sum_{j=1}^{N}\beta_k^j\right)\right]\cdot r(\hat{X}_k^i)=\sum_{i=1}^{N}\tilde{\beta}_k^i\cdot r(\hat{X}_k^i) \tag{26}$$

where

$$\begin{aligned}\tilde{\beta}_k^i &= p(\hat{X}_k^i \mid \hat{Y}_k) \Big/ q(\hat{X}_k^i \mid \hat{Y}_k) \Bigg/ \left(\sum_{j=1}^{N} p(\hat{X}_k^j \mid \hat{Y}_k) \Big/ q(\hat{X}_k^j \mid \hat{Y}_k) \right) \\ &= \frac{p(\hat{x}_0^i)}{q(\hat{X}_k^i \mid \hat{Y}_k)} \cdot \prod_{m=1}^{k} p(\hat{y}_m \mid \hat{x}_m^i) \cdot p(\hat{x}_m^i \mid \hat{x}_{m-1}^i) \Bigg/ \left(\sum_{j=1}^{N} \frac{p(\hat{x}_0^j)}{q(\hat{X}_k^j \mid \hat{Y}_k)} \cdot \prod_{m=1}^{k} p(\hat{y}_m \mid \hat{x}_m^j) \cdot p(\hat{x}_m^j \mid \hat{x}_{m-1}^j) \right)\end{aligned} \tag{27}$$

Therefore, the factor $p(\hat{Y}_k)$ in (21) has been cancelled due to the use of the normalized importance weights $\left\{ \tilde{\beta}_k^i : i = 1, ..., N \right\}$, i.e. $\sum_{i=1}^{N} \tilde{\beta}_k^i = 1$. Also, the likelihood functions $p(\hat{y}_m \mid \hat{x}_m^i)$ and $p(\hat{x}_m^i \mid \hat{x}_{m-1}^i)$ can be readily evaluated using the prescribed PDFs for v_m and w_m if the mappings in (1) uniquely specify v_m and w_m, given y_m, x_m and x_{m-1}. We select $q(\hat{X}_k^i \mid \hat{Y}_k)$ so it can be readily evaluated too. The proof for the asymptotic unbiasedness and consistency of $r_{k,N}^2$ is given in Ching *et al.* (2004).

The selection of an importance sampling PDF that admits a real-time procedure is discussed in Ching *et al.* (2004). The conclusion is that the following importance sampling PDF performs better:

$$q(X_k \mid \hat{Y}_k) = p(x_0) \cdot \prod_{m=1}^{k} p(x_m \mid x_{m-1}, \hat{y}_m) \tag{28}$$

The corresponding modified non-normalized importance weight is:

$$\beta_k = \prod_{m=1}^{k} \frac{p(\hat{y}_m \mid x_m) \cdot p(x_m \mid x_{m-1})}{p(x_m \mid x_{m-1}, \hat{y}_m)} = \beta_{k-1} \cdot \frac{p(\hat{y}_k \mid x_k) \cdot p(x_k \mid x_{k-1})}{p(x_k \mid x_{k-1}, \hat{y}_k)} \tag{29}$$

Doucet and Godsill (1998) and Liu and Chen (1998) discuss the optimality of this importance sampling PDF.

Because of the structure of the algorithm, at any time k, we are only required to store the sampled states and weights in the most recent two time steps, i.e. k and $k-1$, if the quantity of

interest is $r(x_k)$ and so depends on the current state (clearly, additional dependence on the previous state x_{k-1} can also be treated). As a result, the following recursive algorithm can be used:

Algorithm 4.1: Basic PF algorithm

(1) Initialize the N samples: Draw $\hat{x}^i$ from $p(x_0)$ and set $\beta^i = 1/N$, $i = 1,...,N$.

(2) At time k, store the previous samples and weights

$$\tilde{x}^i = \hat{x}^i \qquad \tilde{\beta}^i = \beta^i \tag{30}$$

For $i = 1,...,N$, draw $\hat{x}^i$ from $p(x_k \mid x_{k-1} = \tilde{x}^i, \hat{y}_k)$ and update the importance weight

$$\beta^i = \tilde{\beta}^i \cdot \frac{p(\hat{y}_k \mid x_k = \hat{x}^i) \cdot p(x_k = \hat{x}^i \mid x_{k-1} = \tilde{x}^i)}{p(x_k = \hat{x}^i \mid x_{k-1} = \tilde{x}^i, \hat{y}_k)} \tag{31}$$

(3) Using the samples $i = 1,...,N$, $E[r(x_k) \mid \hat{Y}_k]$ can be approximated based on (26) and (30):

$$E[r(x_k) \mid \hat{Y}_k] \approx \sum_{i=1}^{N} \left[\beta^i \Big/ \left(\sum_{j=1}^{N} \beta^j \right) \right] \cdot r(\hat{x}^i) \tag{32}$$

where $r(\cdot)$ is a function that maps from x_k to the quantity of interest.

(4) Do Steps (2) and (3) for timesteps $k = 1,...,T$.

Usually, $p(x_k \mid x_{k-1} = \tilde{x}^i, \hat{y}_k)$ in Step 2 is difficult to sample. Note that estimating the first two moments of $p(x_k \mid x_{k-1} = \tilde{x}^i, \hat{y}_k)$ is a problem that can be solved using a single-time-step EKF algorithm. The least-informative PDF (i.e., the maximum-entropy PDF; see Jaynes 1957) given the estimated two moments, which is a Gaussian PDF (denoted by $p_{LI}(x_k \mid x_{k-1} = \tilde{x}^i, \hat{y}_k)$; LI subscript means 'least-informative'), can be used for the importance sampling PDF. The use of $p_{LI}(x_k \mid x_{k-1} = \tilde{x}^i, \hat{y}_k)$ is discussed in Doucet and Godsill (1998) and van der Merwe *et al.* (2000).

Algorithm 4.2: Determining $p_{LI}(x_k \mid x_{k-1} = \tilde{x}^i, \hat{y}_k)$

(1) Uncertainty propagation: compute

$$\begin{aligned} &E_{LN}\left[x_k \mid x_{k-1} = \tilde{x}^i\right] = f_{k-1}(x_{k-1} = \tilde{x}^i, u_{k-1}, w_{k-1} = 0) \equiv \tilde{x}^i_{k|k-1} \\ &Cov_{LN}\left[x_k \mid x_{k-1} = \tilde{x}^i\right] = (G^{LN}_{k-1}) \cdot Cov\{w_{k-1}\} \cdot (G^{LN}_{k-1})^T \equiv \tilde{P}^i_{k|k-1} \end{aligned} \tag{33}$$

where $G^{LN}_{k-1} \equiv \nabla_w f_{k-1}\big|_{x_{k-1}=\tilde{x}^i, w_{k-1}=0}$ is the Jacobian matrix, and

$$\begin{aligned} &E_{LN}\left[y_k \mid x_{k-1} = \tilde{x}^i\right] = h_{k-1}(\tilde{x}^i_{k|k-1}, u_k, 0) \equiv \tilde{y}^i_{k|k-1} \\ &Cov_{LN}\left[y_k \mid x_{k-1} = \tilde{x}^i\right] = \left(C^{LN}_k\right)\tilde{P}^i_{k|k-1}\left(C^{LN}_k\right)^T + \left(H^{LN}_k\right)\left(H^{LN}_k\right)^T \equiv \tilde{P}^{y,i}_{k|k-1} \\ &Cov_{LN}\left[x_k, y_k \mid x_{k-1} = \tilde{x}^i\right] = \tilde{P}^i_{k|k-1}\left(C^{LN}_k\right)^T \equiv \tilde{P}^{xy,i}_{k|k-1} \end{aligned} \tag{34}$$

where $C^{LN}_k \equiv \nabla_x h_k\big|_{x_k=\tilde{x}^i_{k|k-1}, v_k=0}$ and $H^{LN}_k \equiv \nabla_v h_k\big|_{x_k=\tilde{x}^i_{k|k-1}, v_k=0}$.

(2) Estimation: compute

$$\begin{aligned} &E_{LI}\left[x_k \mid x_{k-1} = \tilde{x}^i, \hat{y}_k\right] = \tilde{x}^i_{k|k-1} + \tilde{P}^{xy,i}_{k|k-1} \cdot (\tilde{P}^{y,i}_{k|k-1})^{-1} \cdot (\hat{y}_k - \tilde{y}^i_{k|k-1}) \\ &Cov_{LI}\left[x_k \mid x_{k-1} = \tilde{x}^i, \hat{y}_k\right] = \tilde{P}^i_{k|k-1} - \tilde{P}^{xy,i}_{k|k-1} \cdot (\tilde{P}^{y,i}_{k|k-1})^{-1} \cdot \tilde{P}^{xy,i\,T}_{k|k-1} \end{aligned} \tag{35}$$

$p_{LI}(x_k \mid x_{k-1} = \tilde{x}^i, \hat{y}_k)$ is then the Gaussian PDF with the two moments in (35).

4.3 Reducing degradation of performance: recursive resampling and parallel particle filters

Note that it is desirable to have the importance weights $\{\beta^i : i = 1, 2, ...N\}$ be approximately uniform so that all samples contribute significantly in (32), but they become far from uniform as k grows, which is due to the recursion in (29) and the fact that $q(X_k \mid \hat{Y}_k) \neq p(X_k \mid \hat{Y}_k)$. Ultimately, a few weights become much larger than the rest, so the effective number of samples is small. Nevertheless, the degradation can be reduced, as described in this section and the next.

Instead of letting the N samples evolve through time independently (Algorithm 4.1), we can resample the samples when the importance weights become highly non-uniform (Kitagawa 1996; Doucet and Godsill 1998; Liu and Chen 1998; Doucet and Andrieu 2000). After the resampling, the importance weights become uniform, therefore the degradation problem is alleviated. The resampling step tends to terminate small-weight samples and duplicate large-weight samples and, therefore, forces the N samples to concentrate in the high probability region of $p(x_k \mid \hat{Y}_k)$.

Although the resampling step sets the weights back to uniform, the price to pay is that the samples become dependent and therefore collectively carry less information about the state. As a result, the resampling procedure should only be executed when the importance weights become highly non-uniform. This can be done by monitoring the coefficient of variation (c.o.v.) of the importance weights. The resampling procedure is executed only when this c.o.v. exceeds a certain threshold, indicating that the variability in the importance weights is large.

Another way to alleviate the dependency induced by the resampling step is to conduct several independent PF algorithms and combine all of the obtained samples. Although the samples obtained in a single algorithm can be highly dependent, the samples from different algorithms are completely independent. The resulting algorithm is as follows:

Algorithm 4.3: Parallel PF algorithm with resampling

(1) Initialize N samples for each of the L parallel PFs: Draw $\hat{x}^{i,j}$ from $p(x_0)$ and set $\beta^{i,j} = 1/N$ for $i = 1,...,N$, $j = 1,...,L$.

(2) Perform the following steps (3)-(4) for $j = 1,...,L$ independently. Since the processes are completely independent, they can be conducted in parallel.

(3) At time k, store the previous samples and weights

$$\tilde{x}^{i,j} = \hat{x}^{i,j} \qquad \tilde{\beta}^{i,j} = \beta^{i,j} \tag{36}$$

For $i = 1,...,N$, draw $\bar{x}^{i,j}$ from $p_{LI}(x_k \mid x_{k-1} = \tilde{x}^{i,j}, \hat{y}_k)$ and update the importance weight

$$\bar{\beta}^{i,j} = \tilde{\beta}^{i,j} \cdot \frac{p(\hat{y}_k \mid x_k = \bar{x}^{i,j}) \cdot p(x_k = \bar{x}^{i,j} \mid x_{k-1} = \tilde{x}^{i,j})}{p_{LI}(x_k = \bar{x}^{i,j} \mid x_{k-1} = \tilde{x}^{i,j}, \hat{y}_k)} \tag{37}$$

(4) Compute the c.o.v. of $\{\bar{\beta}^{i,j} : i = 1,...,N\}$.

If the c.o.v. is larger than the prescribed threshold, then execute the resampling step for $i = 1,...,N$:

$$\hat{x}^{i,j} = \bar{x}^{i,j} \qquad w.p. \quad \bar{\beta}^{i,j} \Big/ \sum_{i=1}^{N} \bar{\beta}^{i,j} \tag{38}$$

and set $\beta^{i,j} = 1/N$ for $i = 1,...,N$. Otherwise, for $i = 1,...,N$:

$$\hat{x}^{i,j} = \bar{x}^{i,j} \qquad \beta^{i,j} = \bar{\beta}^{i,j} \Big/ \sum_{i=1}^{N} \bar{\beta}^{i,j} \tag{39}$$

Store $\hat{r}_{k,N}^{j} = \sum_{i=1}^{N} r(\hat{x}^{i,j}) \cdot \beta^{i,j}$.

(5) $E[r(x_k) \mid \hat{Y}_k]$ can be then approximated by

$$E[r(x_k) \mid \hat{Y}_k] \approx \left(\sum_{j=1}^{L} \hat{r}_{k,N}^{j} \right) \Big/ L \tag{40}$$

(6) Do Steps 2 to 5 for $k = 1,...,T$.

After the resampling step in Algorithm 4.3, large-weight samples are duplicated; therefore, some samples are the same samples of $p(x_k \mid \hat{Y}_k)$, which is not desirable from the point of view of preventing degradation. Andrieu *et al.* (1999) use the Markov chain Monte Carlo (MCMC) technique to force the duplicated samples to take a random walk at each time step, where $p(x_k \mid \hat{Y}_k)$ is the stationary PDF of the Marlov chain. In Ching *et al.* (2004), we summarize the procedure of the MCMC step.

4.4 Advantages and disadvantages of the PF technique

The advantages of the PF technique include (1) as N (the number of samples per algorithm) approaches infinity, the value of any function of the state x_k estimated by PF converges to its expected value; therefore, the PF technique can be used to validate other methodologies; and (2) parallel computations are possible for PF algorithms. A disadvantage of the PF technique is that it is computationally expensive, especially when the degradation is severe so that we need large N and L to have the algorithm converge. In general, the required N and L grow with the size of the effective support region of $p(x_k \mid \hat{Y}_k)$. A simple test for convergence is to add parallel particle filters until the estimated quantities of interest, $r(x_k)$, do not significantly change.

For linear systems with time-varying unknown parameters, we derive an efficient PF algorithm in Ching *et al.* (2004). With this algorithm, the convergence rate can be significantly faster than the rate when standard PF is used.

5. CASE STUDY OF RECORDED SEISMIC RESPONSE

5.1 Building description

The selected building for the case study is a 7-story, 66,000 square-foot (6,200 m^2) hotel located in the San Fernando Valley of Los Angeles County, California. The building is 63 ft by 150 ft in plan, consisting of 3 bays by 8 bays, with the long direction oriented east-west. It is approximately 65 ft tall: the first story is 13 ft, 6 inches; stories 2 through 6 are 8 ft, 6-½ inches; the 7th story is 8 ft, 6 inches. We refer to this building as the Van Nuys hotel. It was built in 1966 according to the 1964 Los Angeles Building Code. The lateral-force-resisting system is a perimeter nonductile reinforced-concrete moment frame in both directions; internal gravity frames also provide some resistance. The gravity system comprises two-way reinforced-concrete flat slabs supported by square columns at the interior and by the rectangular columns of the perimeter

frame. The building was lightly damaged by the M6.6 1971 San Fernando event, approximately 20 km to the northeast, and severely damaged by the M6.7 1994 Northridge Earthquake, whose epicenter was approximately 4.5 km to the southwest. In particular, both the south and north frames of the building were seriously damaged during the Northridge earthquake. The building has been studied extensively, e.g., by Jennings (1971), Scholl *et al.* (1982), Islam (1996a, 1996b), Islam *et al.* (1998), Li and Jirsa (1998) and Beck *et al.* (2002). A detailed description for the building can be found in Beck *et al.* (2002).

Strong motion data was obtained from sixteen channels that recorded motions during the Northridge earthquake. Among the sixteen channels, five channels measured the accelerations in the longitudinal (east-west: E-W) direction at the ground, second, third, sixth floors and the roof. The locations of the five accelerometers were at the south-east corner of the ground floor and near the east wall at the second, third, sixth floors and the roof. Figure 1 shows the measured E-W acceleration time histories during the earthquake. These data are used in this case study.

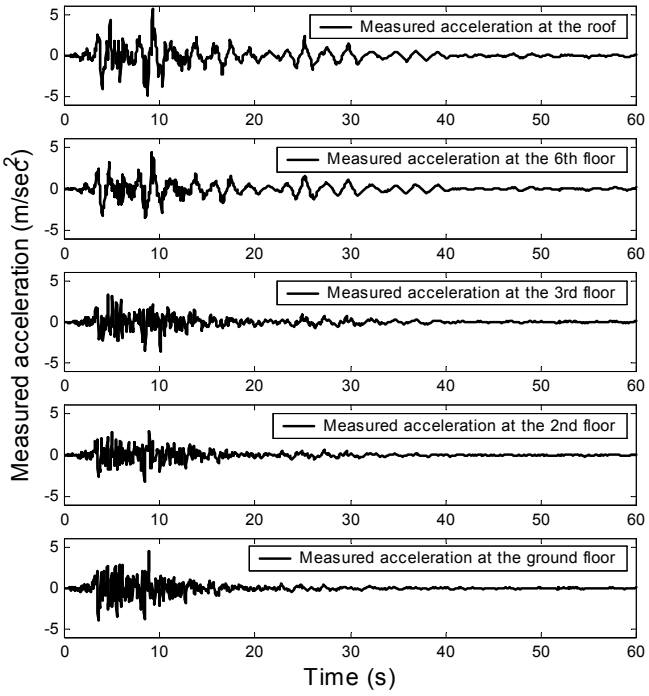

Figure 1. Measured E-W accelerations from the Van Nuys hotel during the Northridge earthquake

The purpose of this case study is to examine the use of Bayesian state-estimation techniques in tracking the system state and parameters of the building during the earthquake. Moreover, we examine two identification models: (1) a time-varying linear model and (2) a simplified time-varying nonlinear degradation model. We show that the latter is better in tracking the system dynamics. We focus exclusively on the dynamics in the E-W direction due to the fact that this involves the south frame that was severely damaged.

5.2 Time-varying linear identification model

We first investigate a linear structural identification model with unknown time-varying inter-story stiffnesses and dampings. This model is our first attempt because linear time-varying structural models are popular for identifying degrading civil engineering systems. The model is a

1-D 7-degree-of-freedom lumped-mass shear-building model with the following continuous-time state-space equations:

$$\frac{d}{dt}\begin{bmatrix} x_t \\ \dot{x}_t \\ \theta_t \end{bmatrix} = \begin{bmatrix} \dot{x}_t \\ -M^{-1}K(\theta_t)x_t - M^{-1}C(\theta_t)\dot{x}_t \\ 0_{18\times 1} \end{bmatrix} - \begin{bmatrix} 0_{7\times 1} \\ 1_{7\times 1} \\ 0_{18\times 1} \end{bmatrix} \cdot u_t + \begin{bmatrix} 0 \\ 0 \\ G \end{bmatrix} \cdot w_t$$

$$y_t = \begin{bmatrix} \ddot{x}_{7,t} + u_t \\ \ddot{x}_{5,t} + u_t \\ \ddot{x}_{2,t} + u_t \\ \ddot{x}_{1,t} + u_t \end{bmatrix} + H(\theta_t)\cdot v_t = -\begin{bmatrix} 1 & 0 & 0 & 0 & 0 & 0 & 0 \\ 0 & 0 & 1 & 0 & 0 & 0 & 0 \\ 0 & 0 & 0 & 0 & 0 & 1 & 0 \\ 0 & 0 & 0 & 0 & 0 & 0 & 1 \end{bmatrix} \cdot M^{-1}[C(\theta_t)\dot{x}_t + K(\theta_t)x_t] + H(\theta_t)\cdot v_t \quad (41)$$

where $0_{m\times n}$ denotes an ($m\times n$) matrix whose entries are all zeros (and similar for $1_{m\times n}$); $\begin{bmatrix} x_t & \dot{x}_t & \theta_t \end{bmatrix}^T \in R^{32\times 1}$ is the augmented state; $x_{i,t} \in R$ denotes the displacement relative to the ground at the ($i+1$)-*th* floor (the eighth floor is the roof) at time t; $u_t \in R$ is the measured acceleration at the ground floor of the building at time t; $y_t \in R^{4\times 1}$ contains the E-W acceleration time histories measured at the second, third and sixth floors and the roof at time t; $\theta_t \in R^{18\times 1}$ is the vector containing uncertain system parameters at time t, including inter-story stiffness $k_{i,t}$ and damping $c_{i,t}$ of each story (index i denotes story number) plus four uncertainty parameters $h_{1,t} \cdots h_{4,t}$, that is $\theta_t = \begin{bmatrix} k_{1,t} & \cdots & k_{7,t} & c_{1,t} & \cdots & c_{7,t} & h_{1,t} & \cdots & h_{4,t} \end{bmatrix}^T$; masses are assumed to be known perfectly and calculated according to the structural drawings: 120.02 tons for the first floor, 102.11 tons for the second to seventh floors, and 95.87 tons for the roof; $w_t \in R^{18\times 1} \sim N(0, I)$, $v_t \in R^{4\times 1} \sim N(0, I)$ and are independent at each time (Gaussian white noise); $G \in R^{18\times 18}$ is a diagonal matrix whose diagonals we specify, as described later;

$$x_t = \begin{bmatrix} x_{7,t} \\ x_{6,t} \\ \vdots \\ x_{1,t} \end{bmatrix} \quad M = \begin{bmatrix} m_7 & 0 & 0 & 0 \\ 0 & m_6 & 0 & 0 \\ 0 & 0 & \ddots & 0 \\ 0 & 0 & 0 & m_1 \end{bmatrix} \quad F = \begin{bmatrix} -m_7 \\ -m_6 \\ \vdots \\ -m_1 \end{bmatrix} \quad H(\theta_t) = \begin{bmatrix} h_{1,t} & 0 & 0 & 0 \\ 0 & h_{2,t} & 0 & 0 \\ 0 & 0 & h_{3,t} & 0 \\ 0 & 0 & 0 & h_{4,t} \end{bmatrix}$$

$$C(\theta_t) = \begin{bmatrix} c_{7,t} & -c_{7,t} & 0 & 0 \\ -c_{7,t} & c_{7,t} + c_{6,t} & \ddots & 0 \\ 0 & \ddots & \ddots & -c_{2,t} \\ 0 & 0 & -c_{2,t} & c_{2,t} + c_{1,t} \end{bmatrix} \quad K(\theta_t) = \begin{bmatrix} k_{7,t} & -k_{7,t} & 0 & 0 \\ -k_{7,t} & k_{7,t} + k_{6,t} & \ddots & 0 \\ 0 & \ddots & \ddots & -k_{2,t} \\ 0 & 0 & -k_{2,t} & k_{2,t} + k_{1,t} \end{bmatrix} \quad (42)$$

Note that the system parameters are unknown so they are augmented into the system state in (41) and are estimated together with the other states. Moreover, the unknown system parameters θ_t are are modeled by a random walk with time, as shown by the dynamic equation $\dot{\theta}_t = G \cdot w_t$ in (41). We do not expect that the building behaved linearly during the Northridge earthquake; instead, the rationale here is to use the time-varying linear model to track the nonlinear behavior. Also, note that the prediction-error term $H(\theta_t) \cdot v_t$ in this model is non-stationary Gaussian white noise.

The prior PDFs for x_0 and $\dot{x}_0$ are taken to be independent zero-mean Gaussian with zero standard deviations, that is, we are confident that the structure starts from an at-rest initial condition; the prior PDFs of $\{k_{i,0} : i = 1, 2, ...7\}$ and $\{c_{i,0} : i = 1, 2, ...7\}$ are taken to be independent Gaussian with mean equal to our best estimate of the undamaged stiffness and damping (the optimal FE-adjusted values, as defined later) with c.o.v. equal to 5% for the stiffnesses and 20% for the dampings. For $h_{1,0}$, … $h_{4,0}$, the prior PDFs have means equal to 0.1 m/sec^2 and c.o.v. equal to 20%. The diagonals of *G* are chosen such that in each time step (set to 0.04 sec), $k_{i,t}$ and $c_{i,t}$ drift with a c.o.v. equal to 1% with a restriction that they cannot drift into negative values, and $h_{1,t}$, …

$h_{4,t}$ drift with c.o.v. equal to 20%. Note that we have allowed the uncertainty parameters to drift more freely to accommodate the possible large fluctuations of these parameters; however, for the stiffness and damping parameters, only limited fluctuations are allowed.

Results and discussion

We first convert (41) to a discrete-time state-space system with a time step of 0.04 sec by using numerical integration over a time step and only implement PF for this identification model. We employ ***Matlab*** routine ODE23 for this purpose. Figure 2 shows the stiffness and damping parameter estimates and the associated 95% confidence intervals from PF (using Algorithm 4.3 with number of samples $N = 200$ and number of parallel filters $L = 10$ and the importance weight c.o.v. threshold = 200%). If more samples are used in PF than the $N \cdot L = 2000$ samples, there is little change in the estimated means and variances of the unknown parameters, indicating that the results are nearly converged.

The predicted output accelerations (the estimated means of $p(y_t \mid D_t)$) and inter-story drifts (which can be derived from the estimated means of $p(x_t \mid D_t)$) from the model are illustrated in Figures 3 and 4, in which the 95% confidence intervals are also shown. The four measured accelerations and the "measured" inter-story drifts in the first and second stories (obtained from double integrating and high-pass filtering the difference between the accelerations measured at the first story and ground floor base, and second and first stories) are also plotted in the figures. The results show a significant amount of uncertainties since the confidence intervals are large, indicating the performance of the time-varying model is not good. However, the results do predict that the largest interstory drift ratio occurs in the fourth story where the hotel was damaged most in the Northridge earthquake.

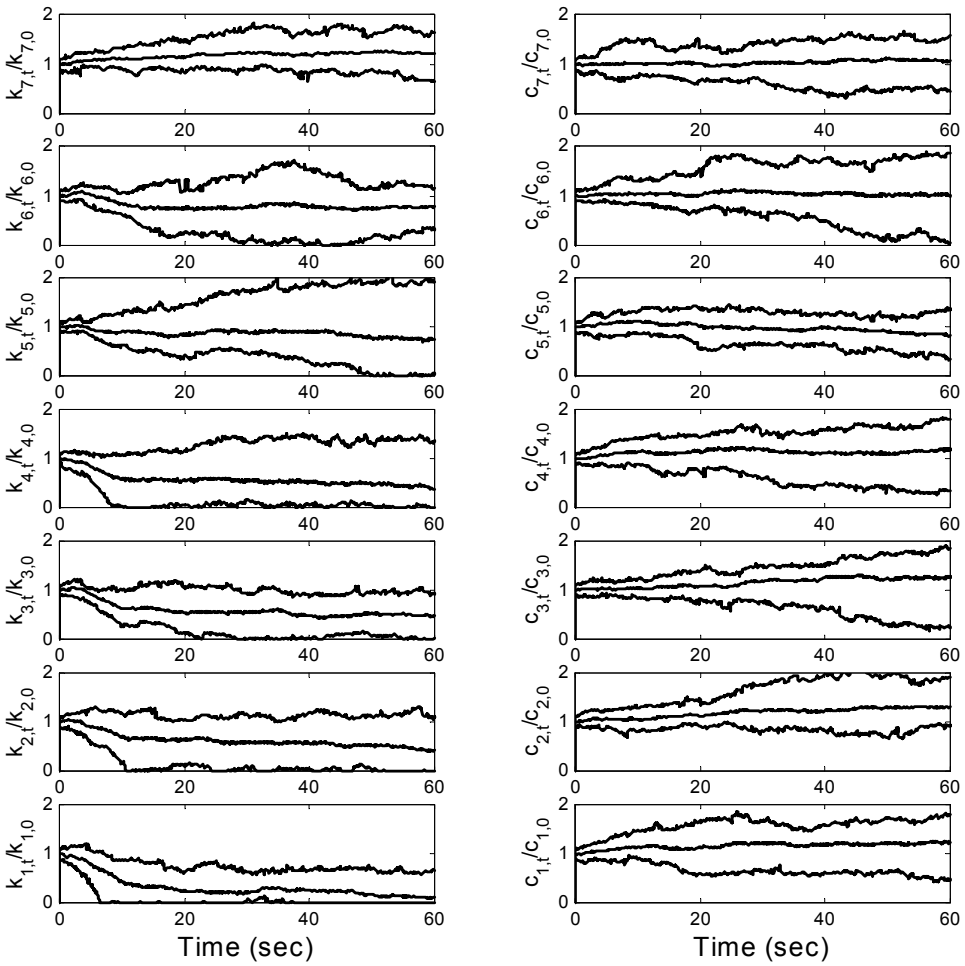

Figure 2. Estimated stiffness (left side) and damping (right side); dotted lines are 95% confidence bounds

To develop a better identification model, we first discuss some issues that are essential for model selection and that caused difficulties when we implemented the time-varying linear model.

(1) **Bias-variance tradeoff**: Consider two extreme cases. First, suppose that the *G* diagonals in (41) are so large that the stiffness and damping values at different time instants have essentially no correlation. Such a model is flexible, that is, one can fit the data quite well by adjusting the time-varying parameters freely, so the model is less biased. But it is

likely that there are numerous possible choices of the time-varying parameters that will also provide a comparable fit, so the model has high parameter variance. Therefore, the problem of estimating the stiffnesses and dampings is ill-posed, and the estimated parameters reflect little about the actual system dynamics.

Now consider the other extreme: the G diagonals are zeros so that the stiffnesses and dampings at different time instants have perfect correlation, that is, it gives a time-invariant linear model. Such a model is rigid, since one may only at best get a moderate fit to the dataset by adjusting the time-invariant parameters, making the model more biased. But there are usually only few possible choices of the parameters that will provide the moderate fit, so the model has low parameter variance.

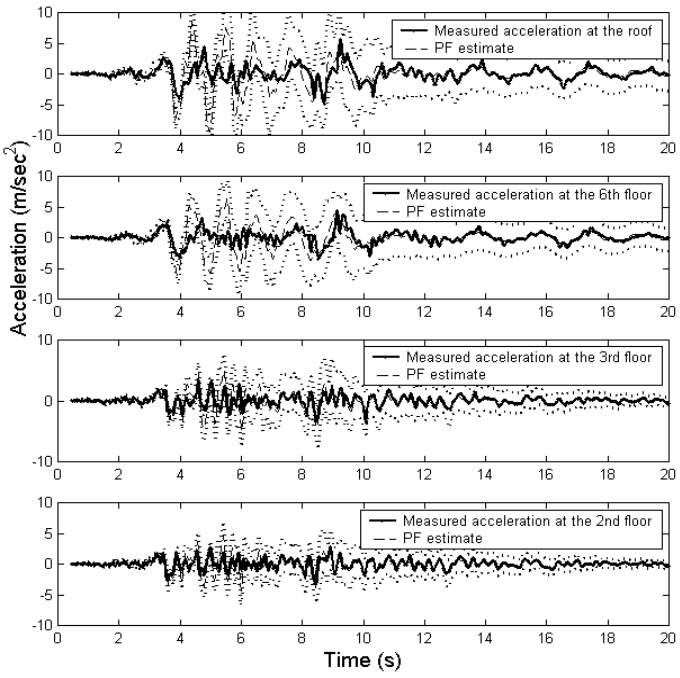

Figure 3. Solid lines are measured accelerations; dashed lines are predicted acceleration time histories; and dotted lines are 95% confidence intervals

Unfortunately, because the Van Nuys hotel was strongly shaken, the time-invariant linear model (the rigid model) is expected to be inappropriate, giving large modeling errors. Therefore, we should choose the G diagonals so that they are relatively large, allowing the linear model to change its parameters rapidly through time to accommodate the nonlinear behavior. By doing so, the resulting model is quite flexible, and the state and parameter estimates have relatively large variances, as seen in Figures 2-4. An ideal model is such that it is relatively rigid, so the parameters are only allowed to change slowly through time (i.e. small variance), but there still exists some choices of the system parameters that can fit the data well (i.e. small bias).

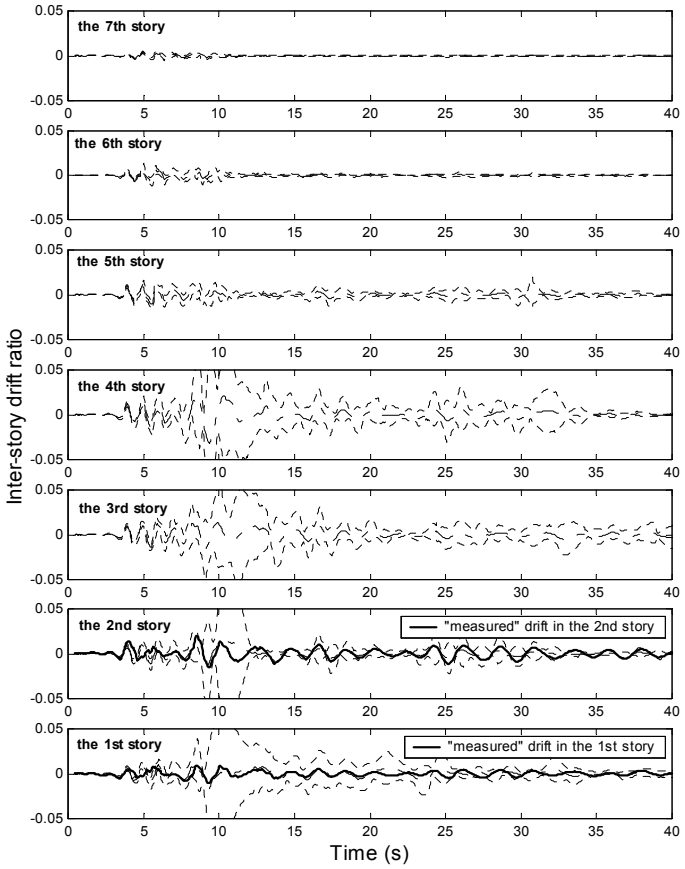

Figure 4. Solid lines are "measured" inter-story drift ratios; dashed lines are predicted inter-story drift ratios; and dotted lines are 95% confidence intervals

(2) **Correlation in prior PDFs**: The prior PDFs imply initially uncorrelated inter-story stiffnesses and dampings. However, it would be better if some correlation is built into the prior PDF because of the following facts. First, when degradation occurs, stiffnesses usually decrease and damping usually increases; therefore, they are in general correlated. Second, the stiffness and damping of adjacent stories could be correlated. This is because two adjacent stories usually have similar inter-story deformation, and hence similar degradation. The linear time-varying model does not provide for this correlation. For instance, in Figure 2, the 1st-story stiffness drops, while the 1st-story damping is basically unchanged. To model this correlation in the prior PDFs, we must use the full G matrix and tune all of the G entries to get the desired correlation instead of only using its diagonals. However, this is not easy.

(3) **Computational effort**: Finally, there are many (eighteen) free parameters in the time-varying linear model, making the computations expensive.

According to the discussion of the bias-variance tradeoff, the following question should be asked: Is it possible to find a model that is relatively rigid by having only a few slowly-changing parameters, and yet there still exist some choices of the system parameters that can fit the data well? In what follows, we first introduce a finite-element model for the Van Nuys hotel developed in previous work at Caltech. We show that this finite-element model provides a satisfactory fit of the measured acceleration data. Then we develop a simplified nonlinear degradation model to capture the behavior of the finite-element model and use this simplified model as our new identification model.

5.3 Caltech finite-element model of Van Nuys Hotel

Caltech researchers in a project on structural loss-estimation developed a nonlinear finite-element (FE) model of the south frame of the Van Nuys hotel (Beck *et al.* 2002). When subjected to the base acceleration recorded in the Northridge earthquake, the FE model is able to produce responses that are similar to the E-W accelerations measured at the second, third, sixth floors and the roof. The inelastic dynamic analysis program Ruaumoko (Carr 2001) was used for performing the FE analyses. For the details of the FE analyses, please refer to Appendix G in Beck *et al.* (2002).

The FE model uses two generic types of element: nonlinear flexural members and nonlinear shear springs. The flexural behavior of the beams and columns of the Van Nuys hotel is represented by one-component Giberson beam with plastic hinges at the ends (Sharpe 1974). Shear deformation for the beams is assumed to be elastic and is incorporated into the flexural elements. Shear deformation of the columns is modeled using nonlinear springs attached to the ends of the flexural elements. Two types of hysteresis rules are used to model the reinforced-concrete members' behavior: the SINA tri-linear hysteresis rule (Saiidi and Sozen 1979) is used to model stiffness degradation of reinforced concrete members in flexure. The Q-HYST bi-linear hysteresis (Saiidi and Sozen 1979) is used to model the stiffness degradation of reinforced concrete members in shear. A strength-degradation pattern introduced by Pincheira *et al.* (1999) is applied to both hysteresis rules.

Using the E-W ground-floor acceleration recorded during the Northridge earthquake as the input, the FE analysis is used to compute the E-W acceleration time histories at the second, third, sixth floors and the roof, which are shown in Figure 5. As seen in this figure, the FE-calculated acceleration adequately captures the trend of the measured accelerations from the

Northridge earthquake, especially in view of the fact that it is a purely theoretical model without any fitting to the earthquake data. However, it is inappropriate to use the FE model directly as our identification model since the FE model possesses a large number of potentially free parameters. Instead, we will employ a simplified nonlinear degradation model that mimics the behavior of the FE model and take that simplified model as our identification model.

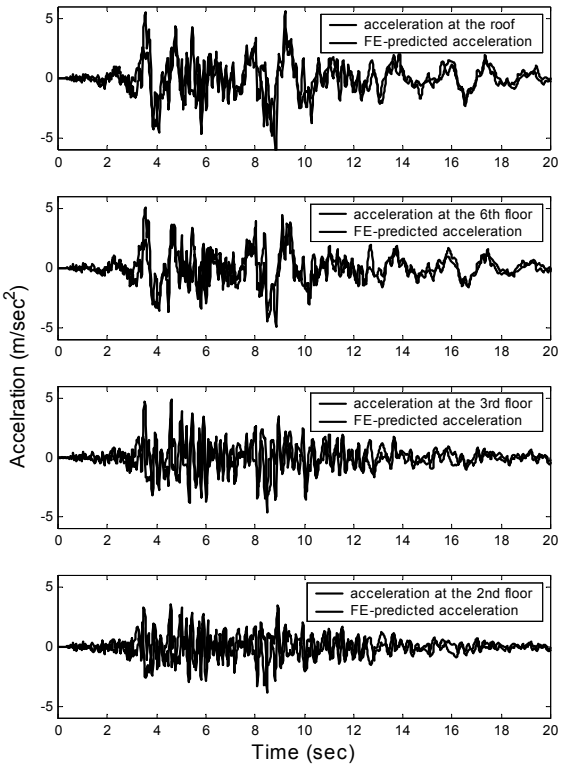

Figure 5. Solid lines are measured accelerations; dashed lines are FE-calculated accelerations

5.4 Development of the simplified nonlinear nonlinear degradation model

In Ching *et al.* (2004), we describe in detail the procedure for developing the simplified nonlinear degradation model that is able to produce relationships for inter-story restoring force versus inter-story drift similar to those produced by the FE model in the previous section. The

simplified nonlinear degradation model is a 1-D 7-DOF lumped-mass shear-building model with the following governing equations:

$$\begin{aligned} &m_1(\ddot{x}_{1,t}+u_t)+f_{1,t}-f_{2,t}=0 \\ &\vdots \\ &m_6(\ddot{x}_{6,t}+u_t)+f_{6,t}-f_{7,t}=0 \\ &m_7(\ddot{x}_{7,t}+u_t)+f_{7,t}=0 \end{aligned} \tag{43}$$

where $f_{i,t}$ is the inter-story restoring force in the *i*-th story and u_t is the acceleration at the ground floor at time t. The relationship between the inter-story restoring force and inter-story drift is as following:

$$f_{1,t}=c_{1,t}\cdot\dot{x}_{1,t}+k_{1,t}\cdot x_{1,t} \qquad f_{i,t}=c_{i,t}\cdot(\dot{x}_{i,t}-\dot{x}_{i-1,t})+k_{i,t}\cdot(x_{i,t}-x_{i-1,t}) \quad for \quad i=2,3,...7 \tag{44}$$

To model the degradation, we first define the ductility index of the *i*-th story as

$$\mu_{1,t}=\max_{0\le k\le t}\left(\left|x_{1,k}\right|/H_1\right) \qquad \mu_{i,t}=\max_{0\le k\le t}\left(\left|x_{i,k}-x_{i-1,k}\right|/H_i\right) \quad for \quad i=2,3,...7$$

where H_i is the story height of the *i*-th story. The degradation (i.e. the behavior that stiffnesses decrease and dampings increase with deformation) is then modeled by the following rule

$$k_{i,t}=k_{i,0}\cdot e^{-\gamma\cdot\mu_{i,t}^{\rho}} \qquad c_{i,t}=\delta+\lambda\cdot\mu_{i,t} \tag{45}$$

This gives a nonlinear model for the inter-story restoring forces versus drift with parameters γ, ρ, δ, λ, and $\{k_{i,0}: i=1,2,...7\}$. Notice that the same parameters γ, ρ, δ, and λ are used for each of the seven stories. We further reduce the model flexibility by parameterizing $\{k_{i,0}: i=1,2,...7\}$ using a single stiffness scaling parameter α such that

$$k_{i,0}=\alpha\cdot k_{i,0}^{FE} \qquad i=1,2,...7 \tag{46}$$

where $k_{i,0}^{FE}$ is the optimal FE-adjusted value for the inter-story stiffness $k_{i,0}$ (as discussed in the following). Assuming $\{k_{i,0} : i = 1,2,...7\}$ to be strongly correlated up to a scaling factor α greatly reduces the flexibility of the model and so it is likely that this assumption will bring in more bias but reduce the variance.

To show that this simplified model is able to mimic the behavior of the FE model, we input the inter-story restoring force $f_{i,t}$ generated by the FE model into (44) and solve the nonlinear differential equation for $\{x_{i,t} : i = 1,...,7; \forall t\}$ to compute the inter-story drifts with the following parameter setting: γ = 5.0, ρ = 0.4, δ = 0.5 MN/m·sec, and λ = 50 MN/m·sec, $k_{1,0}$ = 100 MN/m, $k_{2,0}$ = 120 MN/m, $k_{3,0}$ = 98 MN/m, $k_{4,0} = k_{5,0} = k_{6,0} = k_{7,0}$ = 80 MN/m (these parameter values are called the optimal FE-adjusted values). The computed inter-story drifts are then compared with the drifts generated by the FE model in Figure 6, where excellent agreement is exhibited.

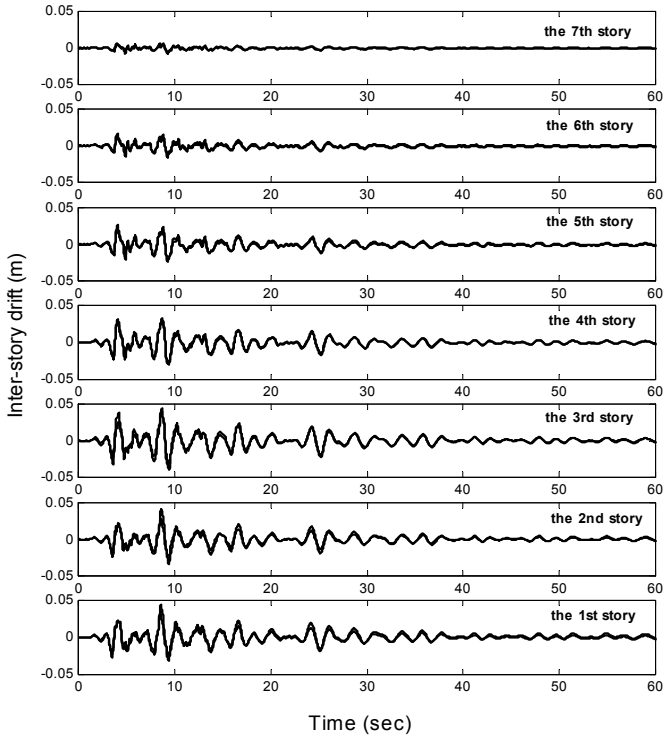

Figure 6. A comparison of the computed inter-story drifts from the simplified force-drift model (solid lines) and the reference FE model (dashed lines) based on the inter-story forces from the FE model.

A continuous-time state-space form for the simplified nonlinear degradation model can built:

$$\frac{d}{dt}\begin{bmatrix} x_t \\ \dot{x}_t \end{bmatrix} = \begin{bmatrix} \dot{x}_t \\ g(x_t, \dot{x}_t, \beta) \end{bmatrix} - \begin{bmatrix} 0_{7\times 1} \\ 1_{7\times 1} \end{bmatrix} \cdot u_t \qquad y_t = \begin{bmatrix} 1 & 0 & 0 & 0 & 0 & 0 & 0 \\ 0 & 0 & 1 & 0 & 0 & 0 & 0 \\ 0 & 0 & 0 & 0 & 0 & 1 & 0 \\ 0 & 0 & 0 & 0 & 0 & 0 & 1 \end{bmatrix} \cdot g(x_t, \dot{x}_t, \beta) \tag{47}$$

where $\beta = \begin{bmatrix} \gamma & \rho & \delta & \lambda & \alpha \end{bmatrix}^T \in R^{5\times 1}$; $g(x_t, \dot{x}_t, \beta) \in R^{7\times 1}$ characterizes (43)-(45). Using the Northridge E-W ground-floor acceleration as the input u_t, the computed output accelerations at the sensor locations using the simplified nonlinear degradation model with parameters equal to the optimal FE-adjusted values are shown in Figure 7, where we see that despite some mismatch, the model output can capture the overall trend of the measured accelerations.

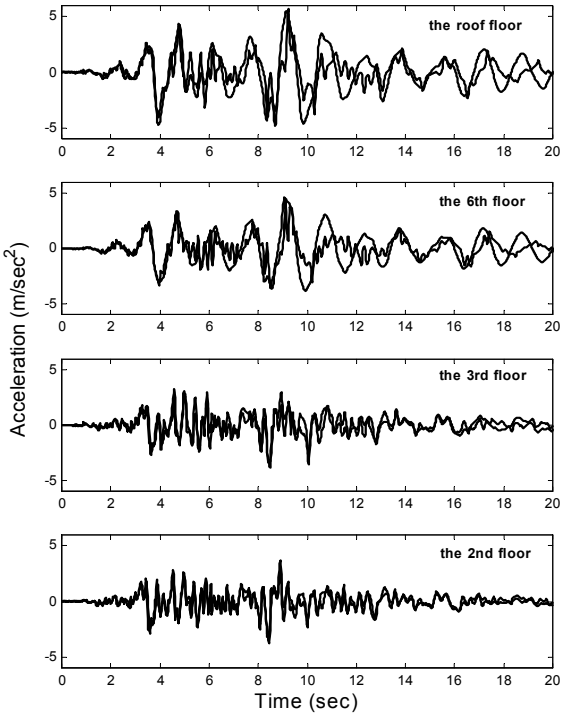

Figure 7. Solid lines are measured accelerations; and dashed lines are acceleration time histories calculated from the simplified nonlinear degradation model using recorded ground floor accelerations as input.

5.5 Time-varying nonlinear degradation identification model

A time-varying state-space stochastic model for identification can be derived from (47). The identification model has time-varying system parameters (i.e. $\beta_t = \begin{bmatrix} \gamma_t & \rho_t & \delta_t & \lambda_t & \alpha_t \end{bmatrix}^T$) and time-varying uncertainty parameters.

The rationale behind allowing the system parameters, such as β_t, to drift with time is as follows: it is very unlikely that the simplified nonlinear degradation model has no modeling error. The modeling error can be partially compensated by allowing the system parameters to vary with time, that is, the model is able to adaptively fit the data by slowly changing its parameter values. Nevertheless, we expect that the modeling error for the nonlinear model is less than that for the linear model considered previously. Therefore, the amount of change in the parameters

required for the nonlinear model should be less than that required for the linear model, so the time-varying nonlinear model is less flexible and should result in less parameter variance.

The resulting identification model is as follows:

$$\frac{d}{dt}\begin{bmatrix} x_t \\ \dot{x}_t \\ \theta_t \end{bmatrix} = \begin{bmatrix} \dot{x}_t \\ g(x_t, \dot{x}_t, \theta_t) \\ 0_{9\times 1} \end{bmatrix} - \begin{bmatrix} 0_{7\times 1} \\ 1_{7\times 1} \\ 0_{9\times 1} \end{bmatrix} \cdot u_t + \begin{bmatrix} 0_{7\times 1} \\ 0_{7\times 1} \\ G \end{bmatrix} \cdot w_t$$

$$y_t = \begin{bmatrix} 1 & 0 & 0 & 0 & 0 & 0 & 0 \\ 0 & 0 & 1 & 0 & 0 & 0 & 0 \\ 0 & 0 & 0 & 0 & 0 & 1 & 0 \\ 0 & 0 & 0 & 0 & 0 & 0 & 1 \end{bmatrix} \cdot g(x_t, \dot{x}_t, \theta_t) + H(\theta_t) \cdot v_t \qquad (48)$$

where $\theta_t = [\gamma_t \quad \rho_t \quad \delta_t \quad \lambda_t \quad \alpha_t \quad h_{1,t} \quad h_{2,t} \quad h_{3,t} \quad h_{4,t}]^T \in R^{9\times 1}$; $w_t \in R^{9\times 1} \sim N(0, I)$; $v_t \in R^{4\times 1} \sim N(0, I)$; matrix $H(\theta_t) \in R^{4\times 4}$ is assumed to be diagonal, so there are four uncertainty parameters $h_{i,t},\ i = 1,...,4,$ on the diagonal entry of the $H(\theta_t)$ matrix; $g(x_t, \dot{x}_t, \theta_t)$ is the same as $g(x_t, \dot{x}_t, \beta_t)$; $G \in R^{9\times 9}$ is a prescribed matrix.

Among the system parameters, several parameters confound together; for example, there is more than one set of α_t, γ_t, and ρ_t that corresponds to the same mathematical relationship between $k_{i,t}$ and $\mu_{i,t}$; this is also the case for δ_t and λ_t. This confounding can be resolved by holding some of the parameters constant. Alternatively, in the Bayesian framework this can be done by constraining the prior PDFs of these parameters, as described later.

To complete the identification model, we have to specify the prior PDFs for $x_0, \dot{x}_0, \theta_0$ and the diagonals of the *G* matrix. The prior PDFs of $x_0, \dot{x}_0$ are taken to be independent zero-mean Gaussian with zero standard deviations, since we are certain that the structure starts from an at-rest initial condition. To resolve the confounding problem, the prior PDFs for ρ_0 and δ_0 are chosen to have means equal to the optimal FE-adjusted values and c.o.v. equal to zero, and ρ_t

and δ_t do not change with time, so they are also fixed at the optimal values: $\rho_t = 0.4$ and $\delta_t = 0.5$. For γ_0 and λ_0, the prior PDFs have means equal to the optimal FE-adjusted values, 5.0 and 50, respectively, each with c.o.v. equal to 20% (since they are quite uncertain), while γ_t does not change with time to avoid the confounding problem and λ_t drifts with a c.o.v. equal to 0.4%. For α_0, the prior PDF has mean equal to 1 and c.o.v. equal to 5% (since we are usually more certain about the initial stiffness scaling parameter), and α_t drifts with a c.o.v. equal to 0.4%.

To sum up, there is only one uncertain time-varying parameter for the stiffnesses (i.e. α_t) and one for the damping (i.e. λ_t) to avoid confounding; two parameters are fixed (i.e. ρ_t and δ_t); and γ_t is an uncertain time-invariant parameter. For $h_{1,0}$, … $h_{4,0}$, the prior PDFs have means equal to 0.1 m/sec^2 and c.o.v. equal to 20% (since they are highly uncertain), and $h_{1,t}$, … $h_{4,t}$ fluctuate with a c.o.v. equal to 10% to allow rapid change of the prediction errors.

Preliminary comparison of the two identification models

As discussed in an early section, selecting the diagonals of *G* is a difficult task in general. Nevertheless, we argue here that with the simplified nonlinear degradation model, selecting the diagonals of *G* is easier. As we have seen, the time-varying linear model must vary its parameters (stiffnesses and dampings) rapidly to accommodate the nonlinearity (or degradation) that is present in the acceleration data; however, the simplified nonlinear degradation model is able to accommodate the degradation to a certain degree even with its parameters fixed. Therefore, in order to accommodate the degradation, the simplified nonlinear degradation model may only need to vary its parameters slowly (except for the uncertainty parameters $h_{1,t}$, … $h_{4,t}$, which need

to vary rapidly). This makes it easier to decide how to choose the diagonals of G in (48), since we should use relatively small diagonal values (again, not for the diagonal values corresponding to $h_{1,t}$, … $h_{4,t}$).

Moreover, the correlation between the inter-story stiffnesses and dampings is directly considered in the simplified nonlinear degradation model since they depend on the inter-story drifts, and the drifts of different stories are, in turn, correlated through the model structure. Lastly, the total number of the active parameters in the simplified nonlinear degradation model is only seven, so the flexibility of the model and the required computation resources are greatly reduced.

Results and discussion

We first convert (48) to a discrete-time system with time step of 0.04 sec. We then implement PF with N = 200 and L = 10 and the importance weight c.o.v. threshold = 200% using Algorithm 4.3. If more samples are used in PF than the $N \cdot L = 2000$ samples, there is little change in the estimated means and variances of the unknown parameters, indicating that the results are nearly converged.

Figure 8 shows the evolution of the estimated system parameters for the simplified nonlinear degradation model (where ρ_t and δ_t are not shown since they are deterministic). Figure 9 shows the predicted output accelerations, i.e. the estimated mean of $p(y_t \mid D_t)$, from the simplified model as well as the measured accelerations. Compared to Figure 3, the predicted acceleration can better capture the trend of the measured accelerations, and the corresponding confidence intervals are much smaller, indicating better performance. Similar observations are found for the predicted inter-story drifts (see Figure 10 and compare it to Figure 4).

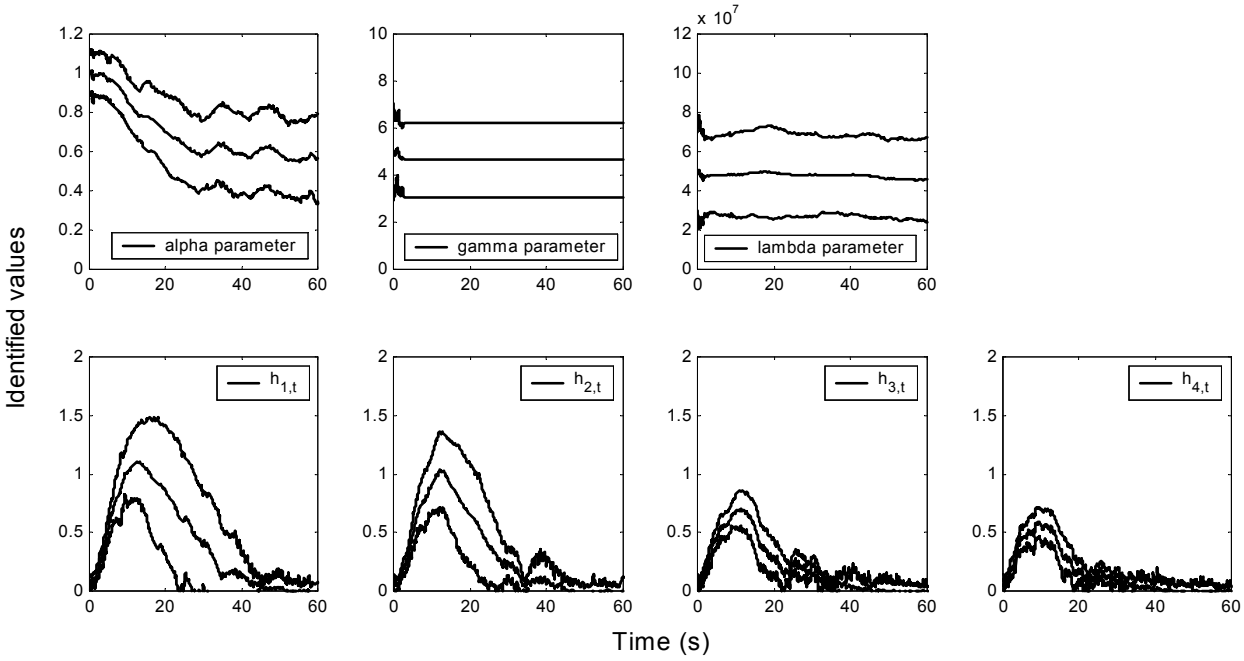

Figure 8. The estimated system parameters by PF; the dotted lines are the 95% confidence intervals (the results for the fixed parameters (i.e. ρ_t and δ_t) are not shown)

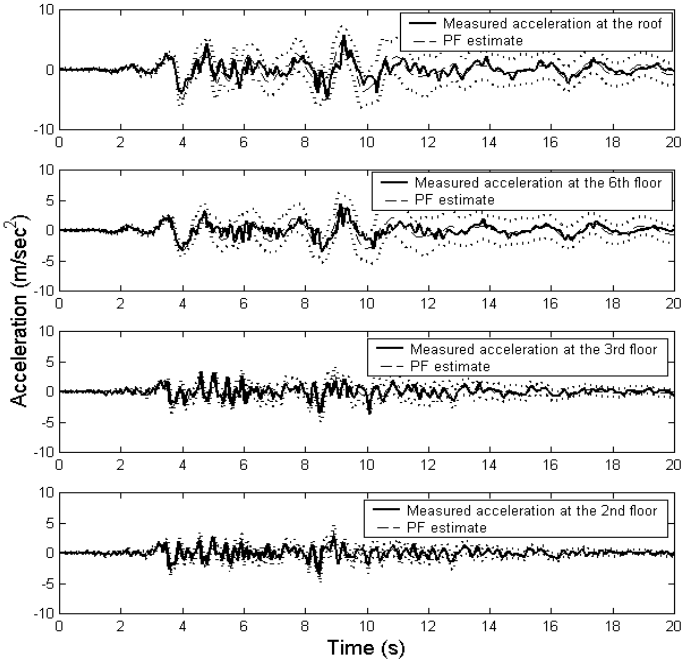

Figure 9. Solid lines are measured accelerations; dashed lines are predicted acceleration time histories; and dotted lines are 95% confidence intervals

Figure 11 shows the estimated inter-story stiffnesses and dampings from the simplified nonlinear degradation model. Compared to Figure 2, the confidence intervals are much smaller and the correlations between stiffnesses and dampings of different stories are more reasonable. The estimated dampings are quite different from those in Figure 2, in which the estimated dampings almost keep constant and do not show any degradation.

Comparison with EKF results

We also implement the EKF algorithm for the simplified nonlinear degradation model. The results from EKF are not consistent with those from PF, as can be seen by comparing Figure 12 for the estimated system parameters from EKF with those from PF in Figure 8. We treat the results from PF as a comparison standard since it asymptotically gives consistent state estimates. Therefore, we conclude that EKF does not provide consistent estimates for this case. Also, there is an unreasonable result from EKF for γ_t (the gamma parameter in the figure), which is a time-invariant parameter and so the prior PDF for γ_0 gives the same degree of constraint on γ_t for $t \neq 0$; as a consequence, the fluctuation of γ_t in Figure 12 is not reasonable since it drifts out of the main support region of the prior PDF of γ_0.

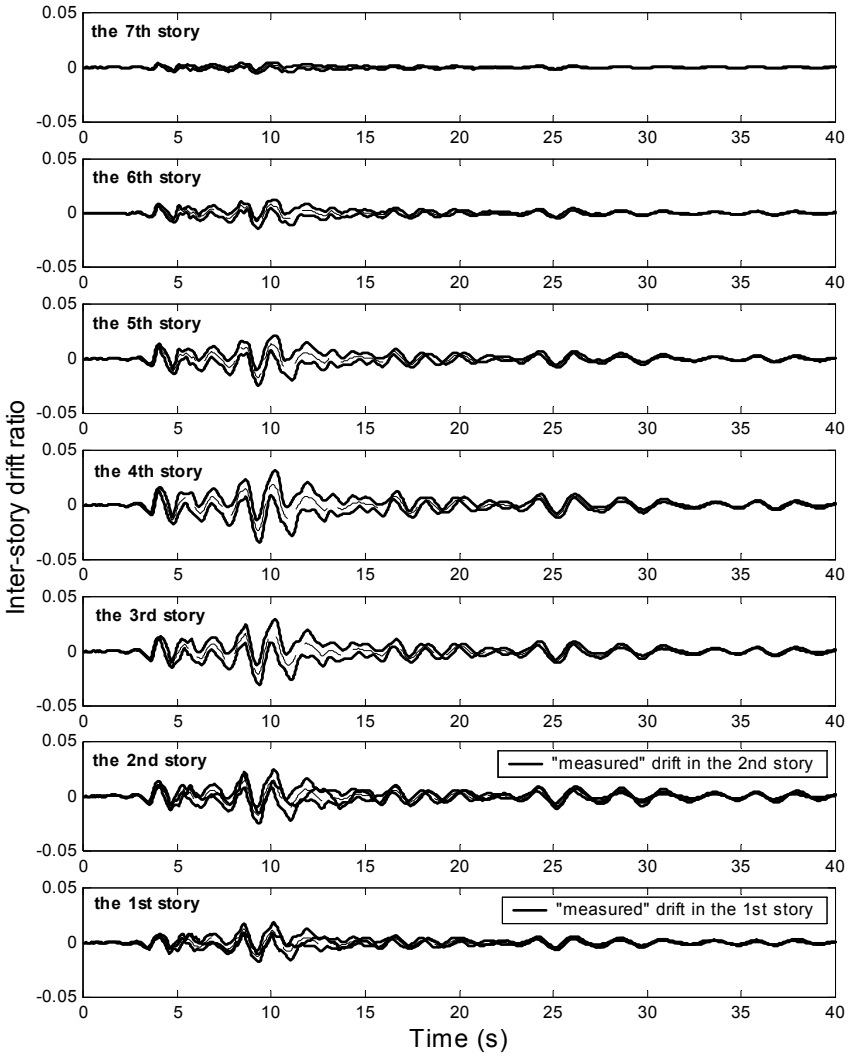

Figure 10. Solid lines are "measured" inter-story drift ratios; dashed lines are predicted inter-story drift ratios; and dotted lines are 95% confidence intervals

Figure 13 shows the predicted output accelerations and the confidence intervals from EKF. It is clear that the confidence intervals from EKF are erroreously smaller than those from PF shown in Figure 9 (the EKF uses the same data as the PF). The 95% confidence intervals for the inter-story drifts (Figure 14) from EKF are also much smaller than those from the PF shown in Figure 10, again giving erroneously higher confidence in the estimates. As a result, the meas-

ured inter-story drift ratios do not fall within the confidence intervals, which is not a desirable outcome. Figure 15 shows the estimated evolution of the inter-story stiffnesses and dampings from EKF; again, the results are not completely consistent with those from PF.

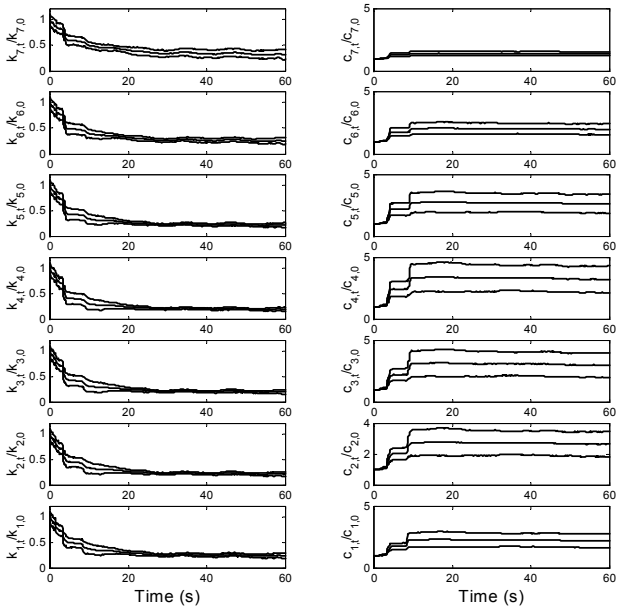

Figure 11. The estimated stiffnesses (left) and dampings (right); the dotted lines are the 95% confidence intervals

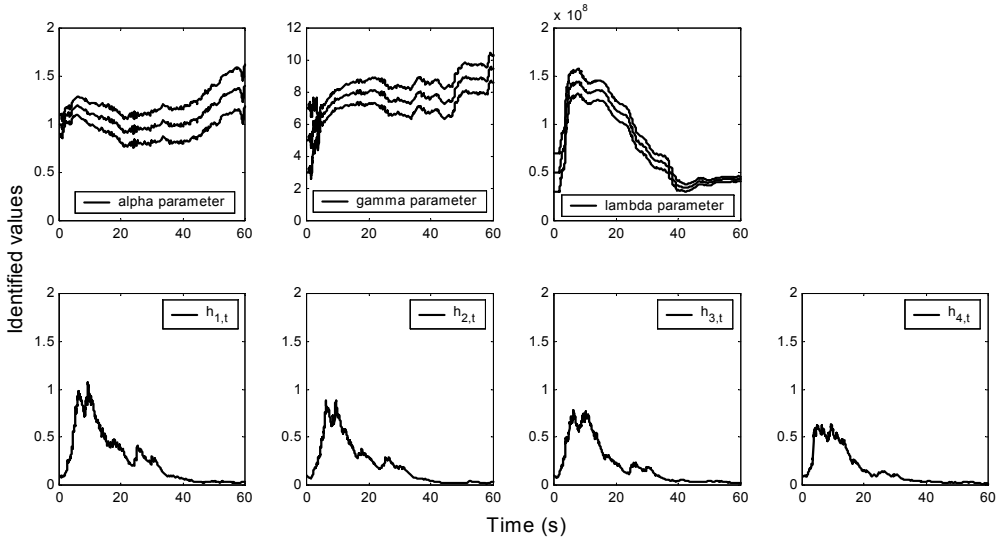

Figure 12. The estimated system parameters by EKF; the dotted lines are the 95% confidence intervals (no confidence intervals available for the uncertainty parameters)

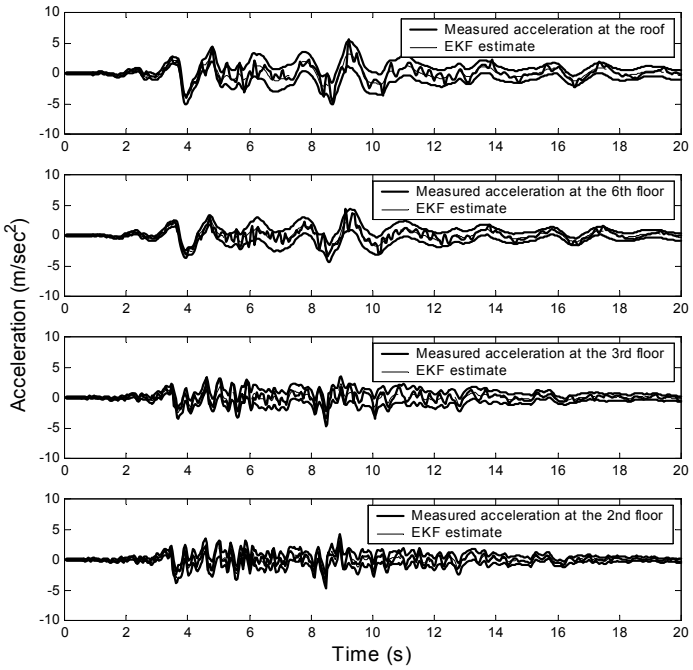

Figure 13. Solid lines are measured accelerations; dashed lines are predicted acceleration time histories by EKF; and dotted lines are 95% confidence intervals

5.6 Discussion

We have seen that for this real-data case study, EKF does not give results that are consistent with those from PF. In contrast, we show in Ching *et al.* (2004) that EKF gives consistent state estimates for several "simulated" examples (although these examples are not discussed in this paper). This may suggest that for real-data problems, it can be misleading if we only consider the first two moments of the system state and unknown parameters; instead, it may be essential to also consider the entire posterior PDFs.

Besides the need to choose a good algorithm among different available algorithms (e.g. EKF, PF, etc.), the results from this section also suggest that selecting a good stochastic identification model is essential. As we have seen, even with a good estimation algorithm (i.e. PF), the estimation results can be unsatisfactory if the time-varying linear model is employed. A better

strategy is to take a nonlinear model that can roughly capture the degrading behavior of the building and select an identification model based on that model. In fact, this is the main idea of developing the simplified nonlinear degradation model. As a result, a successful state-estimation technique should at least consist of (1) a good model for the underlying processes and (2) a good estimation algorithm. For the Van Nuys hotel case study, it is preferable to use the simplified nonlinear degradation model with the PF algorithm.

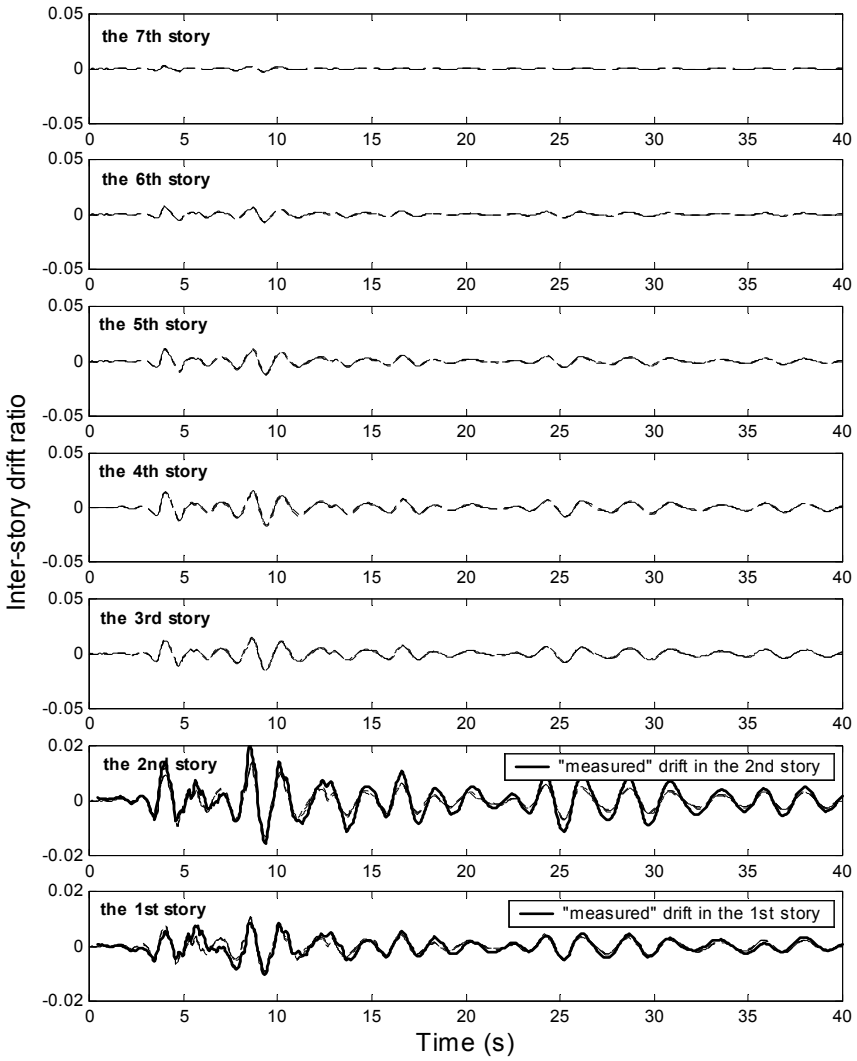

Figure 14. Solid lines are "measured" inter-story drift ratios; dashed lines are predicted inter-story drift ratios by EKF; and dotted lines are 95% confidence intervals (the confidence intervals are very small and so the dotted lines and the dashed lines almost overlap).

Although the simplified nonlinear degradation model performs satisfactorily for the case study, it is not necessarily the best model to use. There may exist other degradation models that are rigid in the sense defined earlier and yet able to fit the acceleration well. To find a better model than the simplified nonlinear degradation model involves model class selection and the bias-variance tradeoff, and we will not pursue this in this paper. A Bayesian approach to model class selection for dynamical systems is given by Beck and Yuen (2004).

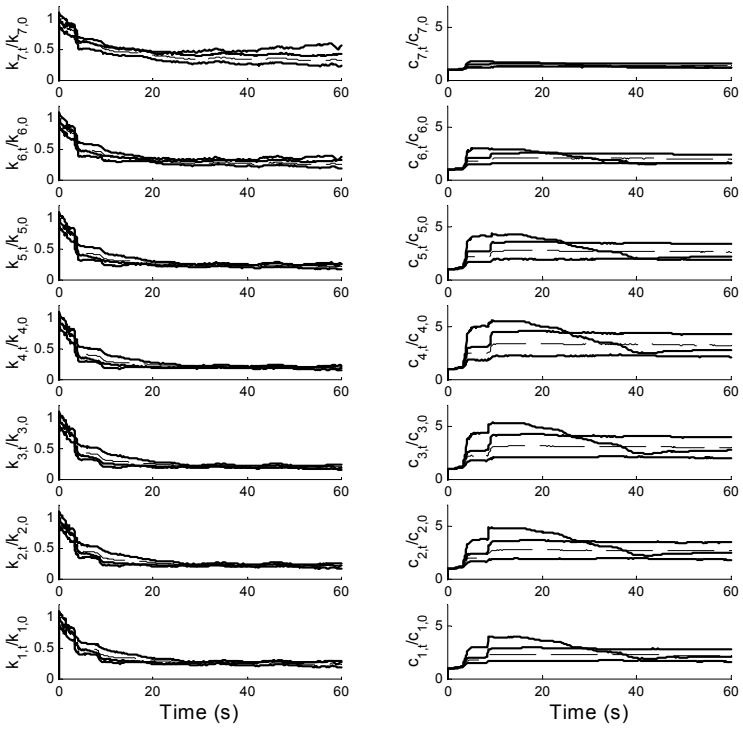

Figure 15. Solid lines: the estimated stiffnesses (left) and dampings (right) from EKF (the 95% confidence intervals are not available). For comparison, the results from PF are also shown as the dashed lines (mean values) and dotted lines (the 95% confidence intervals).

Although not shown in this paper, the maximum inter-story drift predicted by the FE model analyses is at the third story, although the actual damage to the south frame in the 1994

Northridge Earthquake was primarily to the beam-column joints at the top of the fourth-story level (see Section 5.3.3 in Beck *et al.* 2002). However, the inter-story drift predicted by the simplified nonlinear degradation model reaches its maximum at the fourth story (see Figure 10). Note that the former results do not incorporate the measured accelerations at the second, third, sixth floors and the roof, while the latter ones (Figure 10) do. It is likely that the inter-story drift prediction from the latter has been improved because the information from these acceleration data is incorporated.

6. CONCLUSION

We have presented two real-time Bayesian state-estimation algorithms in detail, the extended Kalman filter (EKF) and the particle filter (PF), which is a stochastic simulation approach. Strong-motion records from the seven-story Van Nuys hotel are studied using two different identification models (a time-varying linear model and a simplified nonlinear degradation model) and the EKF and PF algorithms. The results show that the simplified nonlinear degradation model significantly outperforms the time-varying linear model, which produces some unreasonable estimation results, and that the PF algorithm performs better than EKF. It is concluded that the following two factors are keys to a successful real-time Bayesian state estimation: (1) an appropriate state estimation algorithm and (2) an appropriate stochastic identification model.

REFERENCES

Alspach, D.L. and Sorenson, H.W. (1972). Nonlinear Bayesian estimation using Gaussian sum approximations, *IEEE Transactions on Automatic Control*, **17**(4), 439-448.

Andrieu, C., de Freitas, J. F. G. and Doucet, A. (1999). Sequential MCMC for Bayesian model selection, IEEE Higher Order Statistics Workshop, Ceasarea, Israel, 130-134.

Beck, J. L. (1978). *Determining Models of Structures from Earthquake Records*, EERL Report 78-01, Earthquake Engineering Research Laboratory, California Institute of Technology, Pasadena, California. <http://resolver.caltech.edu/CaltechEERL:1978.EERL-78-01>

Beck, J.L., Porter, K.A., Shaikhutdinov, R., Au, S.K., Moroi, T., Tsukada, Y., and Masuda, M. (2002). *Impact of Seismic Risk on Lifetime Property Values, Final Report, CUREe-Kajima Joint Research*

Program Phase IV, Consortium of Universities for Research in Earthquake Engineering, Richmond, CA. <http://resolver.caltech.edu/CaltechEERL: 2002.EERL-2002-04>

Beck, J.L. and Yuen, K.-V. (2004). Model selection using response measurements: Bayesian probabilistic approach, *Journal of Engineering Mechanics*, **130**(2), 192-203.

Carr, A.J. (2001). *Ruaumoko*, University of Canterbury, Christchurch, New Zealand.

Ching, J., Beck, J.L., Porter, K.A., and Shaikhutdinov, R. (2004) *Real-time Bayesian State Estimation of Uncertain Dynamical Systems*. EERL Report 2004-01, California Institute of Technology, Pasadena, CA. <http://caltecheerl.library.caltech.edu/>

Doucet, A. and Godsill, S. (1998). *On Sequential Simulation-based Methods for Bayesian Filtering*, Report CUED/F-INFENG/TR310, Department of Engineering, Cambridge University.

Doucet, A. and Andrieu, C. (2000). *Particle Filtering for Partially Observed Gaussian State Space Models*, Report CUED/F-INFENG /TR393, Department of Engineering, Cambridge University.

Doucet, A., de Freitas, J.F.G. and Gordon, N. (2000). Introduction to sequential Monte Carlo methods, in *Sequential Monte Carlo Methods in Practice*, Doucet, A., de Freitas, J.F.G., and Gordon, N.J. (eds), Springer-Verlag.

Ghanem, R. and Shinozuka, M. (1995). Structural-system identification. I: Theory, *Journal of Engineering Mechanics*, **121**(2), 255-264.

Glaser, S.D. (1996). Insight into liquefaction by system identification, *Geotechnique*, 46(4), 641-655.

Gordon, N.J., Salmond, D.J. and Smith, A.F.M. (1993). Novel approach to nonlinear/non-Gaussian Bayesian state estimation, *IEEE Proceedings-F*, **140**(2): 107-113.

Hoshiya, M and Saito, E. (1984). Structural identification by extended Kalman filter. *Journal of Engineering Mechanics*, **110**(12), p. 1757.

Islam, M.S. (1996a). Analysis of the response of an instrumented 7-story nonductile concrete frame building damaged during the Northridge Earthquake, *Proceedings of the 1996 Annual Meeting of the Los Angeles Tall Buildings Structural Council*, Los Angeles, CA.

Islam, M.S. (1996b). Holiday Inn, *1994 Northridge Earthquake Buildings Case Study Project Proposition 122: Product 3.2,* Sacramento CA: Seismic Safety Commission, 189-233.

Islam, M.S., Gupta, M., and Kunnath, B. (1998). Critical review of the state-of-the-art analytical tools and acceptance criterion in light of observed response of an instrumented nonductile concrete frame building, *Proceedings Sixth US National Conference on Earthquake Engineering*, Seattle, Washington.

Jaynes, E. T. (1957). Information theory and statistical mechanics, *Physical Review*, **106**, 620-630. Also in Rosenkrantz, R. D. (Ed) (1982). *E. T. Jaynes, Papers on Probability, Statistics and Statistical Physics*, Dordrecht, Holland: D. Reidel Publishing Co.

Jazwinski, A.H. (1970). *Stochastic Processes and Filtering Theory*, Academic Press, New York.

Jennings, P.C. (1971). *Engineering Features of the San Fernando Earthquake of February 9, 1971*, EERL Report 71-02, California Institute of Technology, Pasadena, CA.

Julier, S.J., Uhlmann, J.K., and Durrant-Whyte, H.F. (2000). A new method for the nonlinear transformation of means and covariances in filters and estimators, *IEEE Transactions on Automatic Control*, **45**(3), 477-482.

Kalman, R.E. (1960). A new approach to linear filtering and prediction problems, *J. Basic Engr.*, **82**D, 35-45.

Kalman, R.E. and Bucy, R.S. (1961). New results in linear filtering and prediction problems, *J. Basic Engr.*, **83**D.

Kitagawa, G. (1996). Monte Carlo filter and smoother for non-Gaussian nonlinear state space models, *Journal of Computational and Graphical Statistics*, **5**, 1-25.

Koh, C. G. and See, L. M. (1994). Identification and uncertainty estimation of structural parameters. *J. Engng. Mech.*, **120**(6), p. 1219.

Li, Y.R., and Jirsa, J.O. (1998). Nonlinear analyses of an instrumented structure damaged in the 1994 Northridge Earthquake, *Earthquake Spectra*, **14**(2), 245-264.

Lin, C.C., Soong, T.T., and Natke, H.G. (1990). Real-time system identification of degrading structures, *Journal of Engineering Mechanics*, **116**(10), 2258-2274.

Liu, J.S. and Chen, R. (1998). Sequential Monte Carlo methods for dynamical systems, *Journal of the American Statistical Association*, **93**, 1032-1044.

Maruyama, O. and Hoshiya, M. (2003). Nonlinear filters using Monte Carlo integration for conditional random fields, *Proceedings of the 9th International Conference on Applications of Statistics and Probability in Civil Engineering*, San Francisco, July.

Pincheira, J.A., Dotiwala, F.S., and D'Souza, J.T. (1999). Seismic analysis of older reinforced concrete columns, *Earthquake Spectra*, **15**(2), 245-272.

Saiidi, M. and Sozen, M.A. (1979). *Simple and Complex Models for Nonlinear Seismic Response of Reinforced Concrete Structures*, Report UILU-ENG-79-2031, Department of Civil Engineering, University of Illinois, Urbana, IL.

Sato, T. and Qi, K. (1998). Adaptive H_∞ filter: Its application to structural identification, *Journal of Engineering Mechanics*, **124**(11), 1233-1240.

Scholl, R.E., Kustu, O., Perry, C.L., and Zanetti, J.M. (1982). *Seismic Damage Assessment for High-rise Buildings,* URS/JAB 8020, URS/John A. Blume & Associates, Engineers, San Francisco, CA.

Sharpe, R.D. (1974). *The Nonlinear Response of Inelastic Structures,* Ph.D. Thesis, Department of Civil Engineering, University of Canterbury, Christchurch, New Zealand.

Shinozuka, M. and Ghanem, R. (1995). Structural-system identification. II: Experimental verification, *Journal of Engineering Mechanics*, **121**(2), 265-273.

Smyth, A.W., Masri, S.F., Chassiakos, A.G., and Caughey, T.K. (1999). On-line parametric identification of MDOF nonlinear hysteretic systems, *Journal of Engineering Mechanics*, **125**(2), 133-142.

van der Merwe, R. and Wan, E.A. (2003). Gaussian mixture sigma-point particle filters for sequential probabilistic inference in dynamic state-space models, *Proceedings of IEEE International Conference on Acoustics, Speech and Signal Processing (ICASSP)*, Hong Kong.

van der Merwe, R., de Freitas, N., Doucet, A. and Wan, E.A. (2000). *The Unscented Particle Filter*, Report CUED/F-INFENG/TR380, Department of Engineering, Cambridge University.

Wan, E.A. and van der Merwe, R. (2000). The unscented Kalman filter for nonlinear estimation, *Proceedings of Symposium 2000 on Adaptive Systems for Signal Processing, Communication and Control*, IEEE, Lake Louise, Alberta, Canada.

Yoshida, I. and Sato, T. (2002). Health monitoring algorithm by the Monte Carlo filter based on non-Gaussian noise, *Journal of Natural Disaster Science*, **24**(2), 101-107.

Yun, C.B. and Shinozuka, M. (1980). Identification of nonlinear dynamic systems, *Journal of Structural Engineering*, **8**(2), 187-203.